İZMİR KÂTİP ÇELEBİ ÜNİVERSİTESİ
2010
GRADUATE SCHOOL OF NATURAL AND APPLIED SCIENCES

# Experimental Investigation of Propagation of Sediment Due to Earth-fill Dam Break

Submitted to the Graduate School of Natural and Applied Sciences in partial fulfillment of the requirements for the degree of

Master of Science

in Civil Engineering

by

Ebru Taşkaya

ORCID 0000-0003-1265-600X

January, 2023

This is to certify that we have read the thesis **Experimental Investigation of Propagation of Sediment Due to Earth-fill Dam Break** submitted by **Ebru Taşkaya**, and it has been judged to be successful, in scope and in quality, at the defense exam and accepted by our jury as a MASTER'S THESIS.

**APPROVED BY:**

**Advisor:** **Prof. Dr. Gökçen Bombar**
İzmir Kâtip Çelebi University

**Committee Members:**

**Prof. Dr. Mehmet SORGUN**
İzmir Kâtip Çelebi University

**Prof. Dr. Gökmen TAYFUR**
İzmir Institute of Technology

**Date of Defense: January 16, 2023**

# Declaration of Authorship

I, **Ebru Taşkaya**, declare that this thesis titled **Experimental Investigation of Propagation of Sediment Due to Earth-fill Dam Break** and the work presented in it are my own. I confirm that:

- This work was done wholly or mainly while in candidature for the Master's degree at this university.
- Where any part of this thesis has previously been submitted for a degree or any other qualification at this university or any other institution, this has been clearly stated.
- Where I have consulted the published work of others, this is always clearly attributed.
- Where I have quoted from the work of others, the source is always given. This thesis is entirely my own work, with the exception of such quotations.
- I have acknowledged all major sources of assistance.
- Where the thesis is based on work done by myself jointly with others, I have made clear exactly what was done by others and what I have contributed myself.

Date: 16.01.2023

# Experimental Investigation of Propagation of Sediment Due to Earth-fill Dam Break


## Abstract

As a result of the break of an earth-fill dam, the materials carried from the dam body may cause changes and destruction in the ground in the downstream region with the effect of the flood wave. Although there are extensive studies on breach development and flow effects experimental and modeling studies in the literature on dam breaks, sediment movement has generally been ignored. Homogeneous earth-fill dams are dams that use a single type of material in their construction. Sediment and flood wave propagation of a homogeneous earth-fill dam as a result of overtopping and piping dam break types were investigated experimentally in an 18.4 m long, 2.0 m wide, and 0.88 m high concrete rectangular open channel in İzmir Katip Çelebi University Hydraulics Laboratory. The dam body is built of uniform material with $d_{50}$ = 0.441 mm, homogeneously 60 cm high, 6 layers in 10 cm thick layers, a transverse base width of 200 cm, a longitudinal base width of 202 cm, crest width of 10 cm, and upstream-downstream slopes 32˚ was built. Each layer of the earth-fill dam body was compacted using standard compaction methods. A total of 8 (2×2×2) dam break experiments were carried out with 2 repetitions in 2 different downstream conditions, rough and smooth, in 2 different break scenarios as overtopping and piping. The roughness elements were placed in a staggered manner by using thirteen concrete blocks with dimensions of 10×10×10 cm at a distance of 1.5 m from the downstream skirt of the dam body. The dams upstream were slowly filled with water until it reached

the crest level. A triangular breach was made in the axis of the dam in order to trigger a dam break in the overtopping experiments. In the piping test, the water was stopped when it reached a certain level and waited for downstream erosion. In the experiments, the water level was measured at 4 different points, 1 upstream and 3 at the downstream of the ruler dam located on the left of the channel. In addition, with the help of ULS-40D ultrasonic level-measured sensors, sediment and water levels were measured at 3 different points on the axis of the channel. At the end of each experiment, the sediment heights taken at 10 cm intervals on the x and y axes were measured. Contour and 3D bathymetry maps of the sediment propagation along the channel of the break dam body were obtained from the sediment measurements obtained with the help of the Surfer program. According to experimental results smooth and rough downstream conditions, rough experiments sediment hight is higher. For overtopping and piping experiments, overtopping type dam break sediment hight is higher than piping type. In water depth and propagation of water, there are no specific differences between experiments.

**Keywords:** Earth-fill dam, overtopping dam break, piping dam break, smooth bed, rough bed

# Toprak Dolgu Baraj Yıkılması Sonucu Oluşan Sediment Taşınımının Deneysel Araştırması

## Öz

Toprak dolgulu bir barajın yıkılması sonucu baraj gövdesinden taşınan malzemeler taşkın dalgasının etkisiyle mansap bölgesindeki zeminde değişmelere ve tahribata sebep olabilir. Baraj yıkılmaları üzerine literatürde gedik gelişimi ve akım etkileri deneysel ve modelleme çalışmaları üzerine kapsamlı çalışmalar olmasına rağmen sediment hareketi genellikle göz ardı edilmiştir. Homojen toprak dolgu barajlar inşasında tek tip materyal kullanılan barajlardır. Homojen toprak dolgu barajın üstten aşma ve borulanma sonucu barajın mansabında oluşan sediment ve taşkın dalgası yayılımı İzmir Katip Çelebi Üniversitesi Hidrolik Laboratuvarı'nda 18,4 m uzunluğunda, 2,0 m genişliğinde ve 0,88 m yüksekliğinde beton dikdörtgen bir açık kanalda deneysel olarak incelenmiştir. Baraj gövdesi, $d_{50}$ = 0.441 mm olan üniform malzeme ile homojen olarak 60 cm yüksekliğinde, 10 cm kalınlığında katmanlar halinde 6 kat olacak şekilde, enine taban genişliği 200 cm, boyuna taban genişliği 202 cm, kret genişliği 10 cm ve memba-mansap eğimleri 32˚ olarak inşa edilmiştir. Toprak dolgu baraj gövdesinin her katı standart sıkıştırma yöntemleri kullanılarak sıkıştırılmıştır. Deneyler, üstten aşma ve borulanma olarak 2 farklı yıkım senaryosu, pürüzlü ve pürüzsüz olmak üzere 2 farklı mansap koşulunda, 2 tekrarlı olarak toplamda 8 ( 2×2×2) tane baraj yıkılma deneyi gerçekleştirilmiştir. Baraj gövdesinin mansap eteğinden 1,5 m uzaklıkta, 10×10×10 cm boyutlarında on üç adet beton blok kullanılarak pürüzlülük elamanları şaşırtmalı olarak yerleştirilmiştir. Baraj membası

kret seviyesine gelene kadar yavaşça doldurulmuştur. Üstten aşma deneylerinde baraj yıkılmasını tetiklemek için barajın ekseninde üçgen gedik açılmıştır. Borulanma deneyinde su belirli bir seviyeye geldiğinde durdurulmuş ve borulanmanın gerçekleşmesi beklenmiştir. Deneylerde su seviyesi kanalın solunda bulunan cetveller barajın membasında 1, mansabında 3 tane olmak üzere 4 farklı noktada ölçülmüştür. Ayrıca ULS-40D ultrasonik seviye ölçer sensörleri yardımıyla kanalın ekseninde 3 farklı noktada sediment ve su seviyesi ölçülmüştür. Her deney sonunda x ve y eksenlerinde 10 cm aralıklarla alınan sediment yükseklikleri ölçülmüştür. Elde edilen sediment ölçümlerinden Surfer programı yardımıyla yıkılan baraj gövdesinin kanal boyunca yayılan sedimentin kontur ve 3 boyutlu batimetri haritaları çıkartılmıştır. Deney sonuçlarına göre pürüzsüz ve pürüzlü mansap koşullundaki deneylerde, pürüzlü deneylerde sediment yüksekliği daha fazladır. Üstten aşma ve borulama deneylerinde, Üstten aşma baraj yıkılmasının sediment yüksekliği borulanmaya göre daha yüksektir. Su derinliği ve suyun yayılmasında, deneylerin arasında belirli bir fark yoktur.

**Anahtar Kelimeler:** Toprak dolgu baraj, üstten aşma baraj yıkılması, borulanma baraj yıkılması, pürüzsüz taban, pürüzlü taban

*I’d like to dedicate this thesis to my family.*

# Acknowledgment

First of all, I would like to thank my esteemed advisor, Assoc. Dr. Gökçen BOMBAR for her help and suggestions during the thesis study. I would like to thank my friends Lec. Zehra BÜYÜKER and Büşra ÖZTÜRK, Ress. Ass. Pelin İLKER, Ress. Ass. Şevket Onur KALKAN, Ress. Ass. İlker GÜCU and Ress. Ass. Tolga ARSLAN with all my heart.

I would like to thank the project coordinator of the project numbered 119M959 supported by TÜBİTAK and my thesis jury Prof. Dr. Gökmen TAYFUR for his support and spare time. I would also like to thank the Technical Research Council of Turkey (TÜBİTAK) for its support to the research.

Finally, I would like to thank my dear parents Ayşe TAŞKAYA and İdris TAŞKAYA, my dear sisters Kadiriye DEMİRHAN and Burcu TAŞKAYA MUTLU, my dear brother Mert TAŞKAYA who have been with me in every decision of my life and have not spared their love and support and I would like to thank my dear fiance Fatih Halil YAVUZ for motivated and supported me throughout my university life.

# Table of Contents

# List of Figures

# List of Tables

# List of Abbreviations

| | |
|---|---|
| WCD | World Commission on Dams |
| ICOLD | International Commission on Large Dams |
| OS | Overtopping Smooth |
| OR | Overtopping Rough |
| PS | Piping Smooth |
| PR | Piping Rough |
| R0 | Ruler 0 |
| R1 | Ruler 1 |
| R2 | Ruler 2 |
| R3 | Ruler 3 |
| Probe 1 | ULS40-D measurement sensor at x = 1.07 m |
| Probe 2 | ULS40-D measurement sensor at x = 2.02 m |
| Probe 2 | ULS40-D measurement sensor at x = 4.5 m |

# List of Symbols

| | |
|---|---|
| $d_{50}$ | Median grain size [mm] |
| $t$ | Time [s] |
| $z$ | Level [cm] |
| $z'$ | Normalized data |

# Chapter 1

# Introduction

Dams are structures built for the purpose of accumulating water by preventing the flow of large rivers or streams. Centuries ago, humanity's first purpose in building the dam was to supply the water needs of the growing population and to irrigate agriculture. According to the report presented by the World Commission on Dams (WCD), the dams used to store water date back to BC. It dates back to 3000 BC [1]. Remains of water storage dams found in Jordan, Egypt, and other parts of the Middle East date back to at least 3000 BC [1]. With the development of civilizations, the needs of society have changed and the importance of dams for society has increased. Today, in addition to meeting the water needs of cities and irrigation of agricultural areas, dams are used to obtain hydroelectric energy, prevent flooding, to provide water for industry, transportation, and fishing purposes. Dams are divided into three in the literature according to their size, purpose of construction, and filling/body material from which the body is made.

1. Dams according to their size;

According to the International Commission on Large Dams (ICOLD) [2], 'A dam with a height of 15 meters or greater from lowest foundation to crest or a dam between 5 meters and 15 meters impounding more than 3 million cubic meters.' Dams outside the definition of a large dam are called ponds (small dams), and dams with a height of more than 50 m are called high dams.

2. Dams according to the purpose of construction;

According to the ICOLD, dams can be built for a single purpose or for multipurpose. According to singe-purpose dams are classified as:

- Flood control 9%
- Hydropower 21 %
- Irrigation 47 %
- Fish farming/Navigation/Tailing 1%
- Recreation 5%
- Water supply 12%
- Others 5%

According to multipurpose dams are classified as:

- Flood control 19%
- Hydropower 16%
- Irrigation 24%
- Fish farming/Navigation/Tailing 8%
- Recreation 11%
- Water supply 17%
- Others 5%

3. Dams by filling/body material

According to the body material of the existing dams by the ICOLD;

- Earth-fill dams 65%
- Rockfill dams 13%
- Gravity dams 14 %
- Buttress dams 0.8 %
- Barrages 0.5 %
- Arch dams 4 %
- Multiple arch dams 0.2 %
- Others 2.5 %

According to the report presented by ICOLD, the most common type of dam in the world is a fill dam. The reason for this is that fill dams are easy to construct and are more cost-effective than other types of dams. Fill dams are suitable for every valley. A rigid foundation feature is not sought in its construction, it can be applied on all

kinds of ground. Since the filling material is natural materials that occur in nature, the material costs are minimal for both rockfill and earth-fill dams. Labor is very less compared to other types of dams. Most of the dam construction is completed with machinery.

Earth-fill dams, which are the most common type of dam in the world, are divided into two. These are homogeneous earth-fill and zoned earth-fill shown in Figure 1.1. One type of material is used in the construction of the homogeneous earth-fill dam. Zoned earth-fill dams are constructed using more than one material. The core zone and outer shells are constructed of different materials.

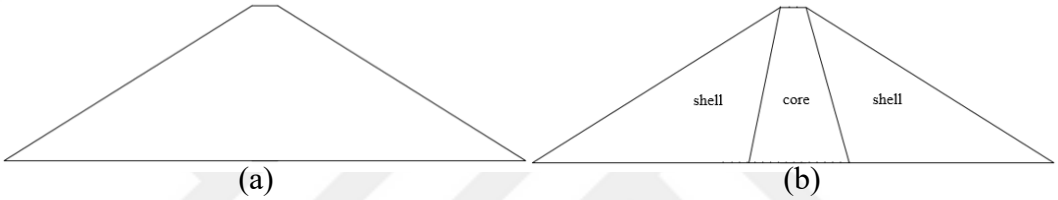


Figure 1. 1: Homogeneous (a) and zoned (b) earth-fill dam

Since dams accumulate large water bodies in their reservoirs, they are structures that are built with high safety coefficients to prevent them for break. However, dams are broken due to various reasons, and as a result of their breaks, serious material damage and loss of life may result. As a result of the break of the dams, all living things in nature; people, animals, and plants are harmed. For example; In the People's Republic of China, on August 8, 1975, with the annual precipitation falling in just 24 hours, the Banqiao and Shimantan Dams were destroyed and 11 million people were affected by this disaster with the break of 62 dams of all sizes. During the flood, 26.000 people lost their lives. Due to effects such as the fields destroyed by the flood and the inability of people to reach clean drinking water, 145.000 more people lost their lives due to hunger and epidemic diseases, and a total of 171.000 people lost their lives. Another example is the break of Teton Dam on 5 June 1976, causing the death of 11 people spread over an area of more than 250.000 acres in the reservoir water [3].

Reasons that can cause a dam to break are generally classified as natural causes (eg heavy rains, storms, tsunamis, landslides, and earth-quakes) or anthropogenic causes

(e.g. dam design errors, water storage mismanagement, maintenance errors, intentional dam, destruction, and terrorism) [4].

Overtopping and piping are common types of breaking dams. Overtopping is simply when the water level upstream of the dam exceeds the dam's crest, causing erosion downstream of the dam.

Piping break is the attempt of the water from the upstream of the dam to pass downstream of the dam due to seepage, which is usually observed at the bottom or middle of the dam by internal erosion.

In Figure 1.2 shows the development of the dam breach for overtopping and piping givin by Brunner [5]. Costa et al. [6] according to, about 34% of dam breaks are caused by overtopping, 30% by foundation defects, and 28% by piping. According to the report of the ICOLD in Bozkuş's study [7] 38% of dam breaks are caused by insufficient spillway capacity, 33% by piping, and 23% by other reasons mentioned above. Abay et al. [8] reported that the causes of dam breaks worldwide were 34% overtopping, 30% foundation problems, 20% piping, 10% pipes and valves, and 6% other causes. According to the report of the ICOLD earth- and rockfill dam breaks 49 % by overtopping, and 28% by piping.

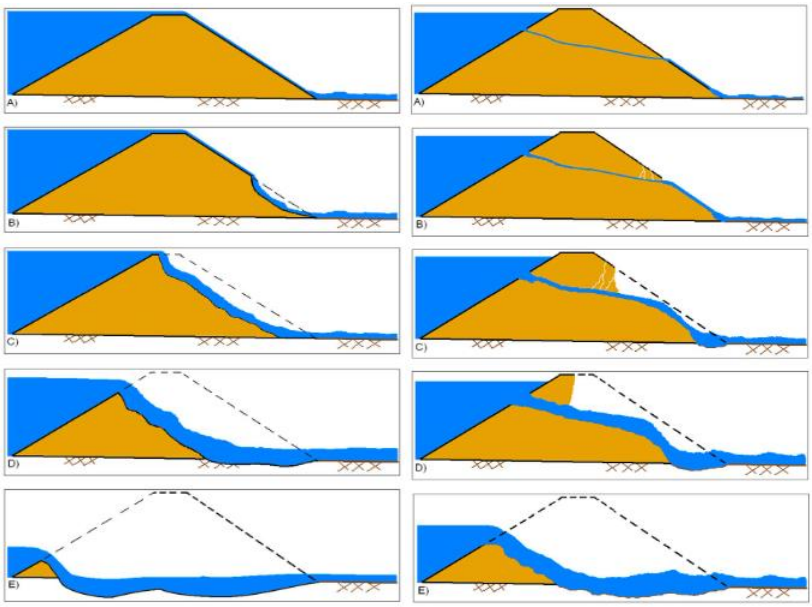

Figure 1. 2: Overtopping and piping schematic drawing by Brunner [5]

Table 1.1: List of major dam failures for overtopping and piping dam break type [9]

| Dam | Date | Country | Fatalities | Details |
|---|---|---|---|---|
| Hogs Back Dam | 1829-04-03 | Upper Canada | Un-known | Piping |
| Iruka Lake Dam | 1868 | Japan | 941 | Overtopping |
| Lower Otay Dam | 1916 | United States | 14 | Overtopping |
| Tigra Dam | 1917-08-19 | British India | 1 000 | Piping |
| Panshet Dam | 1961-07-12 | India | 1 000 | Piping |
| Vajont Dam | 1963-10-09 | Italy | 2 000 | Overtopping |
| Sempor Dam | 1967-11-29 | Indonesia | 138 | Overtopping |
| Teton Dam | 1976-06-05 | United States | 11 | Piping |
| Laurel Run Dam | 1977-07-19 | United States | 40 | Overtopping |
| Machchu-2 Dam | 1979-08-11 | India | 5 000 | Overtopping |
| Lawn Lake Dam | 1982-07-15 | United States | 3 | Piping |
| Val di Stava dam | 1985-07-19 | Italy | 268 | Piping |
| Belci dam failiure | 1991-07-29 | Romania | 25 | Overtopping |
| Virgen Dam | 1998 | Nicaragua | 0 | Overtopping |
| Zeyzoun Dam | 2002-06-04 | Syria | 22 | Overtopping |
| Glashütte dam | 2002-08-12 | Germany | 0 | Overtopping |
| Taum Sauk reservoir | 2005-12-14 | United States | 0 | Piping. |
| Niedow Dam | 2010-08-07 | Poland | 1 | Overtopping |
| Sanford Dam, Patricia Lake | 2018-09-15 | United States | 0 | Overtopping |
| Tiware Dam | 2019-07-02 | India | 23 | Overtopping and breached the dam. |

Table 1.1 shows the dams that have broken due to overtopping and piping from past to present [9]. Although it is impossible to prevent all possible dam breaks, it is possible to avoid the damage of breaks [9]. The design of each dam is unique and therefore the development of break differs from dam to dam, even for dams of the same type [11]. Therefore, making plans for the break of each dam that is built and preventing and predetermining dam breaks will ensure that people living downstream of the dam are evacuated in a shorter time and prevent possible loss of life. Thereupon, various scientific studies have been carried out in the literature to prevent or reduce the effects of disasters that may occur as a result of dam breaks. Various experimental and modeling studies have been conducted to predict the flood that will occur as a result of a dam break [12].

Shock wave occurs because the flood wave reaches its peak flow value in a very short time as a result of a dam break. Due to this shock wave, large amounts of debris, solids, and sediment are transported, causing scour and accumulating sediment in the upstream areas of the dam. As a result, significant morphological changes may occur downstream of the dam. In the literature, there are modeling and experimental studies on this and many other dam breaks, and flood waves. In this study, the break of an earth-fill dam is experimentally investigated. The aim of this study is to examine the propagation of sediment to the downstream due to the dam break of an earth-fill dam as a result of overtopping and piping with two different break mechanisms. Experiments were carried out for the smooth and the rough condition in the downstream region. In summary, a total of 8 experiments were carried out under 2 different break mechanisms, 2 different roughness conditions, and 2 repetitions. During the break, the levels of the water were measured with the help of the ULS 40-D device and metal rulers attached to the channel, and after the experiment, the sediment heights and propagation downstream of the dam were examined.

## 1.1 Scope

In the first part of this thesis, dams and dams breaks is explained by making a short introduction, the importance of the subject and the purpose of the study are explained.

In Chapter 2, experimental and numerical studies on dam breaks are summarized.

In Chapter 3, the experimental set-up, the devices used in the experiments, and the experimental procedure are explained in detail.

In Chapter 4, the experimental results and the interpretation of the experimental findings are given and the results are discussed.

In Chapter 5, conclusions are drawn, and suggestions for future work are made.

In the References section, all the references cited during the formation process of the current study are included.

# Chapter 2

# Literature Review

In Chapter 2, numerical and physical studies in the literature on the break of earth-fill dams are mentioned.

In the study published by Güngör [14], the piping problem in earth-fill dams was numerically solved using the finite element model. As a result of this study, it was aimed to precisely find the velocity and potential value of the seepage flow in the dam body.

Zorluer [13] published a study describing dam breaks with piping in earth-fill dams and designed an internal drainage system that can prevent the earth-fill dam from collapsing by piping. This internal drainage system is formed by laying thin and thick filter materials in layers on the body at the downstream surface of the dam.

Foster et al. [15] presented the results of statistical analysis on earth-fill dam accidents in their work. Accordingly, piping breaks affect earth-fill dams more than other types of dams. In addition, it has been stated that the presence of rock fill downstream of the dam is less likely to be destroyed by piping, and it has been stated that the probability of piping occurring on soils affected by glaciation is high. Finally, it was explained that excessive piping occurred in the first reservoir filling of the dam and approximately 66.7% of each piping break occurred in the first 5 years of the dam.

Tingsanchali and Chinnarasri [16] conducted overtopping experiments on a homogeneous dam body in a channel and modeled in a one-dimensional form.

Capart et al. [17] studied the hydrodynamic and geomorphic behavior of the dam-breaking flow. The changes in the base morphology of the dam breaks in real life in the literature were examined, and laboratory experiments and modeling studies were

carried out to determine the similarities between them and they found some qualitative similarities in the debris flows. However, it was stated that the characteristics of the land in the downstream region were effective in the changes in the base topography (in the accumulation and scour zones).

Fell et al. **Error! Reference source not found.** presented an estimated method for determining the time it takes for internal erosion and piping to occur that can cause breaks in fill dams and foundations. In addition to determining this period, the initiation, progression, and detection of internal erosion or piping are explained. As a result of the study, it was concluded that the risk of piping is high in earth-fill dams and it occurs in a short time, and continuous leakage should be observed.

Bozkus [7] conducted numerical breaks analyses of the break of the Kestel fill dam in Turkey with its overtopping and found out when the peak elevations and flood flows occurred in 6 sections determined in the downstream of the dam. According to the results of the analysis, he explained that the areas in danger were the areas close to the dam, and stated the importance of creating an emergency action plan and what needs to be done.

Hanson et al. [18] performed 7 different experiments with and without cohesion in order to better understand the process of break of the dam by overtopping and to provide data for numerical modeling to be made, and the movement of overtopping and breach erosion was observed. It has been determined that the most important effect on the development of breach erosion is the properties of the soil material.

Wu and Wang [19] examined the bed forms formed as a result of a dam break due to the flood wave.

Alcrudo and Mulet [20] carried out numerical modeling of the breaks of the Tous Dam in Spain on October 20, 1922. The aim of this study is to obtain the flood wave propagation, its downstream effects, and results in real-life dam failure in numerical modeling.

Zhang et al. [23] compiled the details of common dam failures occurring around the world and aimed to provide a better understanding of the causes and potential risks of failure by conducting a statistical study on earth-fill dams since 66% of these failures

occurred in earth- dams. Among the 593 earth-fill dams that have been demolished worldwide, 89.8% of the filling materials are unknown and the most destroyed 6.4% of them are homogeneous earth-fill dams. 36.4% of the embankment dams were destroyed due to overtopping, 42.5% due to piping reasons, 1.3% due to faulty operation, 3% due to natural disasters, 5.2% due to other reasons, and 11.6% of them were not known due to the reasons for the break.

Carrivick [24] investigated the effect of the water level downstream of the dam on the development of the breach and the hydraulic changes of the flow, the effect of bed roughness on the flow and suspended sediment transport. It has been stated that suspended sediment transport causes energy loss and does not exhibit a mountainous change downstream of the dam with the effect of bed roughness. It has been stated that the propagation of the flood wave depends on the Froude number depending on the reservoir height of the dam, the slowdown of the flow is associated with the decrease of the Froude number over time, and other effective forces are examined in detail.

Kocaman and Güzel **Error! Reference source not found.** investigated the propagation of the flood wave downstream as a result of a dam break, based on experimental and mathematical studies, in 3D. Experimental results and finite volumes method and the modeling they obtained in Flow-3D showed very high similarities in propagation velocity and geometry.

Wu et al. [25] examined the studies on homogeneous earth-fill dams, especially on overtopping and piping, and made evaluations to improve and develop the studies in the literature. According to Wu, the biggest deficiency in the current studies is to determine the erosion rate in the development of the breach, the sediment carried by the flood wave. To address this deficiency, it is to improve modeling studies with large-scale experiments and field studies.

Zhang et al. [26] carried out overtopping dam break experiments on a homogeneous dam body from the laboratory channel. In study; homogeneous earth-fill dam by overtopping dam break experiments were studied in one-dimensional and modeled in one-dimensional.

Hsu et al. [27] examined the transport of sediment carried by the flood wave by numerical modeling method and compared the flood wave formed as a result of the

break of the dam by taking snapshots from the experiments carried out to verify the method. Compared to the experimental results, the water level spreading downstream of the dam is higher beyond the downstream, as a result of which the flood wave propagation downstream of the dam is in two different regimes.

Güney et al. [28] constructed a distorted model of the Ürkmez dam in Turkey and conducted dam break experiments to examine the flood wave resulting from the dam break. During the dam break, the depths of the flood wave were measured at 8 different points, and the velocity at 4 different points with experimental devices. Downstream of the dam, it has been observed that the flow velocities in the sparsely populated areas are high and the flow rates are low in the dense areas, but the flow depths are high due to the low flow rates in the dense areas.

Okeke and Wang [30] conducted experiments on the sloped channel bottom to evaluate the piping mechanism in the dam body. As a result, they observed that there are 5 main stages of piping. These are, respectively, “piping formation, development, fee settlement, hydraulic fracturing, and slow demolition”.

Msadala **Error! Reference source not found.** has developed an equation that can be used to determine the sediment carried by the break of the homogeneous earth-fill dam. For this purpose, 87 laboratory experiments were performed using 3 different channel base slopes and 3 different sediments. It has been stated that the empirical equation developed based on the experimental results is compatible with some sediment transport equations in the literature.

Haltas et al. [19] created flood maps in a GIS environment for the town of Ürkmez as a result of the break of the Ürkmez Dam. Haltaş et al. [31] carried out a similar scenario to generate flood maps of the downstream areas of the Porsuk Dam in Eskişehir and the Alibey Dam in Istanbul.

Elci et al. [34] analyzed the spread of the flood wave in the downstream region as a result of the break of the Porsuk and Alibey dams, which are close to the settlements in Turkey. In the analysis performed by HEC-RAS and FLO-2D, the maximum flow depths and velocities that may occur as a result of the breaks of the dams at their downstream were determined, and the occurrence times of the flood wave were given in detail for both dam break scenarios.

Zhong et al. **Error! Reference source not found.** presented physically-based modeling to calculate the breaking process of core dams. They validated their results in the modeling using the data obtained from the break of the Banqiao dam. They also studied ten dam breaks including the Banqiao dam. It was stated that the analysis results of the proposed modeling were more detailed than the parametric model.

Chen et al. [35] developed a new numerical model based on model tests of piping cracks in earth-fill dams. The authors stated that the most important feature of their study that distinguishes it from other modeling studies is that the cross-section of the pipe channel is different from the others. It is stated that the new numerical model developed gives better results than the NWS BREACH model and the first location where the piping flow occurs has a significant effect on the estimation of the discharge.

Khosravi et al. [37] conducted an experimental study in order to find the differences in the change in the bottom morphology of the river bed downstream of the dam as a result of a dam break, in the case of uniform and non-uniform base material downstream of the dam. As a result, the fine-grained substrates of the non-uniform substrate were more stable, while the coarse-grained substrates exhibited more erosive behavior. In other words, it can be said that the sediment transport at the non-uniform base is high. In the experimental conditions where the water level in the reservoir is high, it was observed that the thin base materials were transported more in the non-uniform base, and the base material became coarser.

Azeez et al. **Error! Reference source not found.** break analysis of Um Al-Khair Dam was carried out in 2D using the flood simulation HEC-RAS program.

Urzica et al. **Error! Reference source not found.** to test the flood control capacity of the Baseu multiple reservoir system in Romania, the way the piping was breached was considered in the Cal Alb dam break scenario.

# Chapter 3

# Experimental Set-up and Procedure

This experimental study was carried out in a concrete channel 18 m long, 2 m wide and 0.88 m deep in the Hydraulics Laboratory of İzmir Kâtip Celebi University (Figure 3.1a). Water is supplied to the channel from the reservoir located on the lower floor of the laboratory with the circulation system. From the main reservoir to the channel with a volume of 24 $m^3$, water reaches the channel with the help of pumps through pipes (Figure 3.1b) and returns to the main reservoir through the cover at the end of the channel.

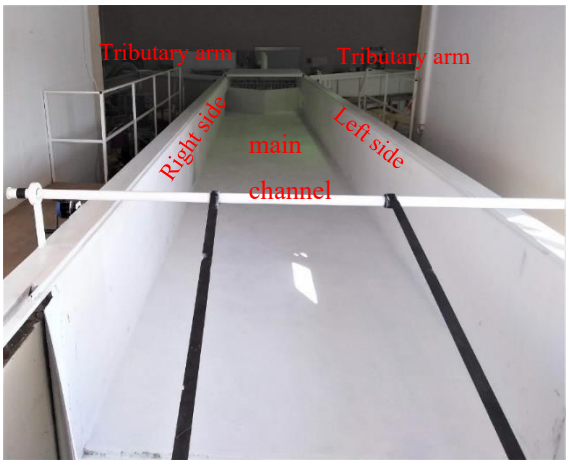


(a)


(b)

Figure 3. 1: Channel

The plan and side view of the channel are presented in Figure 3.2. The 1 m wide right (4.93 m) and left (4.92 m) tributary arms, connected at a 45° angle symmetrically to the sides of the main channel, were used to increase the water volume of the dam in the reservoir. The dam body was constructed between x = 0 m and x = 2.02 m of the main channel, 2 m wide, 2.02 m long, and 0.6 m high, as seen in Figure 3.2.

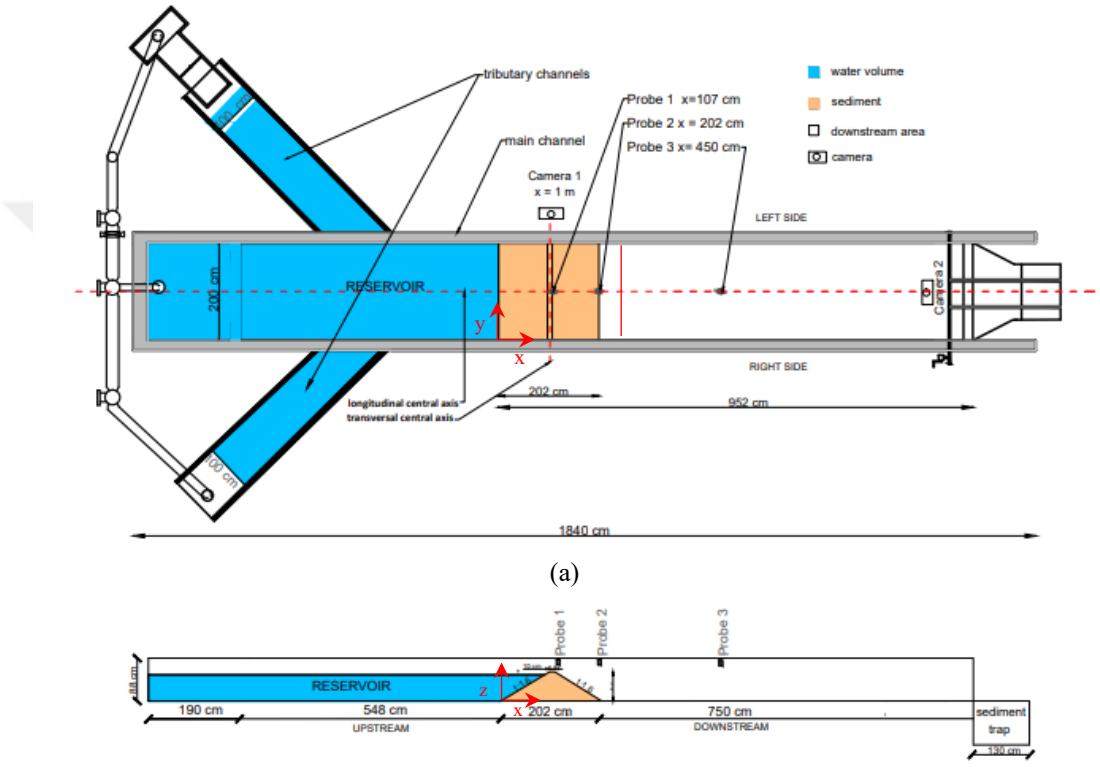


(a)




(b)

Figure 3. 2: Experimental setup; plan (a) and side (b) view

The experiments were carried out in 2 different downstream conditions, smooth and rough. 10×10×10 cm concrete cubes were used as the roughness element to represent the settlements. The cubes are spaced equally between 3.47 m – 5.07 m of the channel in 5 rows as shown in Figure 3.3.

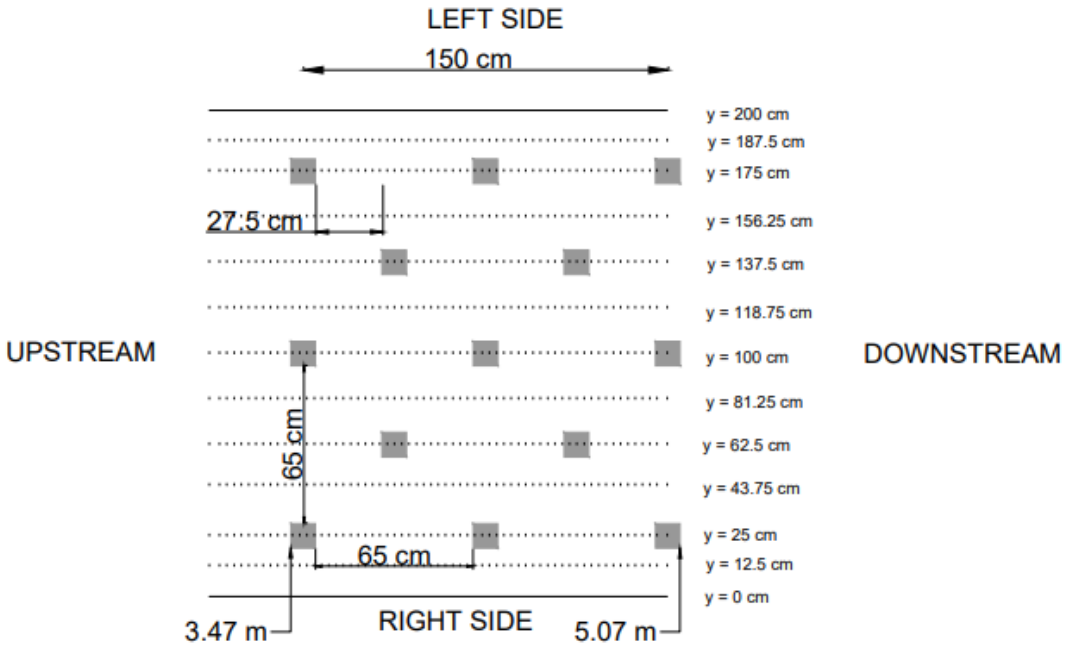


Figure 3. 3: Schematic representation of roughness elements

The homogeneous earth-fill dam body was constructed as six layers (Figure 3.4). The first layer is 2 m wide and 2.02 m long. The dam body was constructed with a crest width of 10 cm by changing the floor length of each layer. The upstream and downstream slopes of the dam were constructed to be 32˚ (1:1.6) with a spirit level.

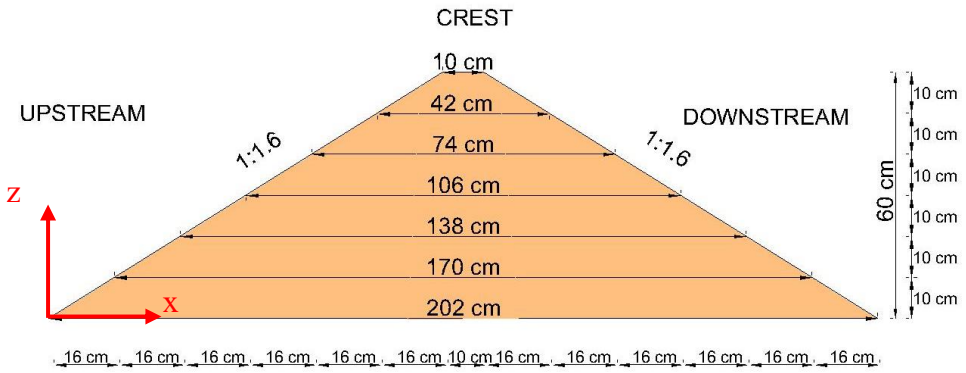


Figure 3. 4: Dam body x-section

While constructing the homogeneous dam body, approximately 1363 kg of sediment with a grain diameter ($d_{50}$) of 0.441 mm was used for each dam. The grain diameter distribution graph is shown in Figure 3.5.

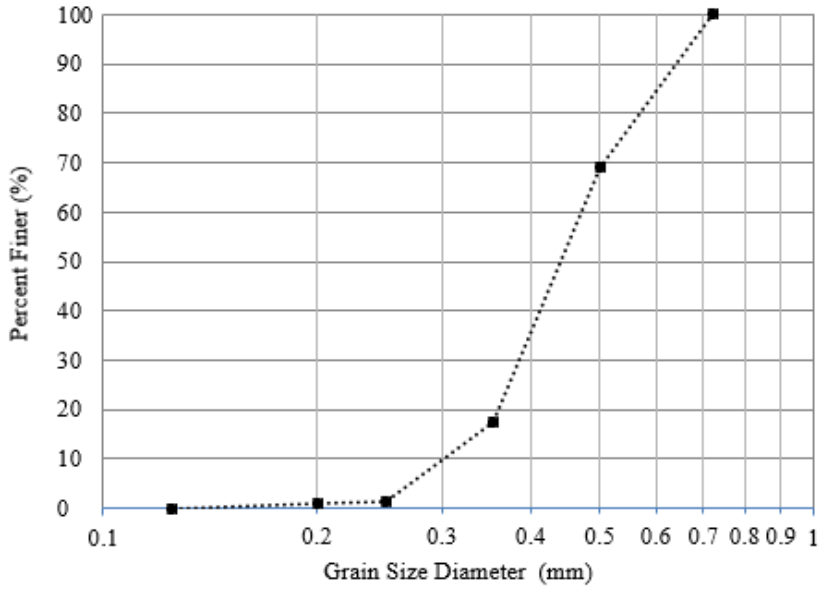


Figure 3. 5: Sediment grain size distrubition

While constructing the dam, standard compression methods were used (ASTM-D1557). Accordingly, the dam body was laid in 10 cm thick layers, and an iron weight of 4.5 kg was dropped 10 times from a height of 46 cm and compressed. (Figure 3.6). In order to compress the dam, the iron weight was dropped on the 40 cm × 40 cm plate and used when compressing the 1$^{st}$ floor from the 5$^{th}$ floor, while the 20 cm × 20 cm plate was used when compressing the 6$^{th}$ floor.

The construction of the dam body was built according to the layer widths given in Figure 3.4 and the construction phase of laying and compaction from the 1$^{st}$ to the 6$^{th}$ floor is shown in Figure 3.7. While the dam body was being constructed, the bricks for the first floor were placed 2 m wide and 2.02 m long as in Figure 3.7a, and laid flat in the sediment. The iron weight was dropped 10 times on a 40 cm × 40 cm plate and this process was repeated at 25 points for the 1$^{st}$ floor, and the sediment compression process was completed by making a total of 250 hits. The same procedure was

performed on the 2nd floor, 3rd floor, 4th floor, and 5th floor. While the 6th floor was being built, the iron weight was dropped on a 20 cm × 20 cm plate 10 times from a height of 46 cm, and the compression process was completed.

Figure 3. 6: Compaction materials; iron weight and plate

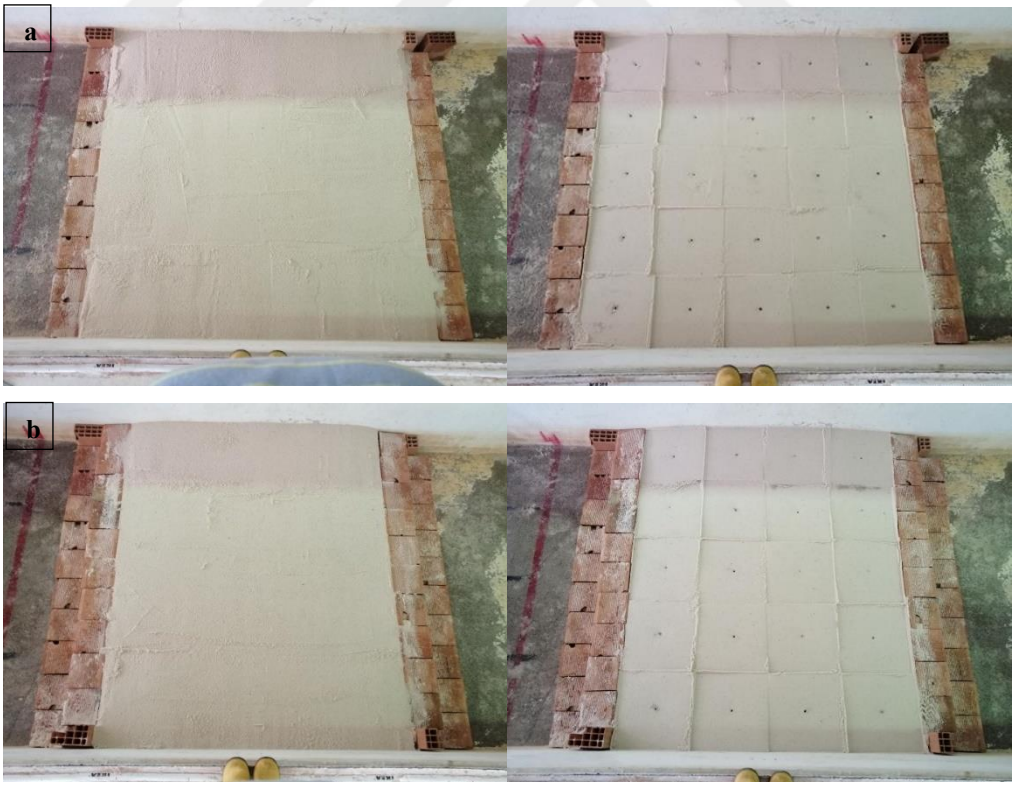

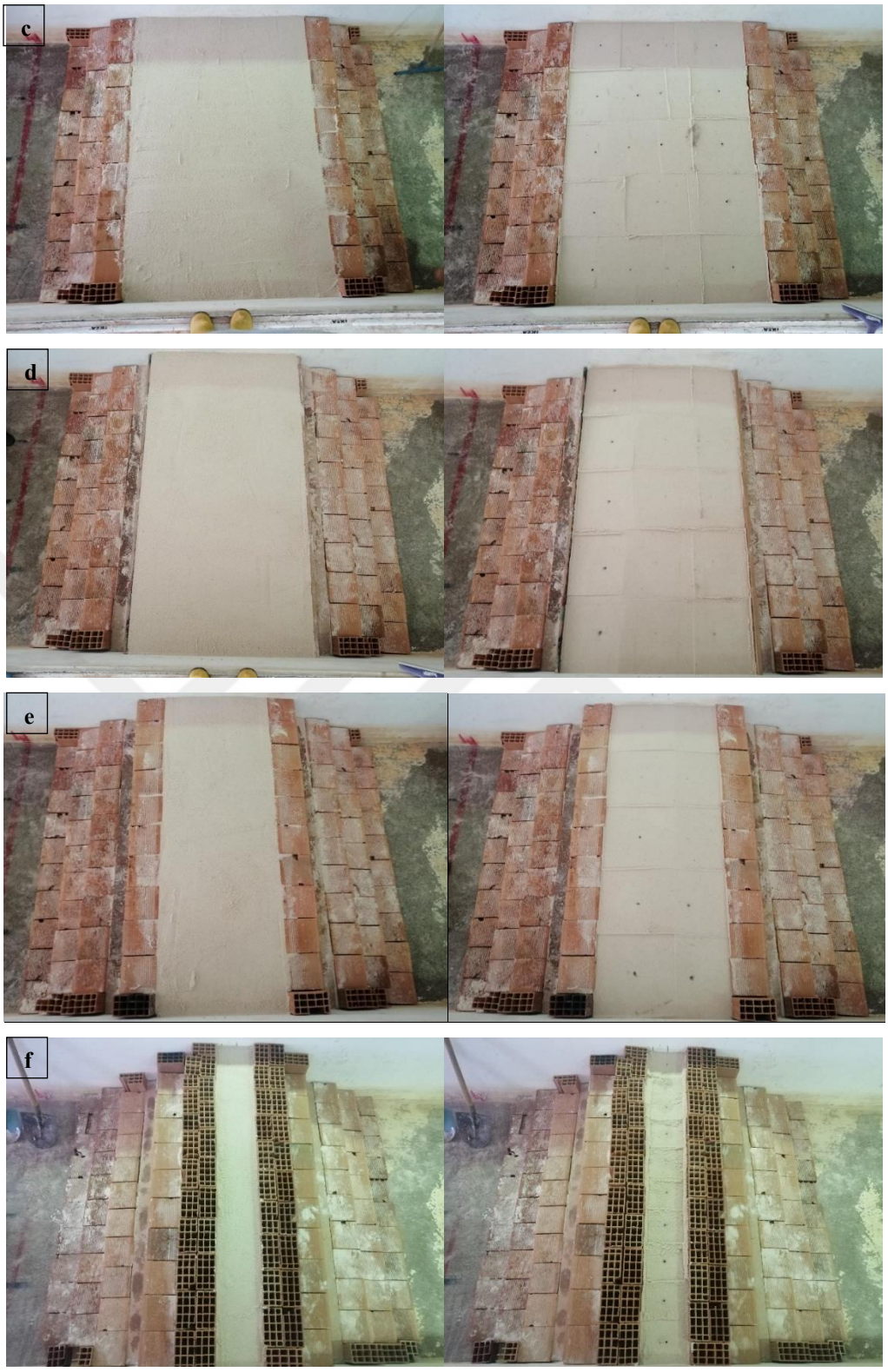


Figure 3. 7: Construction steps of the dam body uncompressed (right side) and compressed (left side) a) 1st floor, b) 2nd floor, c) 3rd floor, d) 4th floor, e) 5th floor, f) 6th floor

After the compression process is completed, the bricks in the upstream and downstream directions of the dam were removed and the construction of the dam body was completed with the help of a digital protractor so that the downstream and upstream slope of the dam was 32 °. (Figure 3.8)

Figure 3. 8: Arrange downstream and upstream slope of dam

For the overtopping experiments, a triangular breach of about 5 cm depth and 10 cm width was open to trigger the dam body to break right in the middle. The dam body whose construction has been completed for the overtopping and piping experiments are given in Figure 3.9.

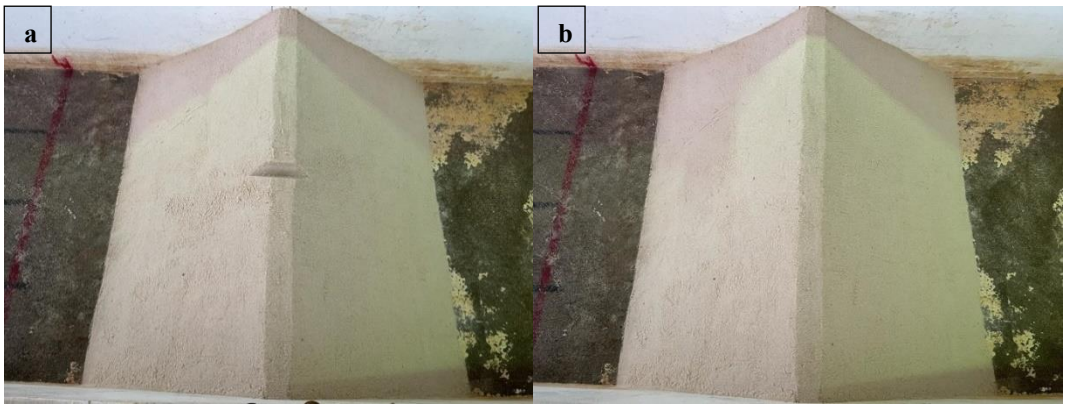


Figure 3. 9: Final state of the dam body for a) overtopping and b) piping experiments

During the experiments, the water level was measured at 4 points with metal rulers attached to the left of the channel. Ruler 0 ($R_0$) x = - 0.5 m, ruler 1 ($R_1$) x = 4.5 m, ruler 2 ($R_2$) x = 6 m, and ruler 3 ($R_3$) x =7.5 m are positioned such that 1 of them is downstream of the dam and the other 3 are upstream of the dam. (Figure. 3.10). In addition, using the ULS-40D (Ultralab Level System) device, time-dependent precise level measurement was made with the sensors of the device at 3 different points of the channel longitudinal central axis during the experiment. One of these sensors is x = 1.07 m of the Probe 1 channel. It is 5 cm below the crest level in the downstream direction. Probe 2 is x = 2.02 m, at the end of the downstream skirt of the dam body, and at Probe 3 x = 4.5 m. With the help of these sensors, 100 data per second is obtained and depth changes are made with precise measurements. In addition, the most important feature of the device is that it can work outside the current and measure distance without disturbing the current.

Figure 3. 10: ULS40-D device and probe

During the experiment, two cameras were placed on the channel in order to observe the propagation sediments of the dam body. Camera 1 is placed at x = 1 m transversal central axis, in a position to show the change in the dam body exactly. The camera 2 is placed at the end of the channels at x = 9.5 m along to longitudinal central axis so that it can see the downstream of the dam (Figure 3.11, Figure 3.12).

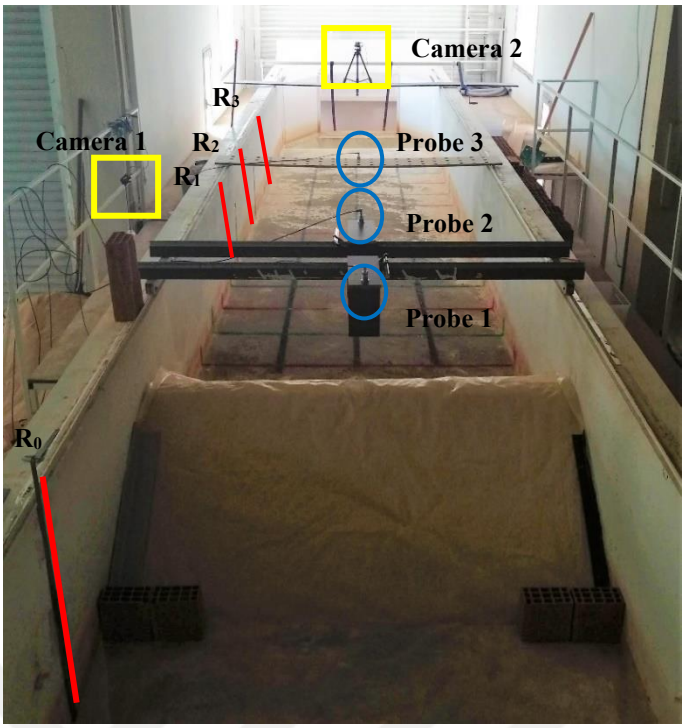


Figure 3. 11: The final form of the dam body and measurement devices (cameras, ULS probes, rulers) for smooth downstream conditions

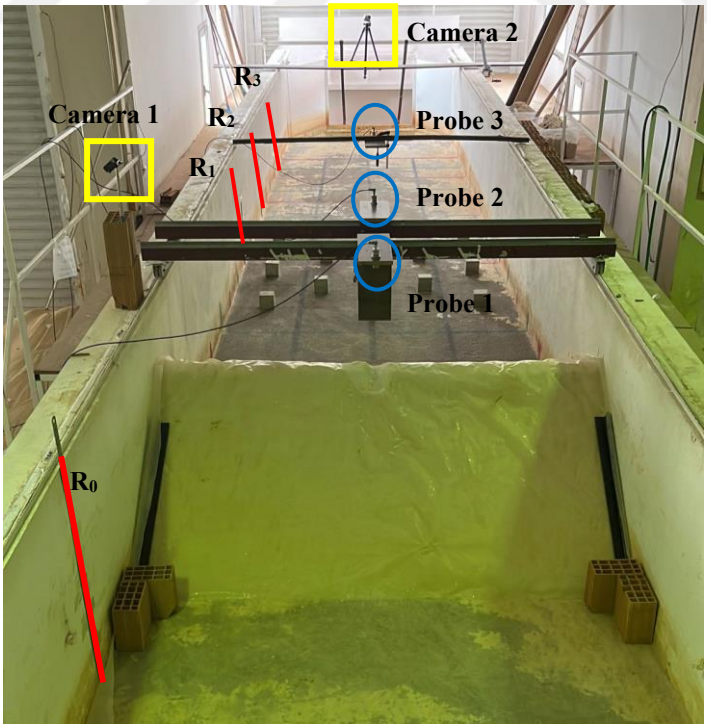


Figure 3. 12: The final form of the dam body and measurement devices (cameras, ULS probes, rulers) for rough downstream conditions

Also colored lines were drawn at 50 cm intervals downstream of the dam to determine the rate of progression of the sediment and water mixture along the channel.

In the dam break overtopping scenario, the dam' reservoirs water level was increased until the water exceeds the breach. After the water had passed through the breach, the experiment started and the measurements were taken. In the piping test, after the water reached a certain level in the reservoir of the dam, the pump was turned off and the test period was started. The filling times, water levels, and volumes of the reservoir are presented in Table 3.1.

Table 3. 1: Dam resevoirs information before dam break

| | | Filling time (min:s) | Water Level (cm) | Volume ($m^3$) |
|---|---|---|---|---|
| Overtopping | OS1 | 11:29 | 57 | 12.53 |
| Smooth (OS) | OS2 | 23:30 | 53.5 | 11.75 |
| Overtopping | OR1 | 13:04 | 58 | 12.76 |
| Rough (OR) | OR2 | 12:18 | 55 | 12.09 |
| Piping | PS1 | 09:19 | 53 | 11.64 |
| Smooth (PS) | PS2 | 12:37 | 51 | 11.19 |
| Piping | PR1 | 13:10 | 53.8 | 11.82 |
| Rough (PR) | PR2 | 12:33 | 53 | 11.64 |

Measurements were carried out at the end of the experiment in order to determine the regional distribution of the height of the sediment to be propagated to the downstream region after the dam break, and the sediment height profile was obtained after the break. In this measurement, the channel length was accepted as the x-axis, the channel width as the y-axis, and the sediment height as the z-axis. Sediment height measurement was made at 10 cm intervals on the x and y axes. Sediment depth

measurements were taken with the sensor of the ULS40-D device and by transferring these measurements to the SURFER digital program, a bathymetry map and contour graph were created.

In summary, a total of 8 experiments were performed under 2 different break mechanisms (overtopping and piping), 2 different roughness (smooth and rough), and 2 repetition conditions.

# Chapter 4

# Experimental Results

In this chapter, the results for each experimental scenario are presented and the experiments are compared with each other. The first scenario is the overtopping experiment in the smooth downstream condition, the second scenario is the overtopping experiment in the rough downstream condition, the third scenario is the piping experiment in the smooth downstream condition, and the fourth scenario is the piping experiment in the rough downstream condition. Under four different scenario conditions, the experiments in the first and second scenarios were a dam break from the middle. The experiments in the third and fourth scenarios dam break from the right side. OS1 experiment in the first scenario, OR1 experiment in the second scenario, PS1 experiment in the third scenario, and PR1 experiment in the fourth scenario was presented. Other experiments are presented in the appendices.

## 4.1 Presentation of Results

When the results of the dam break experiments were examined, the experiment times of each experiment, the height of the reservoir, the start movement time of the sediment, and the change in the water level showed differences from each other. More than one calculation was made to determine the appropriate moment $t_0$ of the 8 experiments. These are respectively; the $t_0$ value was taken as the passage of water and sediment from a certain point in the channel (50 cm away from the end of the dam), the moment of stopping the water level in the reservoir (the moment of closing the pump), the moment when the first water level drops in $R_0$. However, the time $t_0$ determined for each experiment was not found suitable for both piping and

overtopping experiments to be compared with each other. ULS-40D measurements were not used in the $t_0$ calculations because not all experiments have ULS-40D measurements. Since the dam bodies break from the middle and the left wall, and the ULS-40D measurements were taken in the longitudinal axis, the obtained ULS-40D could not be used to determine the $t_0$ moment in the data. In the experiments, the maximum water level in the reservoir varied between 51 cm and 58 cm. It has been observed that the output hydrographs of the experiments show almost a similar decrease curve. Therefore, in order to compare the results of the overtopping and piping experiments with each other, the water levels taken with $R_0$ were determined at $t_0$ using the feature scaling / min-max normalization method.

Min-max normalization, one of the most widely used methods in data scaling, refers to the reduction of the data set so that the available data falls within the range of 0 to 1 [38]. The purpose of normalization is to bring the data to a common range, to ensure that they can be compared, and to eliminate large differences between the data. In the normalization process, all data were brought to the range of 0 - 1 by dividing each water level data by the maximum water level. The equation used for normalization is as in Equation 1. Here z refers to the level.

$$z' = \frac{z - \min(z)}{\max(z) - \min(z)} \tag{4.1}$$

After the normalization, it is seen that approximately the first 50 seconds of the output hydrographs of all experiments overlap as shown in Figure 4.1. Accordingly, the moment when the graphs started to overlap was accepted as the starting time (0 s) of all experiments, and 5 minutes before the found '0' moment is determined as the $t_0$ moment. In order to be able to evaluate and show the results of all experiments within each other, the same moment, $t_0$, was determined with each experiment. While comparing the experiments, the results such as the 'special moments' we observed during the experiment, the water coming to $R_1$, and the progress differences of $R_1$, $R_2$, and $R_3$ were evaluated for each experiment in itself.

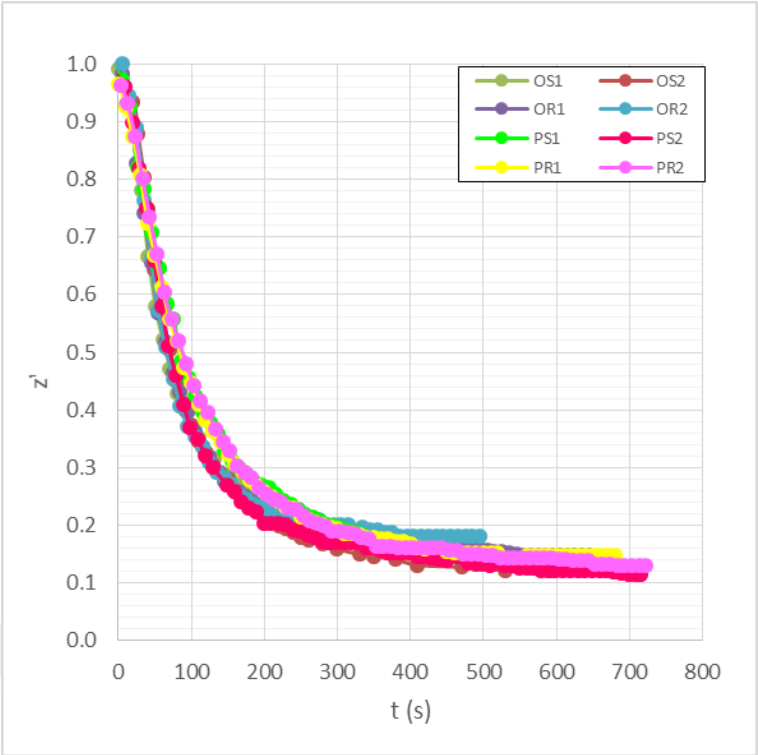


Figure 4.1: t = 0 s when the output hydrographs of all experiments are overlapped

## 4.2 First Scenario: Overtopping Dam Break Type, Smooth Downstream Condition

Simultaneous images of the OS1 experiment at camera 2 (left column) and camera 1 (right column) at 282 s, 307 s, 322 s, 342 s, 357 s, and 387 s are given in Figure 4.2. When t = 260 s, the water has passed over the breach. The propagation of water flow and sediment downstream of the dam after the water crosses the breach, and the widening of the breach in the dam body is presented in Figure 4.2. (a - f), respectively. The breach in the dam body expanded rapidly within 82 s (Figure 4.2 (a - d)) from the top. After 20 seconds, the sediment-water flow mixture propagated completely along the channel (Figure 4.2.b). As seen in Figure 4.2.d, it was observed that a hydraulic jump occurred at approximately 5 m in the longitudinal axis. This splash that occurred expanded towards the right and left walls of the channel, advanced towards the upstream (Figure 4.2.d), and disappeared (Figure 4.2.e). At the end of 387 seconds,

while there is no visible change in the sediment propagation, the water flow continues (Figure 4.2.f).

The time for the sediment and water mixture to reach the first red line (x = 2.5 m) after water pass from the breach is 22 s (Figure 4.2 a), from the red line to $R_1$ is 15 s, from $R_1$ to $R_2$ is 7 s, and from the $R_2$ to come to $R_3$ is 3 s.

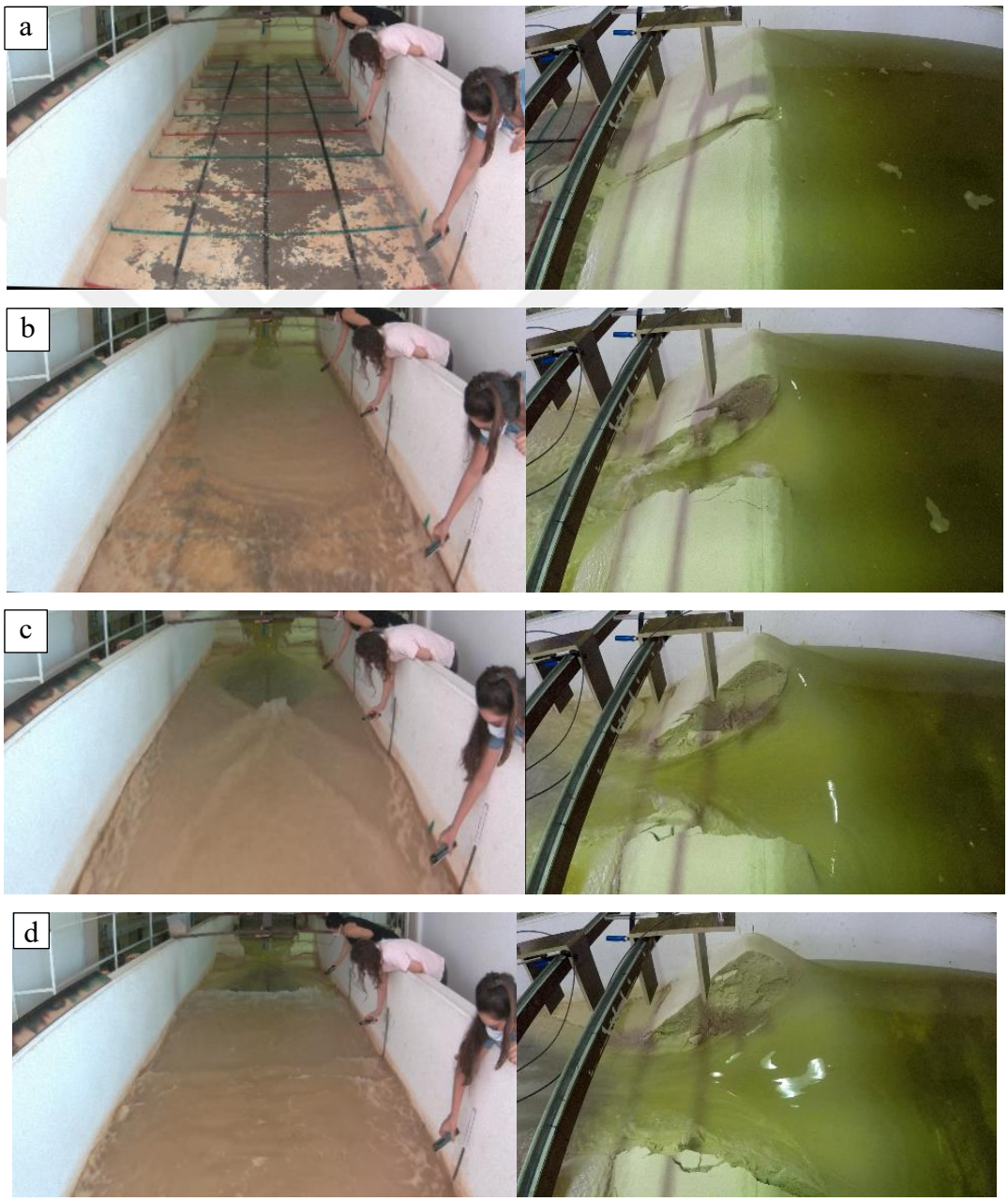


Figure 4.2 : Camera 2 (flow and sediment transport at downstream area) and Camera 1 (stages of breach formation) at a) 282 s, b) 307 s, c) 322 s, d) 342 s, e) 357 s, f) 387 s for experiment OS1

In Figure 4.3, a photograph of the sediment propagation that occurred after the dam break at the end of the OS1 experiment is presented. As seen in the figure, it is observed that the sediment height is shallower in the area closer to the longitudinal axis due to the high velocity water flow in the area approximately 4 m from the downstream skirt of the dam. It was observed that the height was higher near the walls on the right and left sides of the sediment channel and the sediment was propagated along the channel.

Figure 4.3: Sediment propagation of end the experiment OS1

At the end of the experiment, sediment height measurements taken at 10 cm intervals on the x and y axis, a two-dimensional contour map, and a three-dimensional bathymetry map obtained with Surfer software were created and presented in Figure 4.4. As shown in Figure 4.4, between 5 m and 6 m is the region with the highest sediment height. The sediment heights between 3.5 m and 8 m along the channel are higher on the right and left sides of the channel, and lower on the longitudinal axis. The body of the dam was mostly exposed to erosion between 50 cm and 150 cm.

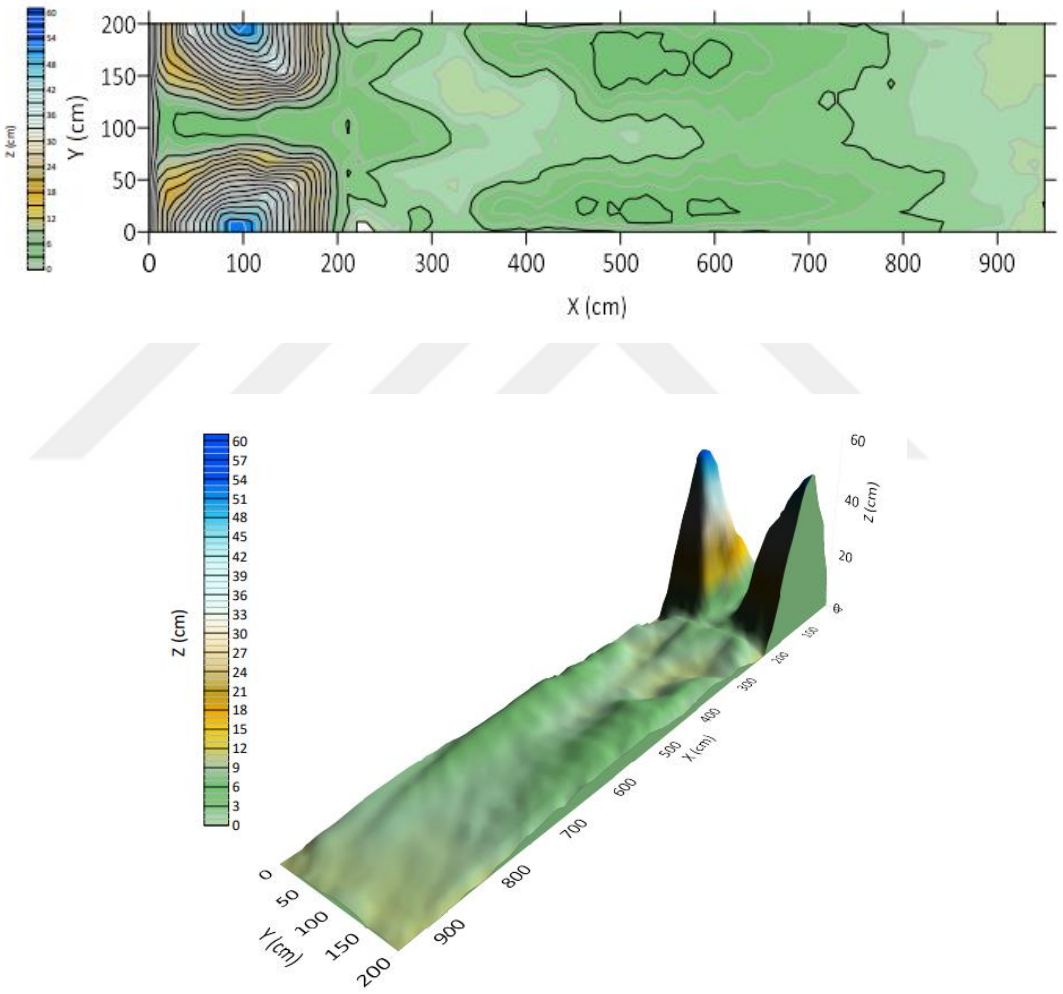


Figure 4.4: 2D and 3D contour maps of sediment distribution at the end of OS1

Symmetrical with respect to the longitudinal axis of experiment OS1, y = 0 cm and 200 cm, y = 12.5 cm and 187.5 cm, y = 25 cm and 125 cm, y = 43.75 cm and 156.25

cm, y = 62.5 cm and 137.5 cm, y= 81.25 cm and 118.75 cm, and y = 100 cm and x = 100 cm with longitudinal and traversal axes graphs of sediment heights are presented in Figure 4.5. Accordingly, in the cross-sections that are symmetrical to each other between y = 0 cm and y = 200 cm (y = 0 cm and 200 cm, y = 12.5 cm and 187.5 cm, y = 25 cm and 125 cm, y = 43.75 cm and 156.25 cm, y = 62.5 cm and 137.5 cm, y = 62.5 cm and 137.5 cm, y = 81.25 cm and 118.75 cm), the approximate sediment heights are almost similar.

y = 0 cm and y = 200 cm while the maximum sediment height in the dam body is 52.4 cm and 54.3 cm, respectively. The sediment height is 5.1 cm at x = 2.02 m, the maximum sediment height is 5.1 cm between x = 2 m and x = 4 m, and the maximum sediment height is between x = 4 m and x = 6 m is 3.8 cm at y = 12.5 cm and 4.9 cm at y = 187.5 cm, between x = 6 m and x = 8 m is 4.2 cm at y = 12.5 cm and 4.6 cm at y = 187.5 cm, between x = 8 m and x = 9.5 m is 3.5 cm at y = 12.5 cm and 1.1 cm at y = 187.5 cm.

y = 12.5 cm and y = 187.5 cm while the maximum sediment heigt in the dam body is 51 cm and 49.1 cm, respectively. The sediment height at x = 2.02 m is 5.4 cm at y = 12.5 cm and 5.1 cm at y = 187.5 cm. The maximum sediment height between x = 2 m and x = 4 m is 5.4 cm at y = 12.5 cm and 5.1 cm at y = 187.5 cm, between x = 4 m and x = 6 m is 6.5 cm at y = 12.5 cm and 4.9 cm at y = 187.5 cm, between x = 6 m and x = 8 m is 5.7 cm at y = 12.5 cm and 4.6 at y = 187.5 cm, between x = 8 m and x = 9.5 m is 3.1 cm at y = 12.5 cm and 1.1 cm at y = 187.5 cm.

y = 25 cm and y = 175 cm while the maximum sediment height in the dam body is 44.8 cm and 46.5 cm, respectively. The sediment height at x = 2.02 m is 5.9 cm at y = 25 cm and 6.5 cm at y = 175 cm. The maximum sediment height between x = 2 m and x = 4 m is 5.9 cm at y = 25 cm and 6.5 cm at y = 175 cm, between x = 4 m and x = 6 m is 6.8 cm at y = 25 cm and 6.8 cm at y = 175 cm, between x = 6 m and x = 8 m is 6.2 cm at y = 25 cm and y = 175 cm, between x = 8 m and x = 9.5 m is 3.2 cm at y = 25 cm and 2.5 cm at y = 175 cm.

y = 43.75 cm and y = 156.25 cm while the maximum sediment height in the dam body is 35.1 cm and 36.8 cm, respectively. The sediment height at x = 2.02 m is 5.9 cm at y = 43.75 cm and 5.6 cm at y = 156.25 cm. The maximum sediment height between

x = 2 m and x = 4 m is 5.9 cm at y = 43.75 cm and 5.6 cm at y = 156.25 cm, between x = 4 m and x = 6 m is 5.5 cm at y = 43.75 cm and 6.9 cm at y = 156.25 cm, between x = 6 m and x = 8 m is 5.7 cm at y = 43.75 cm and 6.1 cm at y = 156.25 cm, between x = 8 m and x = 9.5 m is 3.5 cm at y = 43.75 cm and 2.2 cm at y = 156.25 cm.

y = 62.5 cm and y = 137.5 cm while the maximum sediment height in the dam body is 22.7 cm and 22.3 cm, respectively. The sediment height at x = 2.02 m is 4.8 cm at y = 62.5 cm and 5.4 cm at y = 137.5 cm. The maximum sediment height between x = 2 m and x = 4 m is 4.8 cm at y = 62.5 cm and 5.4 cm at y = 137.5 cm, between x = 4 m and x = 6 m is 4.9 cm at y = 62.5 cm and 6.1 cm at y = 137.5 cm, between x = 6 m and x = 8 m is 4.5 cm at y = 62.5 cm and 5.2 cm at y = 137.5 cm, between x = 8 m and x = 9.5 m is 3 cm at y = 62.5 cm and 2.2 cm at y = 137.5 cm.

y = 81.25 cm and y = 118.75 cm while the maximum sediment height in the dam body is 10.8 cm and 10.2 cm, respectively. The sediment height at x = 2.02 m is 4.6 cm at y = 81.25 cm and 4.9 cm at y = 118.75 cm. The maximum sediment height between x = 2 m and x = 4 m is 4.8 cm at y = 81.25 cm and 5 cm at y = 118.75 cm, between x = 4 m and x = 6 m is 3.7 cm at y = 81.25 cm and 4.3 cm at y = 118.75 cm, between x = 6 m and x = 8 m is 4 cm at y = 81.25 cm and 4.2 cm at y = 118.75 cm, between x = 8 m and x = 9.5 m is 2.3 cm at y = 81.25 cm and 2.2 cm at y = 118.75 cm

y = 100 cm while the maximum sediment height in the dam body is 6.7 cm. The sediment height at x = 2.02 m is 4.1 cm. The maximum sediment height between x = 2 m and x = 4 m is 4.5 cm, between x = 4 m and x = 6 m is 3.7 cm, between x = 6 m and x = 8 m is 4.1 cm, between x = 8 m and x = 9.5 m is 2.2 cm. It is the section with the lowest sediment height at y=100 cm. The reason for this is that since the dam body break is in the middle, the fastest water flow occurred in this section, occurrence more sediments to be transported. It is possible to say that almost half of the dam body is exposed to erosion at x = 100 cm.

a

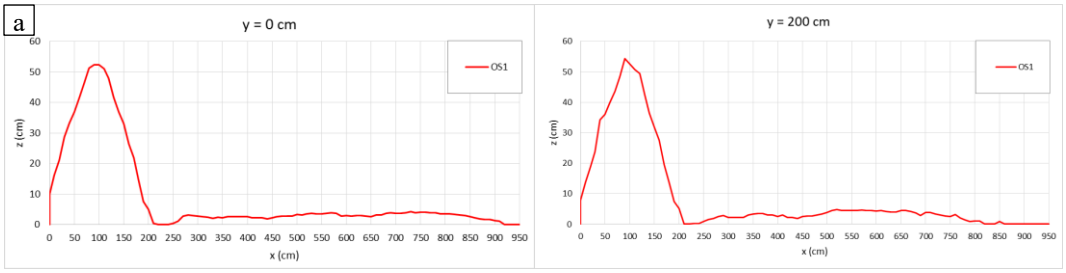
y = 0 cm
y = 200 cm
OS1
z (cm)
x (cm)

b

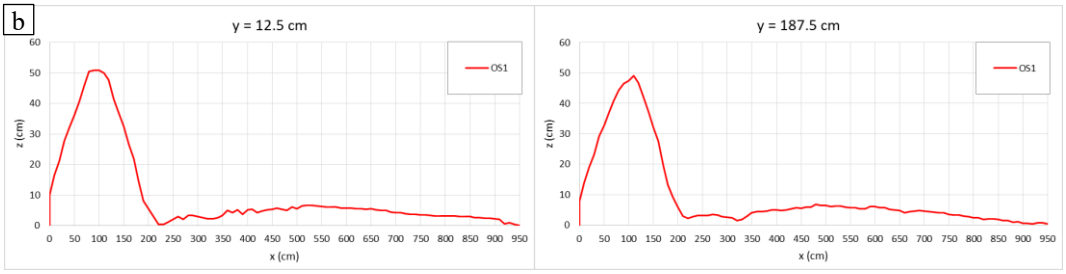
y = 12.5 cm
y = 187.5 cm
OS1
z (cm)
x (cm)

c

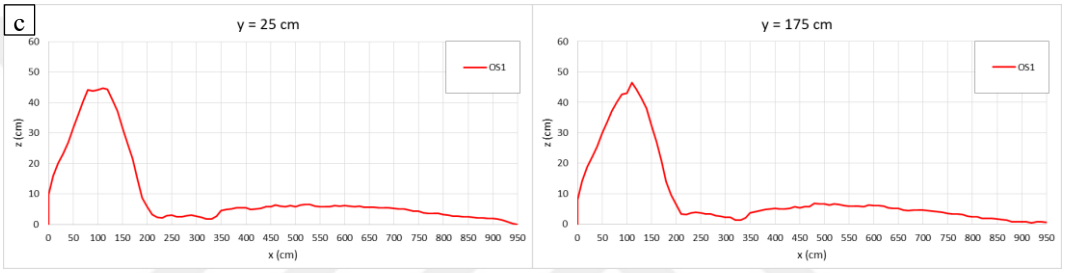
y = 25 cm
y = 175 cm
OS1
z (cm)
x (cm)

d

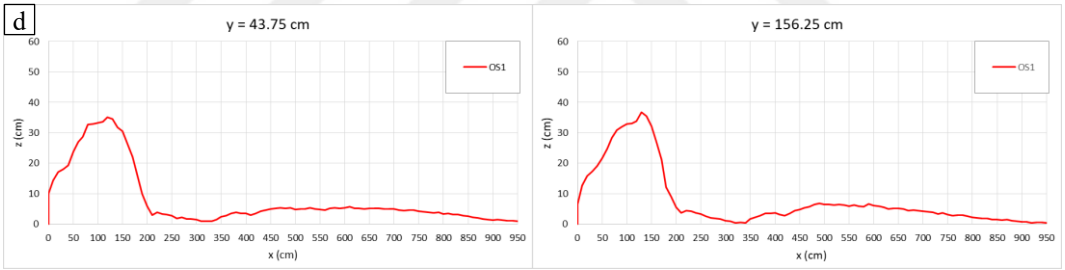
y = 43.75 cm
y = 156.25 cm
OS1
z (cm)
x (cm)

e

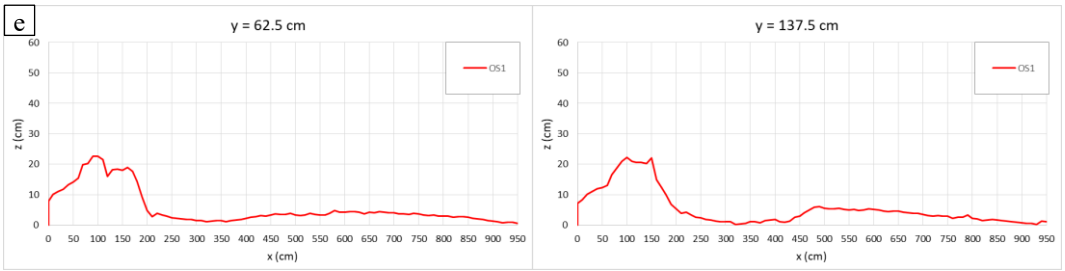
y = 62.5 cm
y = 137.5 cm
OS1
z (cm)
x (cm)

f

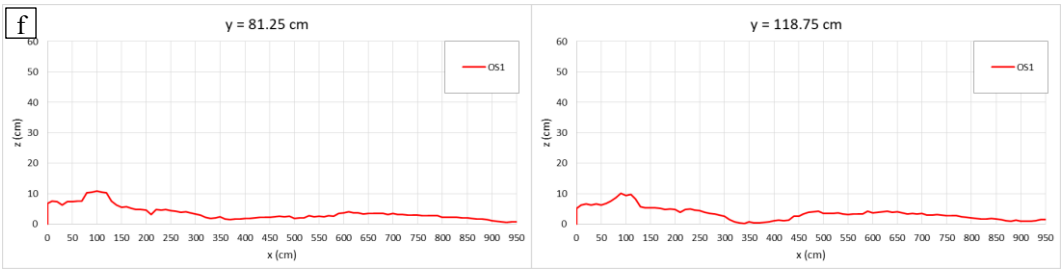
y = 81.25 cm
y = 118.75 cm
OS1
z (cm)
x (cm)

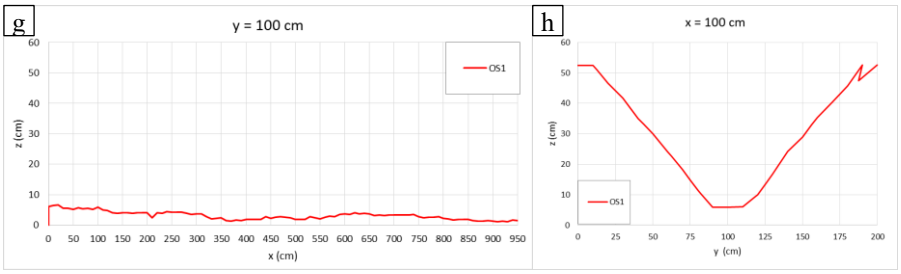


Figure 4.5: Longitudinal sediment height profiles measured at a) y = 0 cm and 200 cm, b) y = 12.5 cm and 187.5 cm, c)y = 25 cm and 125 cm, d) y = 43.75 cm and 156.25 cm, e)y = 62.5 cm and 137.5 cm, f) y= 81.25 cm and 118.75 cm, and g) y = 100 cm and along the channel width and, transversal crest section of the dam at h) x = 100 cm of OS1

Figure 4.6 a shows the levels measured by Probe 1, $R_0$ for OS1, Figure 4.6.b $R_1$, $R_2$, $R_3$, Probe 2 and Probe 3. Probe 1 shows the elevation change at the dam body (x = 1.07 m), and Probe 2 shows the elevation change at the end of the dam body (x = 2.02 m). Probe 3 and $R_1$ take measurements from the same section (x = 4.5 m) on the x-axis, but Probe 3 measures the level change on the longitudinal axis, on the left wall of the $R_1$ channel (y = 200 cm).

Accordingly, in Figure 4.6. a, it can be said that the decrease in the dam body (Probe 1) started to decrease later than the decrease in the water level, but the decrease in the level was faster. Probe 1 and $R_0$ reached the same level at 344. sec and the level decrease continued at the same rate for about 32 seconds. After 376 seconds, the level in Probe 1 decreased more than $R_0$. In Probe 1, the maximum level decreased from 55 cm to 5.5 cm. $R_0$ decreased from 57 cm to 8.3 cm. In Figure 4.6.b, the maximum water level is 343 s, 352 s, 17 cm, 12 cm, and 16 cm at 352 s at $R_1$, $R_2$, and $R_3$, respectively. The maximum water level at Probe 2 and Probe 3 is 8.7 cm and 18.1 cm at 367 s and 395 s, respectively.

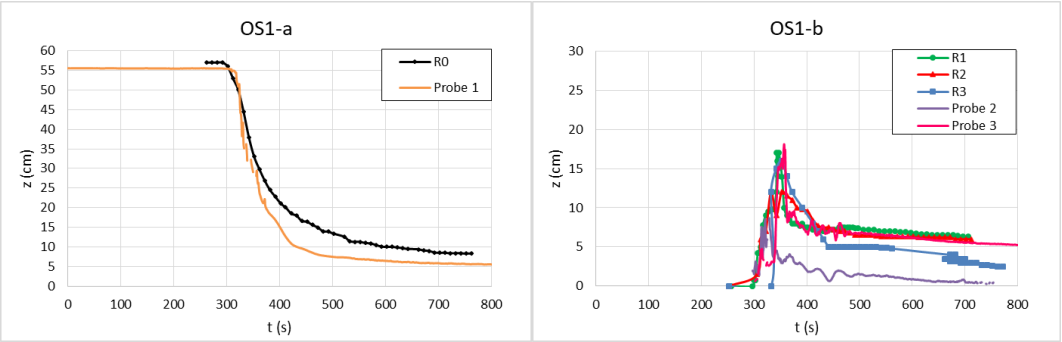


Figure 4.6: Level measurements for OS1 experiment a) measured from $R_0$ and Probe 1, b) measured from $R_1$, $R_2$, $R_3$, Probe 2 and Probe 3

### 4.2.1 Repeatability of First Scenario Experiments

The first break scenario was performed in 2 repetitions under the same condition. In Figure 4.7, for experiments OS1 and OS2 sediment height graphs y = 0 cm and 200 cm, y = 12.5 cm and 187.5 cm, y = 25 cm and 125 cm, y = 43.75 cm and 156.25 cm, y = 62.5 cm, 137.5 cm, y= 81.25 cm and 118.75 cm, y = 100 cm and x = 100 cm are given. Accordingly, it is seen that the sediment section graphs of the experiments carried out in the smooth downstream condition are compatible with each other and the sediment distributions are almost the same.

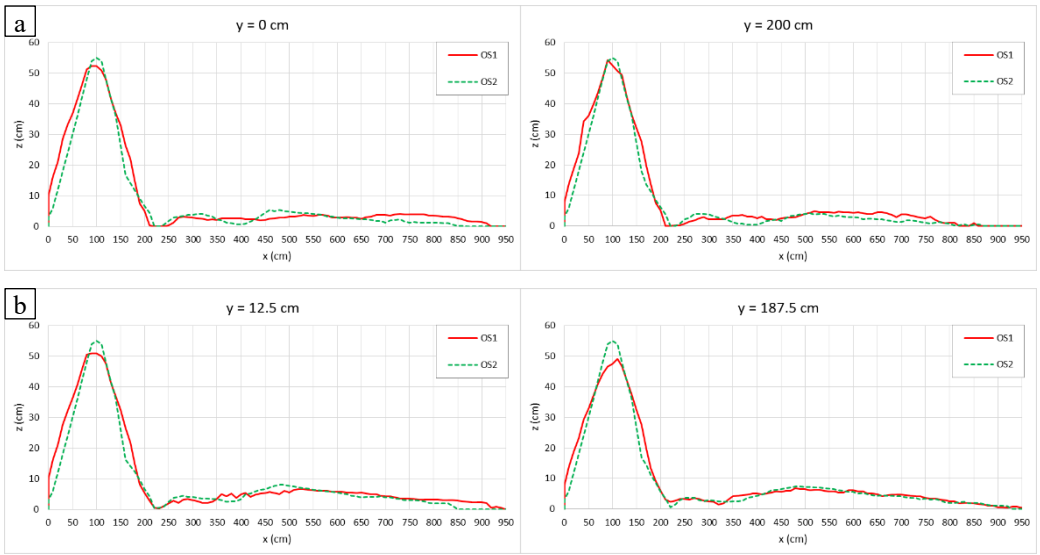

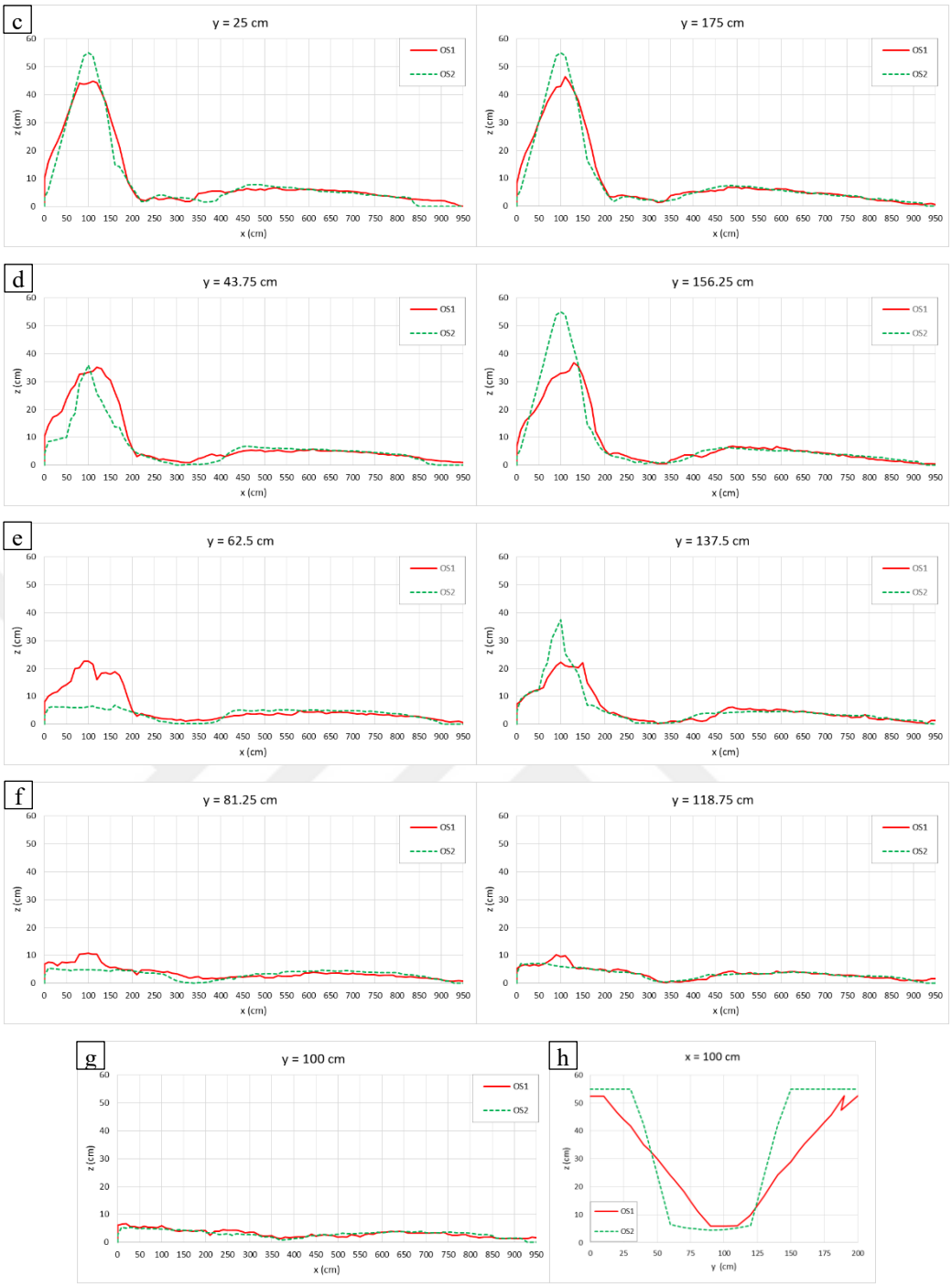


Figure 4.7: Longitudinal sediment height profiles measured at a) y = 0 cm and 200 cm, b) y = 12.5 cm and 187.5 cm, c)y = 25 cm and 125 cm, d) y = 43.75 cm and 156.25 cm, e)y = 62.5 cm and 137.5 cm, f) y= 81.25 cm and 118.75 cm, and g) y = 100 cm and along the channel width and, transversal crest section of the dam at h) x = 100 cm of OS1 and OS2

For the OS2 experiment, the time for, the sediment and water mixture to reach the first red line after water pass from the breach is 86 s, from the red line to $R_1$ is 22 s, from $R_1$ to $R_2$ is 3 s, and from the $R_2$ to come to $R_3$ is 3 s. In the OS2 experiment, the time for the sediment to come to the red line after water pass from the breach is 64 s, the time to reach $R_1$ from the red line is 7 s longer then OS1, and the time from $R_1$ to $R_2$ is 4 s shorter then OS1 experiment. Figure 4.8 shows the graph of the measurements of $R_0$, $R_1$, $R_2$, $R_3$, Probe 1, Probe 2 and Probe 3 measurements of experiment OS1 and $R_0$ and $R_3$ of experiment OS2. Accordingly, it is seen that the ruler and probe measurements are compatible with each other in the experiments.

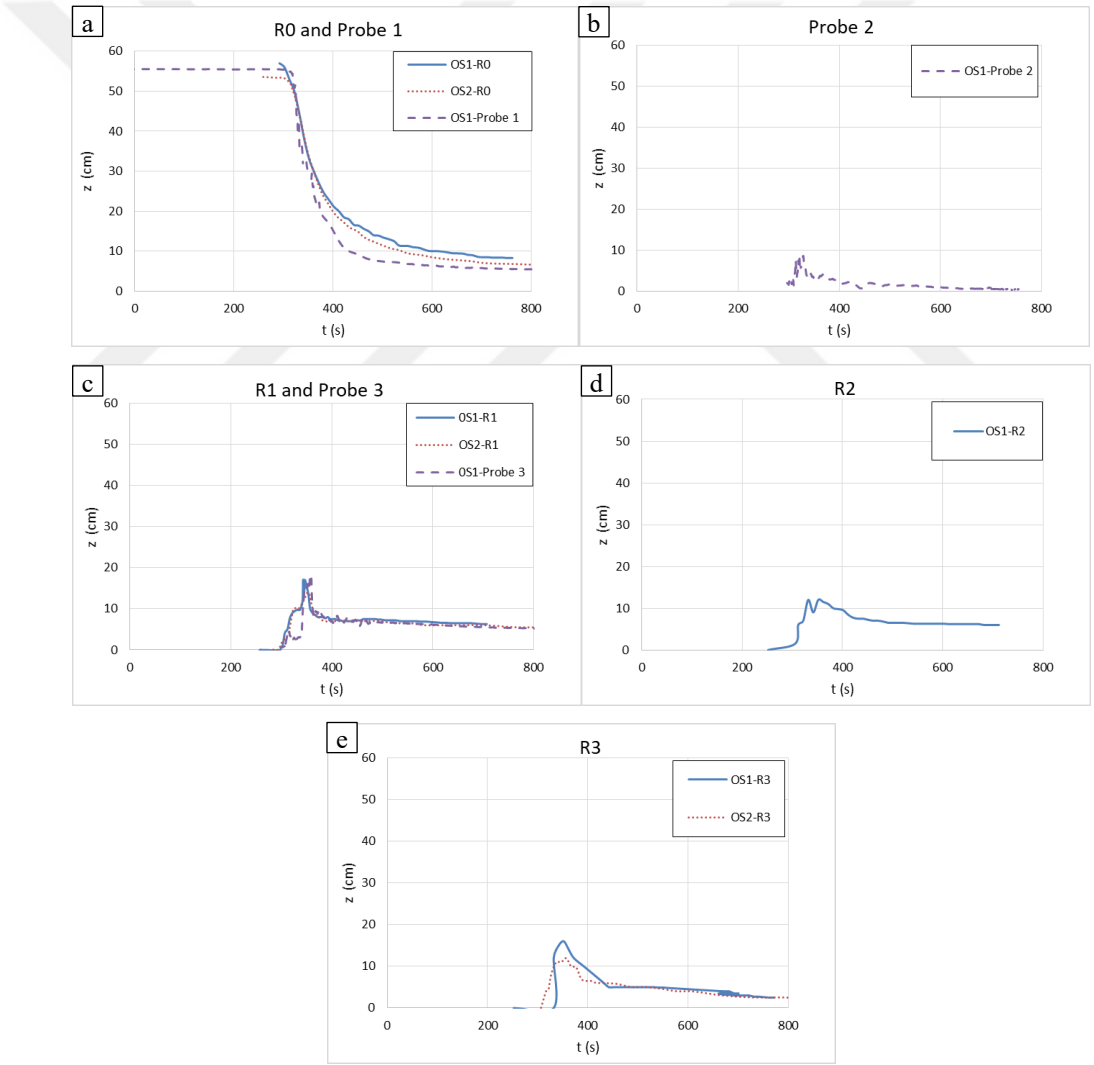


Figure 4.8: Level measurements for experiment OS1 and OS2 experiments measured from a) $R_0$ and Probe 1, b) Probe 2, c) $R_1$ and Probe 3, d) $R_2$ and e) $R_3$

## 4.3 Second Scenario: Overtopping Dam Break Type, Rough Downstream Condition

The simultaneous images of the OR1 experiment in camera 2 (left column) and camera 1 (right column) at 278 s, 304 s, 309 s, 320 s, 342 s, and 402 s are given in Figure 4.9. When t = 240 s, the water has passed over the breach. The propagated water flow and sediment downstream of the dam after the water crosses the breach, and the widening of the breach in the dam body is presented in Figure 4.9 (a-e), respectively. The breach in the dam body widened rapidly within 102 s (Figure 4.9 (a-d)) from the top. The water and sediment mixture completely covered the roughness region 38 s after overtopping from the breach, and hydraulic jumps were observed around the cubes as they progressed downstream (b-e). At t=304 s, the hydraulic jump (b) on the upstream side increased and continued for 16 s (c, d) and then disappeared with a decrease in intensity (e, f).

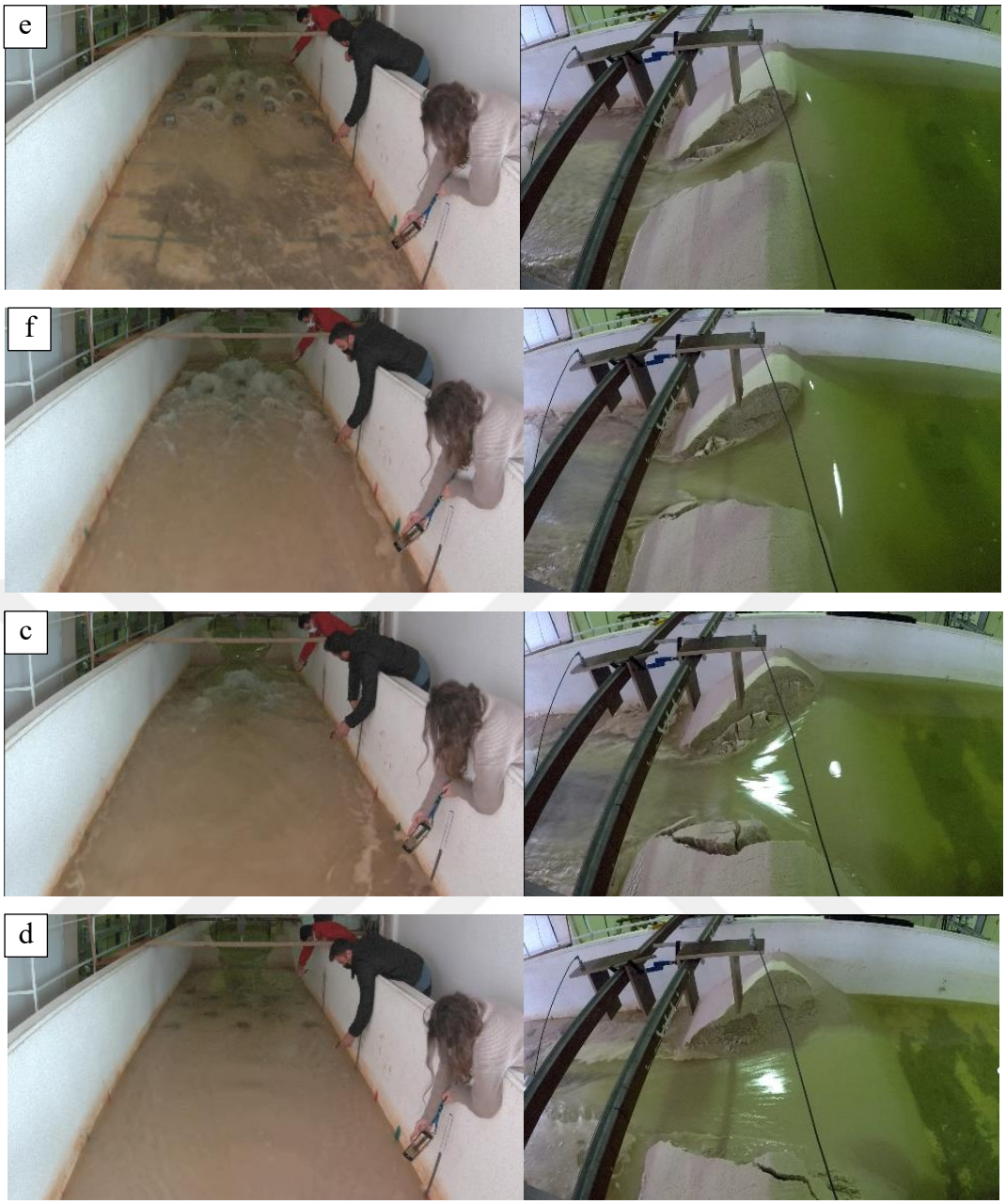


Figure 4.9: Camera 2 (flow and sediment transport at downstream area) and Camera 1 (stages of breach formation) at a) 278 s, b) 304 s, c) 309 s, d) 320 s, e) 342 s, f) 402 s for experiment OR1

The time differences for the sediment and water mixture to reach the first red line after water pass from the breach is 39 s, from the red line to $R_1$ is 21 s, from $R_1$ to $R_2$ is 3 s, and from the $R_2$ to come to $R_3$ is 4 s.

Figure 4.10 shows a picture of sediment propagated along the channel at the end of the OR1 experiment. Almost half of the dam body (middle part) was moved downstream. While high sediment heights are observed around the concrete blocks close to the right and left sides of the channel, some blocks are almost buried under the sediment. There was no sediment accumulation around the blocks located in the areas where the flood wave was severe, especially in the middle block in the first row close to the dam body.

Figure 4.10: Sediment propagation of end the experiment OR1

Three-dimensional bathymetry and contour maps are presented in Figure 4.11. The sediment heights around the blocks vary between 0 cm and almost 10 cm depending on the location of the block. As can be seen in Figure 4.11, most of the sediment accumulation from the dam body has accumulated around the cubes close to the right and left banks, and in the region close to the downstream of the roughness elements.

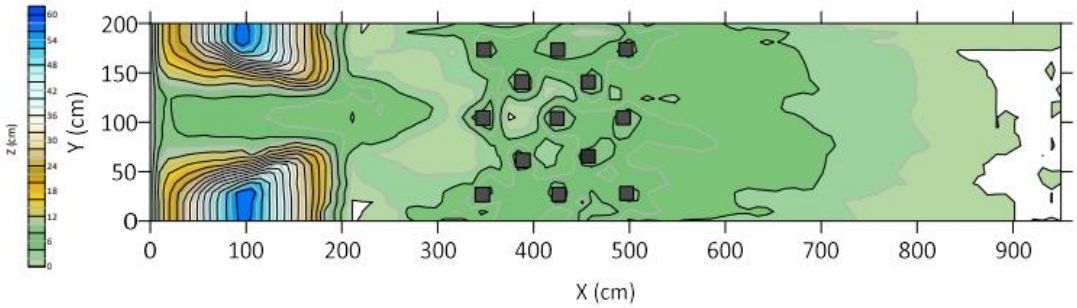

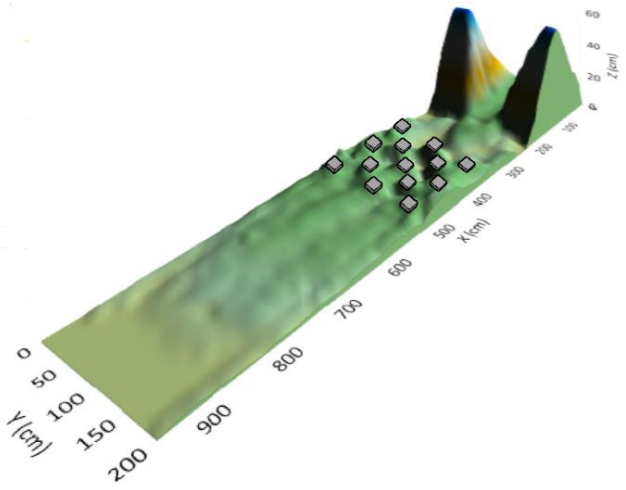


Figure 4.11: 2D and 3D contour maps of sediment distribution at the end of OR1

Symmetrical with respect to the longitudinal axis of experiment OR1, y = 0 cm and 200 cm, y = 12.5 cm and 187.5 cm, y = 25 cm and 125 cm, y = 43.75 cm and 156.25 cm, y = 62.5 cm and 137.5 cm, y= 81.25 cm and 118.75 cm, and y = 100 cm and x = 100 cm with longitudinal and traversal axes graphs of sediment heights are presented in Figure 4.12.

Accordingly, in the cross-sections that are symmetrical to each other between y = 0 cm and 200 cm, y = 12.5 cm and 187.5 cm, y = 25 cm and 125 cm, y = 43.75 cm and 156.25 cm, the approximate sediment heights are almost similar like OS1 experiment.

y = 0 cm and y = 200 cm while the maximum sediment height in the dam body is 57.5 cm and 57.6 cm, respectively. The sediment height at x = 2.02 m is 3.3 cm at y = 0 cm and 6.3 cm at y = 200 cm. The maximum sediment height between x = 2 m and x = 4 m is 6.6 cm at y = 0 cm and 6.3 cm at y = 200 cm, between x = 4 m and x = 6 m is 9.5 cm at y = 0 cm and 9.4 cm at y = 200 cm, between x = 6 m and x = 8 m is 3.4 cm at y = 0 cm and 3.9 cm at y = 200 cm, between x = 8 m and x = 9.5 m is 1.8 cm at y = 0 cm and 1.1 cm at y = 200 cm.

y = 12.5 cm and y = 187.5 cm while the maximum sediment heigt in the dam body is 57.5 cm and 57.6 cm, respectively. The sediment height at x = 2.02 m is 4 cm at y = 12.5 cm and 5.2 cm at y = 187.5 cm. The maximum sediment height between

x = 2 m and x = 4 m is 7.2 cm at y = 12.5 cm and 7.8 cm at y = 187.5 cm, between x = 4 m and x = 6 m is 9.2 cm at y = 12.5 cm and 9.4 cm at y = 187.5 cm, between x = 6 m and x = 8 m is 4.5 cm at y = 12.5 cm and 4.7 at y = 187.5 cm, between x = 8 m and x = 9.5 m is 1.5 cm at y = 12.5 cm and 1 cm at y = 187.5 cm.

y = 25 cm and y = 175 cm while the maximum sediment height in the dam body is 57.6 cm and 54.8 cm, respectively. The sediment height at x = 2.02 m is 5.7 cm at y = 25 cm and 5.2 cm at y = 175 cm. The maximum sediment height between x = 2 m and x = 4 m is 8.6 cm at y = 25 cm and 8.5 cm at y = 175 cm, between x = 4 m and x = 6 m is 8.8 cm at y = 25 cm and 8.9 cm at y = 175 cm, between x = 6 m and x = 8 m is 4.3 cm at y = 25 cm and 4.6 at y = 175 cm, between x = 8 m and x = 9.5 m is 0.9 cm at y = 25 cm and 1.3 cm at y = 175 cm.

y = 43.75 cm and y = 156.25 cm while the maximum sediment height in the dam body is 48.2 cm and 36.6 cm, respectively. The sediment height at x = 2.02 m is 6.6 cm at y = 43.75 cm and 5.7 cm at y = 156.25 cm. The maximum sediment height between x = 2 m and x = 4 m is 7.5 cm at y = 43.75 cm and 7.5 cm at y = 156.25 cm, between x = 4 m and x = 6 m is 7.3 cm at y = 43.75 cm and 7.7 cm at y = 156.25 cm, between x = 6 m and x = 8 m is 5 cm at y = 43.75 cm and 5.2 cm at y = 156.25 cm, between x = 8 m and x = 9.5 m is 1.7 cm at y = 43.75 cm and 1.8 cm at y = 156.25 cm.

y = 62.5 cm and y = 137.5 cm while the maximum sediment height in the dam body is 31.1 cm and 18.5 cm, respectively. The sediment height at x = 2.02 m is 5.5 cm at y = 62.5 cm and 6.9 cm at y = 137.5 cm. The maximum sediment height between x = 2 m and x = 4 m is 9.5 cm at y = 62.5 cm and 9.2 cm at y = 137.5 cm, between x = 4 m and x = 6 m is 9.5 cm at y = 62.5 cm and 9.3 cm at y = 137.5 cm, between x = 6 m and x = 8 m is 5.3 cm at y = 62.5 cm and 5 cm at y = 137.5 cm, between x = 8 m and x = 9.5 m is 1.7 cm at y = 62.5 cm and 2 cm at y = 137.5 cm.

y = 81.25 cm and y = 118.75 cm while the maximum sediment height in the dam body is 9.7 cm and 8.4 cm, respectively. The sediment height at x = 2.02 m is 6 cm at y = 81.25 cm and 5.9 cm at y = 118.75 cm. The maximum sediment height between x = 2 m and x = 4 m is 7.2 cm at y = 81.25 cm and 8.7 cm at y = 118.75 cm, between x = 4 m and x = 6 m is 8.3 cm at y = 81.25 cm and 7.7 cm at y = 118.75 cm, between

x = 6 m and x = 8 m is 5.9 cm at y = 81.25 cm and 4.6 cm at y = 118.75cm, between x = 8 m and x = 9.5 m is 2.1 cm at y = 81.25 cm and 2.2 cm at y = 118.75 cm.

y = 100 cm while the maximum sediment height in the dam body is 8.4 cm. The sediment height at x = 2.02 m is 4.9 cm. The maximum sediment height between x = 2 m and x = 4 m is 9.8 cm, between x = 4 m and x = 6 m is 9.5 cm, between x = 6 m and x = 8 m is 4.9 cm, between x = 8 m and x = 9.5 m is 1.9 cm. As in the OS3 experiment, it is the section with the lowest sediment height at y = 100 cm. It is possible to say that almost half of the dam body is exposed to erosion at x = 100 cm.

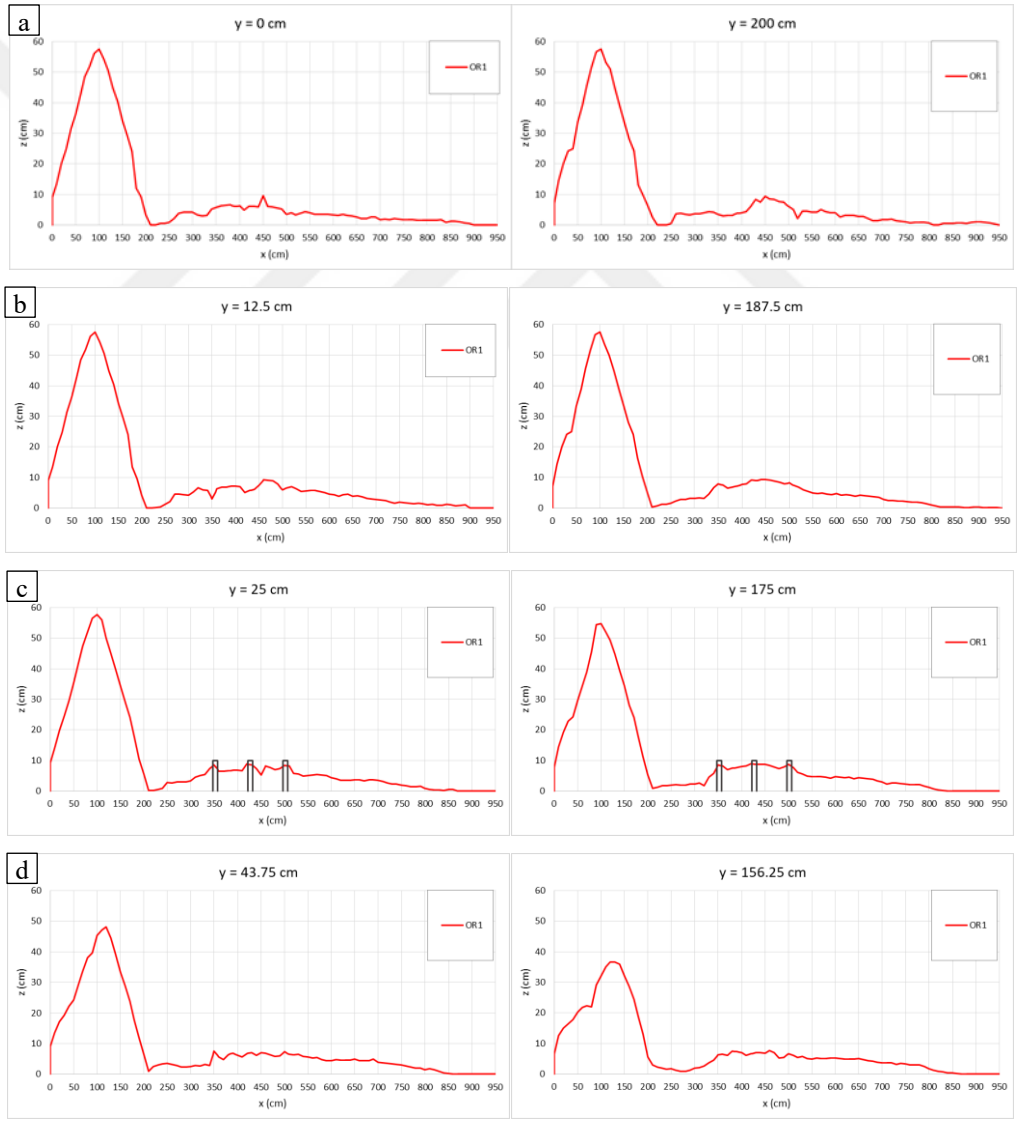

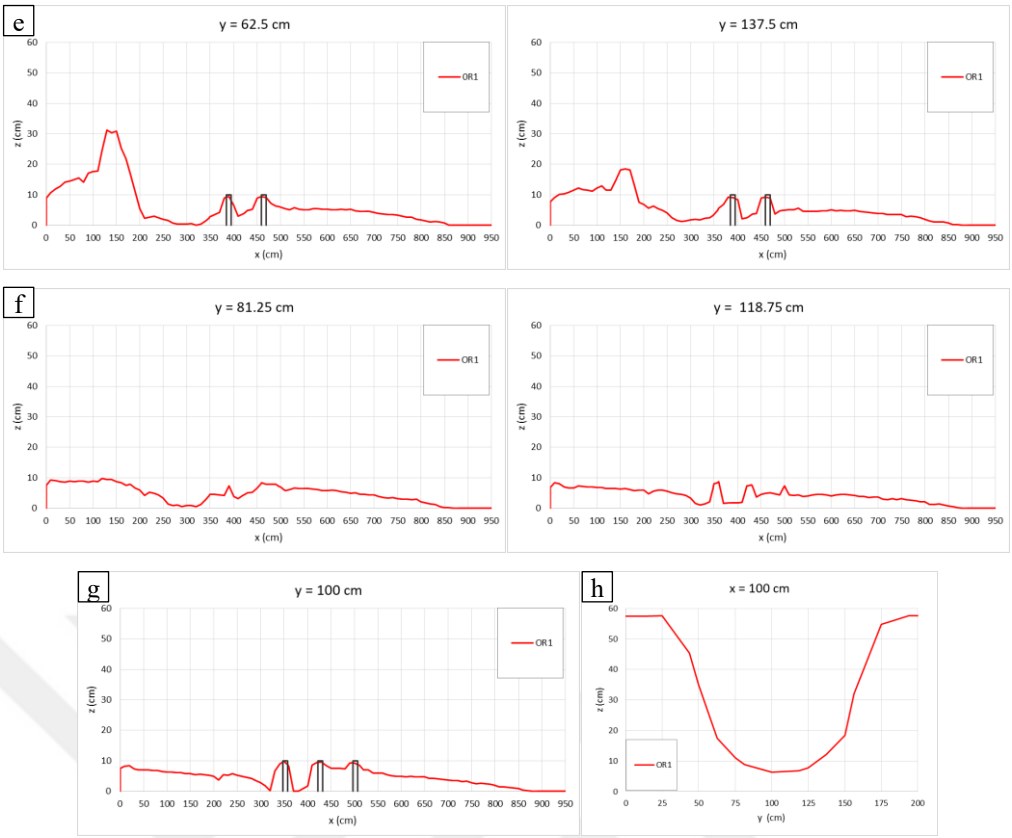


Figure 4.12: Longitudinal sediment height profiles measured at a) y = 0 cm and 200 cm, b) y = 12.5 cm and 187.5 cm, c)y = 25 cm and 125 cm, d) y = 43.75 cm and 156.25 cm, e)y = 62.5 cm and 137.5 cm, f) y= 81.25 cm and 118.75 cm, and g) y = 100 cm and along the channel width and, transversal crest section of the dam at h) x = 100 cm of OR1

Figure 4.13.a shows the levels measured by Probe 1, $R_0$ for OR1, Figure 4.13.b $R_1$, $R_2$, $R_3$, Probe 2 and Probe 3. Accordingly, the decrease in the dam body (Probe 1) in Figure 4.13 a, the decrease in the water level is almost the same until 370 s. After 370 seconds, the level in Probe 1 decreased more than in $R_0$. In Probe 1, the maximum level decreased from 55 cm to 5.2 cm. $R_0$ decreased from 58 cm to 9 cm at the end of 800 seconds. In Figure 4.13 b, the maximum water level in 328 s, 354 s, 347 s is 13 cm, 13 cm, and 14.5 cm at $R_1$, $R_2$, and $R_3$, respectively. The maximum water level at Probe 2 and Probe 3 is 7.7 cm and 15.7 cm at 404 s and 377 s, respectively.

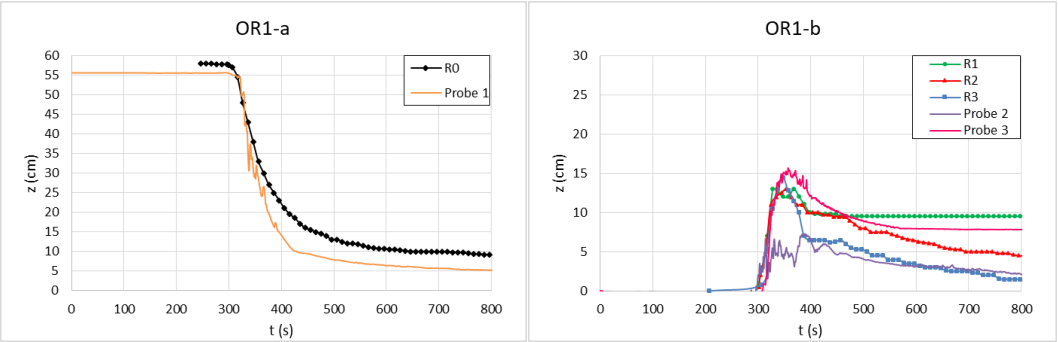


Figure 4.13: Level measurements for OR1 experiment a) measured from $R_0$ and Probe 1, b) measured from $R_1$, $R_2$, $R_3$, Probe 2 and Probe 3

### 4.3.1 Repeatability of Second Scenario Experiments

The second break scenario was performed in 2 repetitions under the same condition. In Figure 4.14, for experiments OR1 and OR2 sediment height graphs y = 0 cm and 200 cm, y = 12.5 cm and 187.5 cm, y = 25 cm and 125 cm, y = 43.75 cm and 156.25 cm, y = 62.5 cm, 137.5 cm, y= 81.25 cm and 118.75 cm, y = 100 cm and x = 100 cm are given. Accordingly, it is seen that the sediment section graphs of the experiments carried out in the rough downstream condition are compatible with each other and the sediment distributions are almost the same.

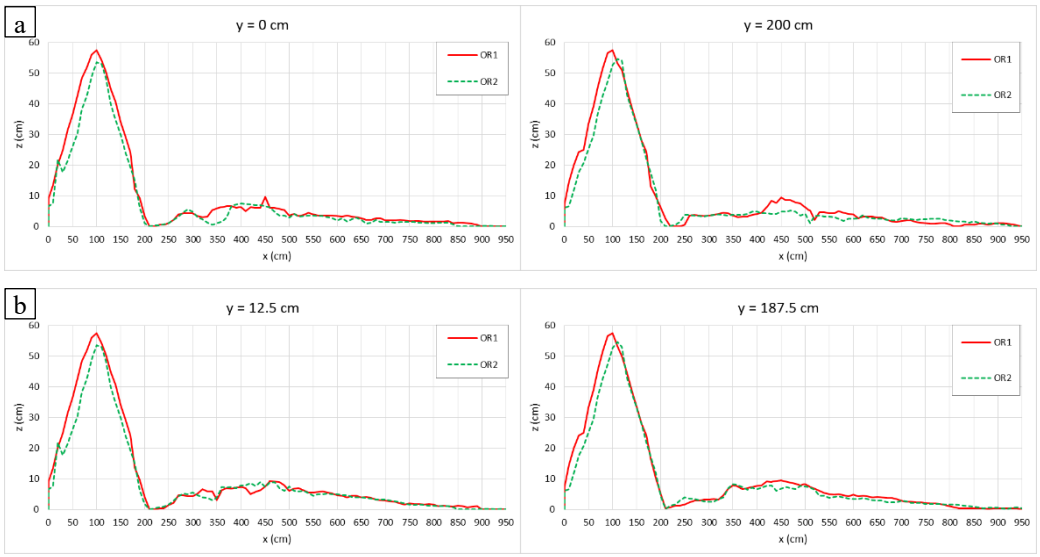

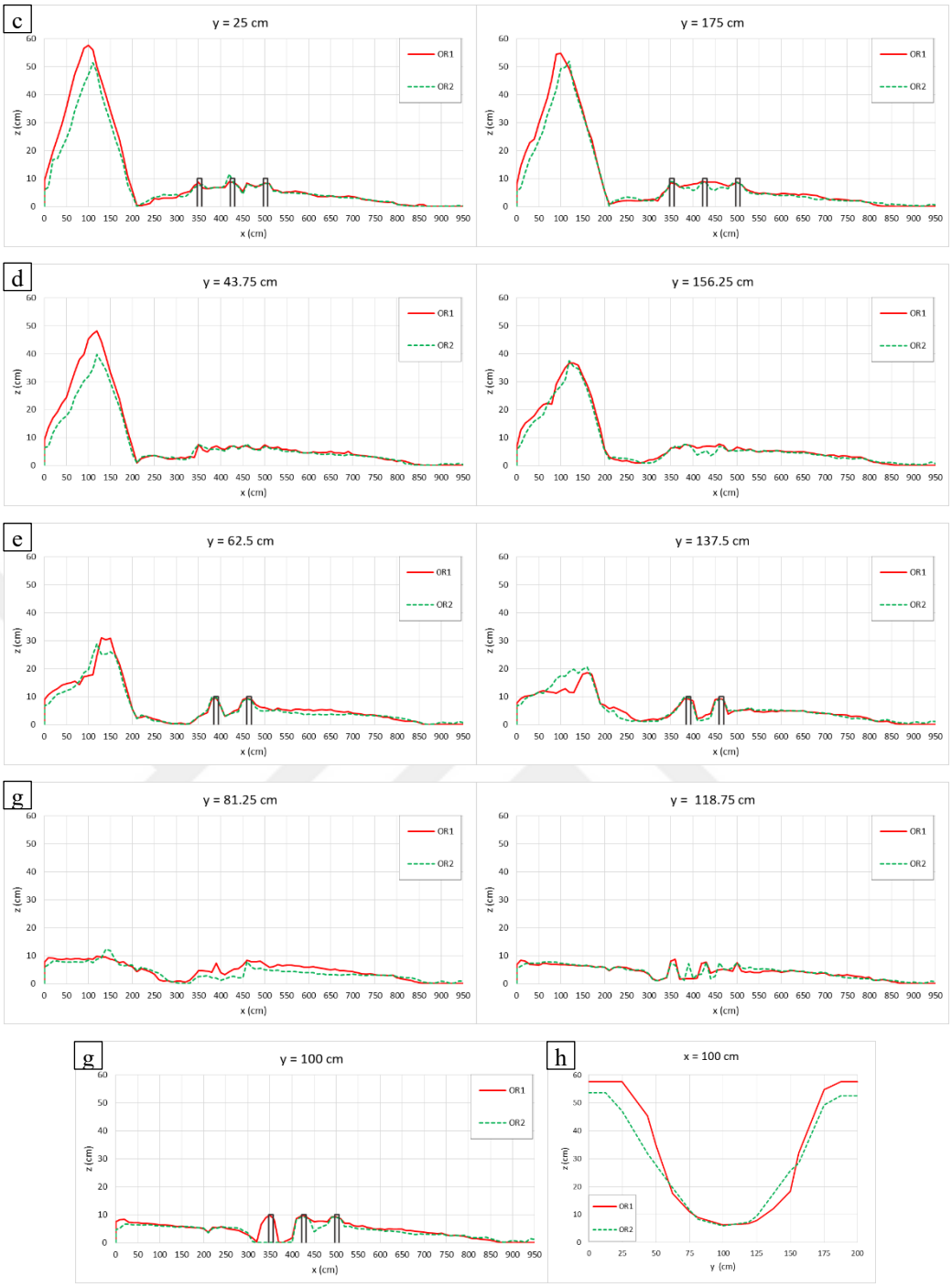


Figure 4.14: Longitudinal sediment height profiles measured at a) y = 0 cm and 200 cm, b) y = 12.5 cm and 187.5 cm, c) y = 25 cm and 125 cm, d) y = 43.75 cm and 156.25 cm, e)y = 62.5 cm and 137.5 cm, f) y= 81.25 cm and 118.75 cm, and g) y = 100 cm and along the channel width and, transversal crest section of the dam at h) x = 100 cm of OR1 and OR2

For the OR2 experiment, the time diffrences for the sediment and water mixture to reach the first red line after water pass from the breach is 32 s, from the red line to $R_1$ is 16 s, from $R_1$ to $R_2$ is 7 s, and from the $R_2$ to come to $R_3$ is 4 s. In the OR2 experiment, the time for the sediment to come to the red line after water pass from the breach is 7 s, the time to reach $R_1$ from the red line is 5 s shorter then OR1, and the time from $R_1$ to $R_2$ is 4 s longer then OR1 experiment.

Figure 4.15 shows the graph of the $R_0$, $R_1$, $R_2$, $R_3$, Probe 1, Probe 2, and Probe 3 measurements of the OR1 and OR2 experiments. Accordingly, it is seen that the ruler and probe measurements are compatible with each other in the experiments.

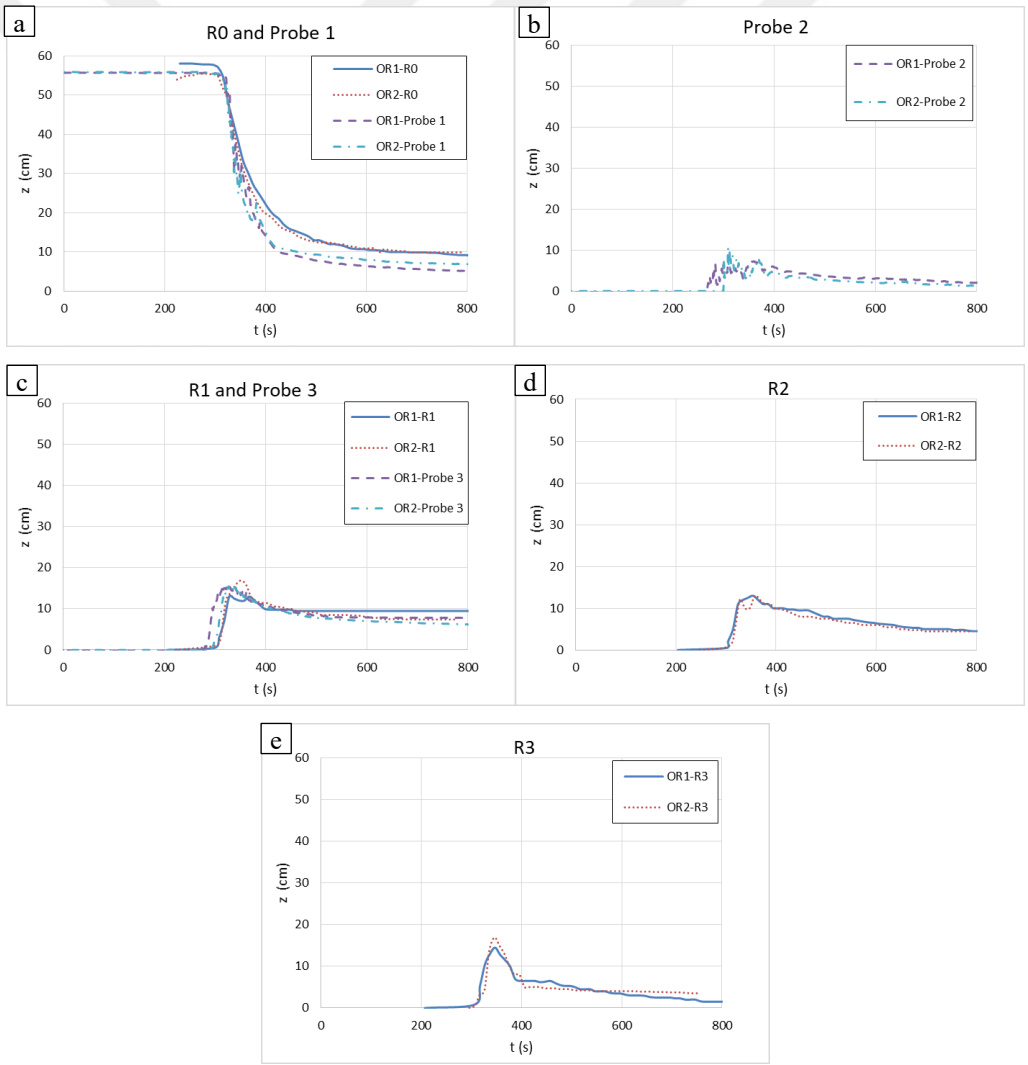


Figure 4.15: Level measurements for experiment OR1 and OR2 experiments measured from a) $R_0$ and Probe 1, b) Probe 2, c) $R_1$ and Probe 3, d) $R_2$, and e) $R_3$

## 4.4 Third Scenario: Piping Dam Break Type, Smooth Downstream Condition

Simultaneous images of the PS1 experiment in camera 2 (left column) and camera 1 (right column) at 137 s, 283 s, 297 s, 329 s, 347 s, and 427 s are given in Figure 4.16. The downstream skirt of the dam started to slide after 81 s and almost half of it was eroded within 137 seconds (Figure 4.16 a). The body of the dam continued to be eroded up to the crest level until the 283$^{rd}$ second, and the crest of the dam was thinned and the water overflowed from the left bank over the crest (Figure 4.16 b). From the left bank to the middle of the channel, the breach widened rapidly within 64 seconds as in Figure 4.16 c-e. As the water and sediment mixture progressed downstream, a hydraulic jump was observed in approximately 6.5 m of the channel and it increased towards the dam body (Figure 4.16 d-e). After t = 427 s, there was no visible change in sediment distribution.

In the piping experiments, the downstream skirt of the dam was eroded before the sediment in the dam body propagated downstream and the water seepage covered the channel. 44 s after the water started to seepage from the skirt of the dam, it reached the first red line. It took 70 s for the seepage water to reach $R_1$ from the red line, 40 s to reach $R_2$ from $R_1$, and 73 s to reach $R_3$ from $R_2$. After the water and sediment mixture started to propagate downstream, it took 6 s to reach $R_1$, 3 s to reach $R_1$ from $R_2$, and 4 s to reach $R_3$ from $R_2$. Water reached $R_2$ in 110 s and the water and sediment mixture reached $R_2$ in 179 s after water passed the first red line.

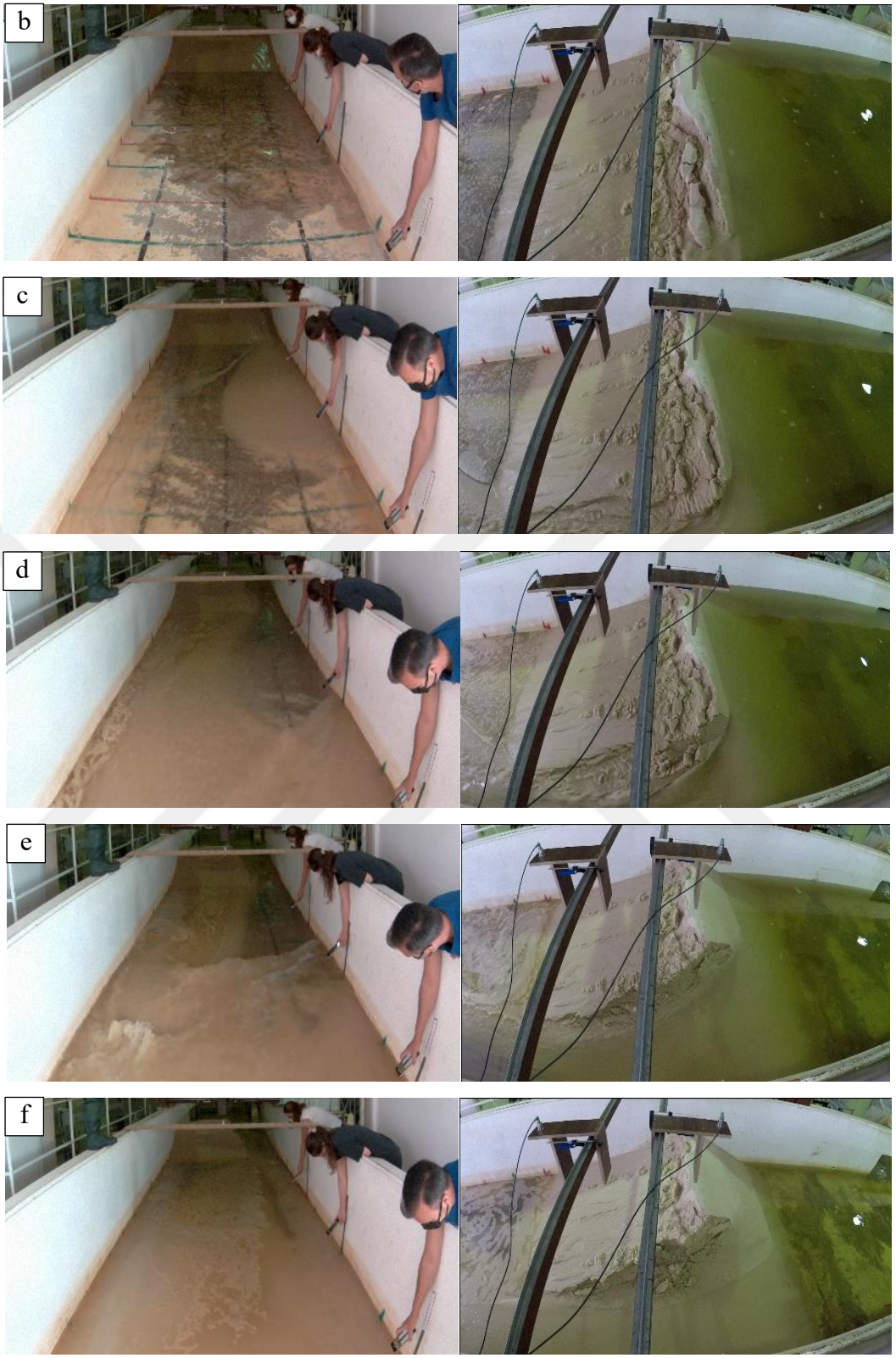


Figure 4. 16: Camera 2 (flow and sediment transport at downstream area) and Camera 1 (stages of breach formation) at a) 137 s, b) 283 s, c) 297 s, d) 329 s, e) 347 s, f) 427 s for experiment PS1

Figure 4.17 shows the final state of sediment propagation after the experiment is complated. As seen in the figure, approximately 50 cm of the dam body from the right bank has been completely eroded, and between 50 cm and 100 cm, the sediment in the dam body has been partially transported. The fact that the flood wave came from the left bank caused the flow to be faster on this axis, and as a result, it caused the sediment to accumulate more on the right wall.

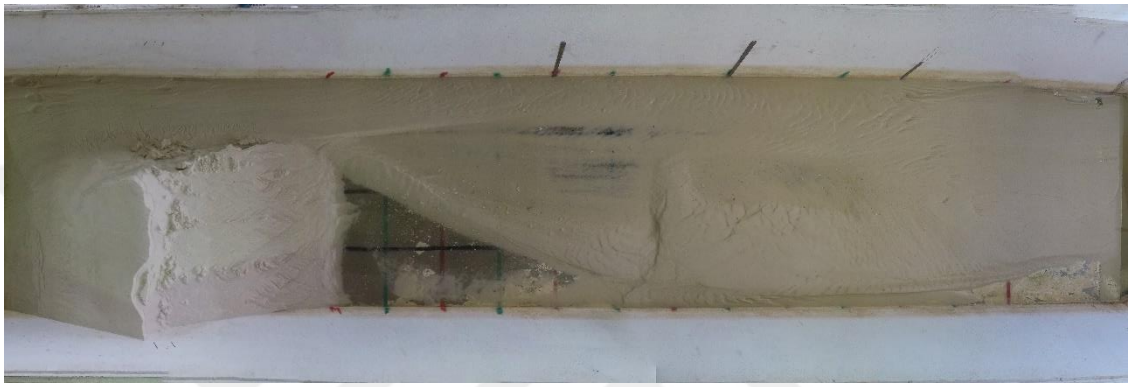

Figure 4.17: Sediment propagation of end the experiment PS1

Contour and bathymetry maps obtained by using the sediment heights obtained as a result of the measurements are presented below in Figure 4.18. According to the bed topography data, the maximum sediment height is between 5.3 m and 8.9 m on the right side of the channel. It can be said that in the region where the water velocity is high, there are values where the sediment depth is 0 between 4 m and 5 m.

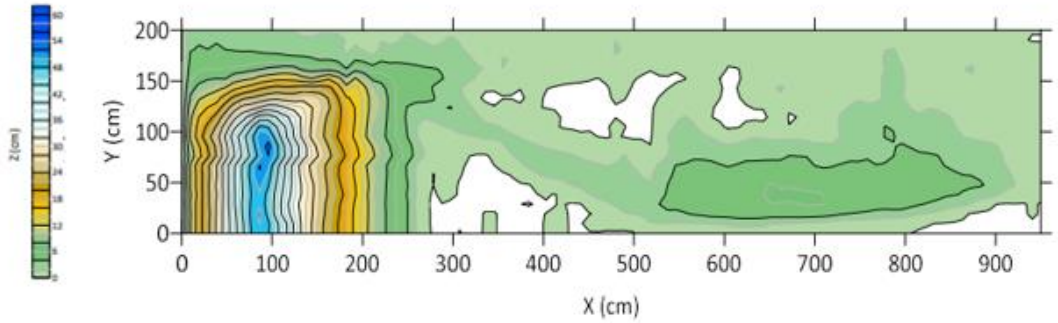

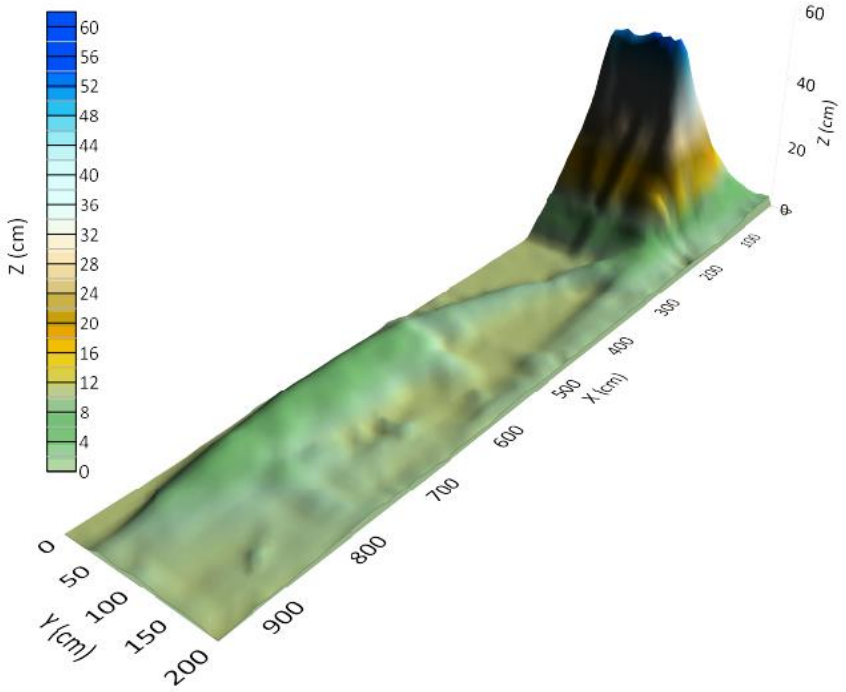


Figure 4.18: 2D and 3D contour maps of sediment distribution at the end of PS1

Symmetrical with respect to the longitudinal axis of experiment PS1, y = 0 cm and 200 cm, y = 12.5 cm and 187.5 cm, y = 25 cm and 125 cm, y = 43.75 cm and 156.25 cm, y = 62.5 cm and 137.5 cm, y= 81.25 cm and 118.75 cm, and y = 100 cm and x = 100 cm with longitudinal and traversal axes graphs of sediment heights are presented in Figure 4.19.

y = 0 cm and y = 200 cm while the maximum sediment height in the dam body is 49.1 cm and 4.2 cm, respectively. The sediment height at x = 2.02 m is 13.8 cm at y = 0 cm and 2.2 cm at y = 200 cm. The maximum sediment height between x = 2 m and x = 4 m is 13.8 cm at y = 0 cm and 2.2 cm at y = 200 cm, between x = 4 m and x = 6 m is 1.8 cm at y = 0 cm and 1.9 cm at y = 200 cm, between x = 6 m and x = 8 m is 1.1 cm at y = 0 cm and 2.1 cm at y = 200 cm, between x = 8 m and x = 9.5 m is 0.4 cm at y = 0 cm and 1.7 cm at y = 200 cm.

y = 12.5 cm and y = 187.5 cm while the maximum sediment heigt in the dam body is 49.9 cm and 5.6 cm, respectively. The sediment height at x = 2.02 m is 13.8 cm at y = 12.5 cm and 2 cm at y = 187.5 cm. The maximum sediment height between x = 2

m and x = 4 m is 13.8 cm at y = 12.5 cm and 2.7 cm at y = 187.5 cm, between x = 4 m and x = 6 m is 3 cm at y = 12.5 cm and 2.2 cm at y = 187.5 cm, between x = 6 m and x = 8 m is 3.6 cm at y = 12.5 cm and 1.9 at y = 187.5 cm, between x = 8 m and x = 9.5 m is 1.3 cm at y = 12.5 cm and 1.5 cm at y = 187.5 cm.

y = 25 cm and y = 175 cm while the maximum sediment height in the dam body is 49.8 cm and 4.7 cm, respectively. The sediment height at x = 2.02 m is 13.9 cm at y = 25 cm and 3.1 cm at y = 175 cm. The maximum sediment height between x = 2 m and x = 4 m is 13.9 cm at y = 25 cm and 3.3 cm at y = 175 cm, between x = 4 m and x = 6 m is 5.6 cm at y = 25 cm and 2.1 cm at y = 175 cm, between x = 6 m and x = 8 m is 5.9 cm at y = 25 cm and 2.4 at y = 175 cm, between x = 8 m and x = 9.5 m is 4.4 cm at y = 25 cm and 1.9 cm at y = 175 cm.

y = 43.75 cm and y = 156.25 cm while the maximum sediment height in the dam body is 50.1 cm and 13.2 cm, respectively. The sediment height at x = 2.02 m is 14.1 cm at y = 43.75 cm and 9 cm at y = 156.25 cm. The maximum sediment height between x = 2 m and x = 4 m is 14.1 cm at y = 43.75 cm and 9 cm at y = 156.25 cm, between x = 4 m and x = 6 m is 5.5 cm at y = 43.75 cm and 1.6 cm at y = 156.25 cm, between x = 6 m and x = 8 m is 6.3 cm at y = 43.75 cm and 2.5 cm at y = 156.25 cm, between x = 8 m and x = 9.5 m is 5.5 cm at y = 43.75 cm and 2.8 cm at y = 156.25 cm.

y = 62.5 cm and y = 137.5 cm while the maximum sediment height in the dam body is 52.6 cm and 25.8 cm, respectively. The sediment height at x = 2.02 m is 13.7 cm at y = 62.5 cm and 13.7 cm at y = 137.5 cm. The maximum sediment height between x = 2 m and x = 4 m is 13.7 cm at y = 62.5 cm and 13.7 cm at y = 137.5 cm, between x = 4 m and x = 6 m is 4.8 cm at y = 62.5 cm and 0.8 cm at y = 137.5 cm, between x = 6 m and x = 8 m is 5.4 cm at y = 62.5 cm and 2.6 cm at y = 137.5 cm, between x = 8 m and x = 9.5 m is 5 cm at y = 62.5 cm and 2.1 cm at y = 137.5 cm.

y = 81.25 cm and y = 118.75 cm while the maximum sediment height in the dam body is 53.7 cm and 38.8 cm, respectively. The sediment height at x = 2.02 m is 14.7 cm at y = 81.25 cm and 14 cm at y = 118.75 cm. The maximum sediment height between x = 2 m and x = 4 m is 14.7 cm at y = 81.25 cm and 14 cm at y = 118.75 cm, between x = 4 m and x = 6 m is 3.9 cm at y = 81.25 cm and 1.9 cm at y = 118.75 cm, between

x = 6 m and x = 8 m is 4.8 cm at y = 81.25 cm and 3.5 cm at y = 118.75cm, between x = 8 m and x = 9.5 m is 4.3 cm at y = 81.25 cm and 2.9 cm at y = 118.75 cm.

y = 100 cm while the maximum sediment height in the dam body is 51.9 cm. The sediment height at x = 2.02 m is 13.7 cm. The maximum sediment height between x = 2 m and x = 4 m is 13.7 cm, between x = 4 m and x = 6 m is 3.1 cm, between x = 6 m and x = 8 m is 4.9 cm, between x = 8 m and x = 9.5 m is 3.2 cm.

In addition, the sediment at the downstream skirt of the dam body shifted from 200 cm to 270 cm at y=0 cm, 12.5 cm, 25 cm, 43.75 cm, 62.5, 81.25, and 100 cm sections. At x = 100 cm, the unbroken right bank height of the dam body decreased from 60 cm to an average of 49 cm. Approximately half of the dam body between x= 90-200 cm has been moved downstream of the dam.

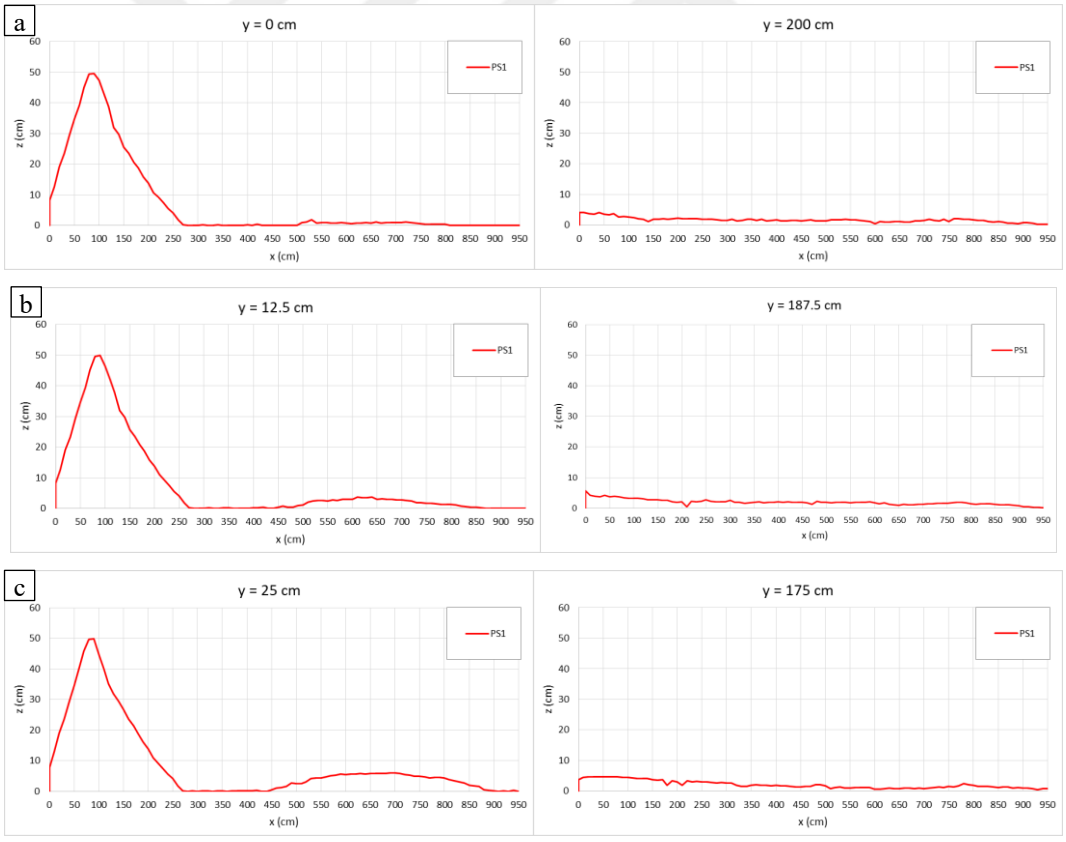

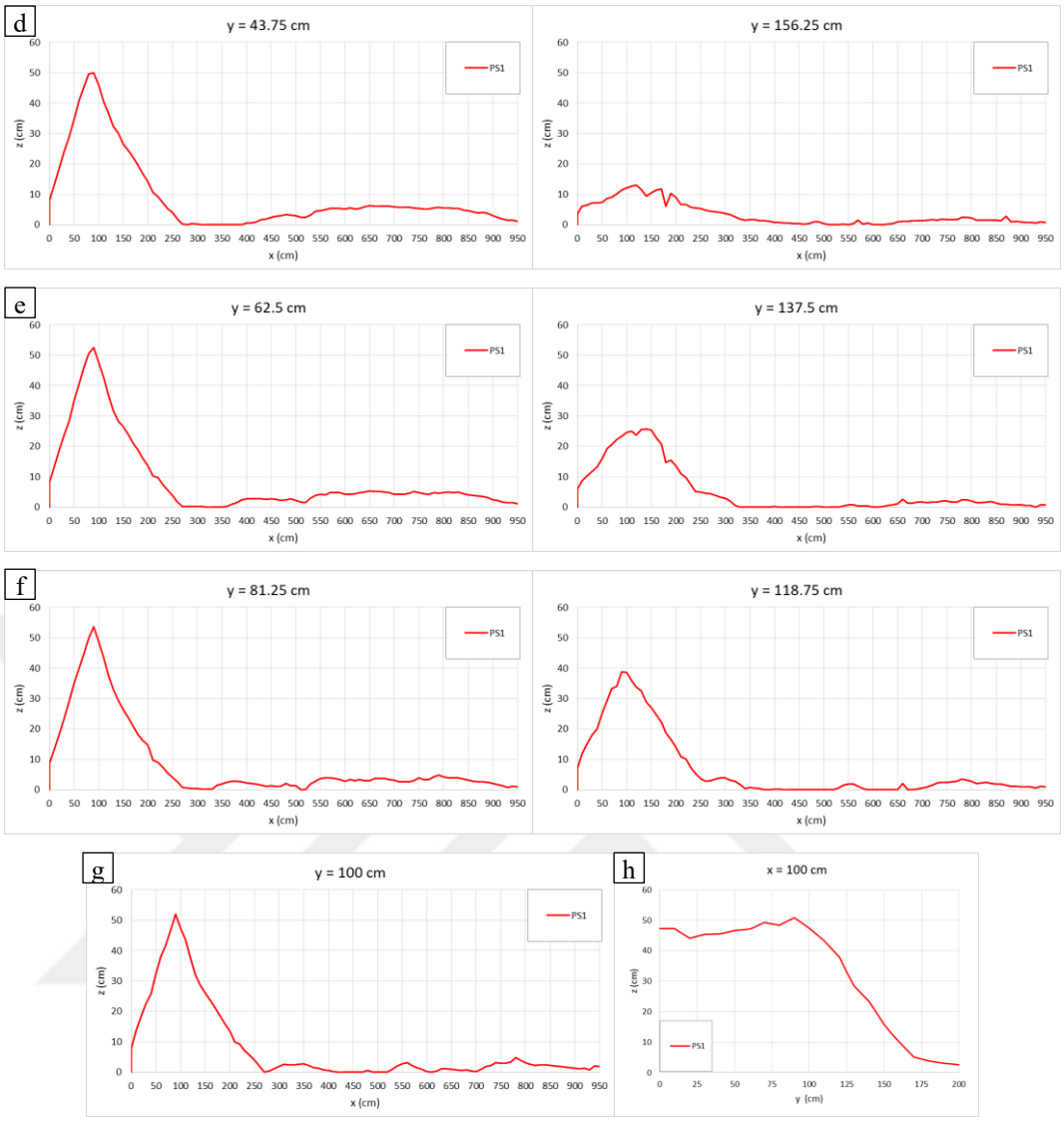


Figure 4.19: Longitudinal sediment height profiles measured at a) y = 0 cm and 200 cm, b) y = 12.5 cm and 187.5 cm, c)y = 25 cm and 125 cm, d) y = 43.75 cm and 156.25 cm, e)y = 62.5 cm and 137.5 cm, f) y= 81.25 cm and 118.75 cm, and g) y = 100 cm and along the channel width and, transversal crest section of the dam at h) x = 100 cm of PS1

Figure 4.20. a shows the levels measured by Probe 1, $R_0$ for PS1, and Figure 4.20.b a shows $R_1$, $R_2$, $R_3$, Probe 2 and Probe 3. Accordingly, the decrease in the dam body (Probe 1) in Figure 4.20.a, the decrease in the dam body 55.5 cm to 54.4 cm. $R_0$ decreased from 53 cm to 8 cm at the end of 800 seconds. In Figure 4.20.b, the maximum water level in 387 s, 367 s, 367 s 10 cm is14 cm, and 13 cm at $R_1$, $R_2$, and

$R_3$, respectively. The maximum level at Probe 2 is 6.38 cm and maximum water level Probe 3 is 7.9 cm at 335 s and 395 s, respectively.

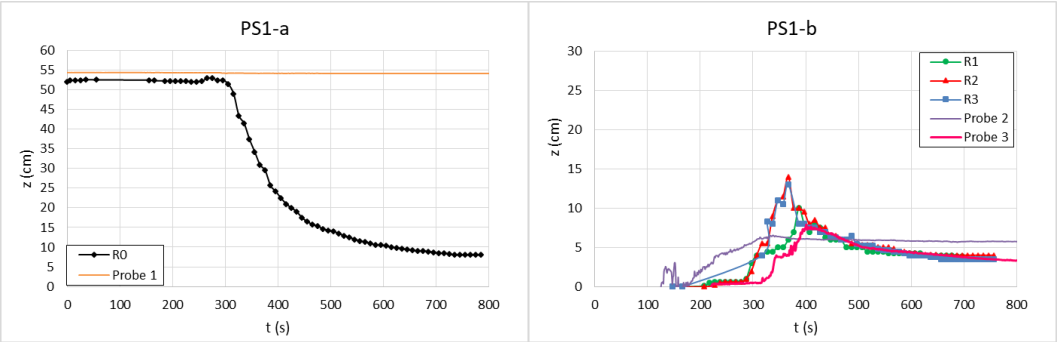


Figure 4.20: Level measurements for PS1 experiment a) measured from $R_0$ and Probe 1, b) measured from $R_1$, $R_2$, $R_3$, Probe 2 and Probe 3

## 4.4.1 Repeatability of Third Scenario Experiments

The third break scenario was performed in 2 repetitions under the same condition. In Figure 4.21, for experiments PS1 and PS2, sediment height graphs y = 0 cm and 200 cm, y = 12.5 cm and 187.5 cm, y = 25 cm and 125 cm, y = 43.75 cm and 156.25 cm, y = 62.5 cm, 137.5 cm, y= 81.25 cm and 118.75 cm, y = 100 cm and x = 100 cm are given.The sediment graphs of PS1 and PS2 experiments are compatible with each other.

For the PS2 experiment, 32 s after the started to water seepage from the skirt of the dam, it reached the first red line. It took 17s for the seepage water to reach $R_1$ from the red line, 61 s to reach $R_2$ from $R_1$, and 78 s to reach $R_3$ from $R_2$. After the water and sediment mixture started to propagate downstream, it took 14 s to reach $R_1$, 6 s to reach $R_1$ from $R_2$, and 4 s to reach $R_3$ from $R_2$. Water reached $R_2$ in 456 s and the water and sediment mixture reached $R_2$ in 78 s after water passed the first red line. In the PS 2 experiment, according to $PR_1$, it was 12 s earlier the first red line after the started to water seepage from the skirt of the dam, and 53 s earlier for the water seepage to reach $R_1$ from the red line. It took 21 s longer from $R_1$ to $R_2$ and 5 s longer from $R_2$ to $R_3$. It

took 8 s longer for the water and sediment mixture to reach $R_1$ and 3 s longer for it to reach $R_2$ from $R_1$ after it started propagating downstream.

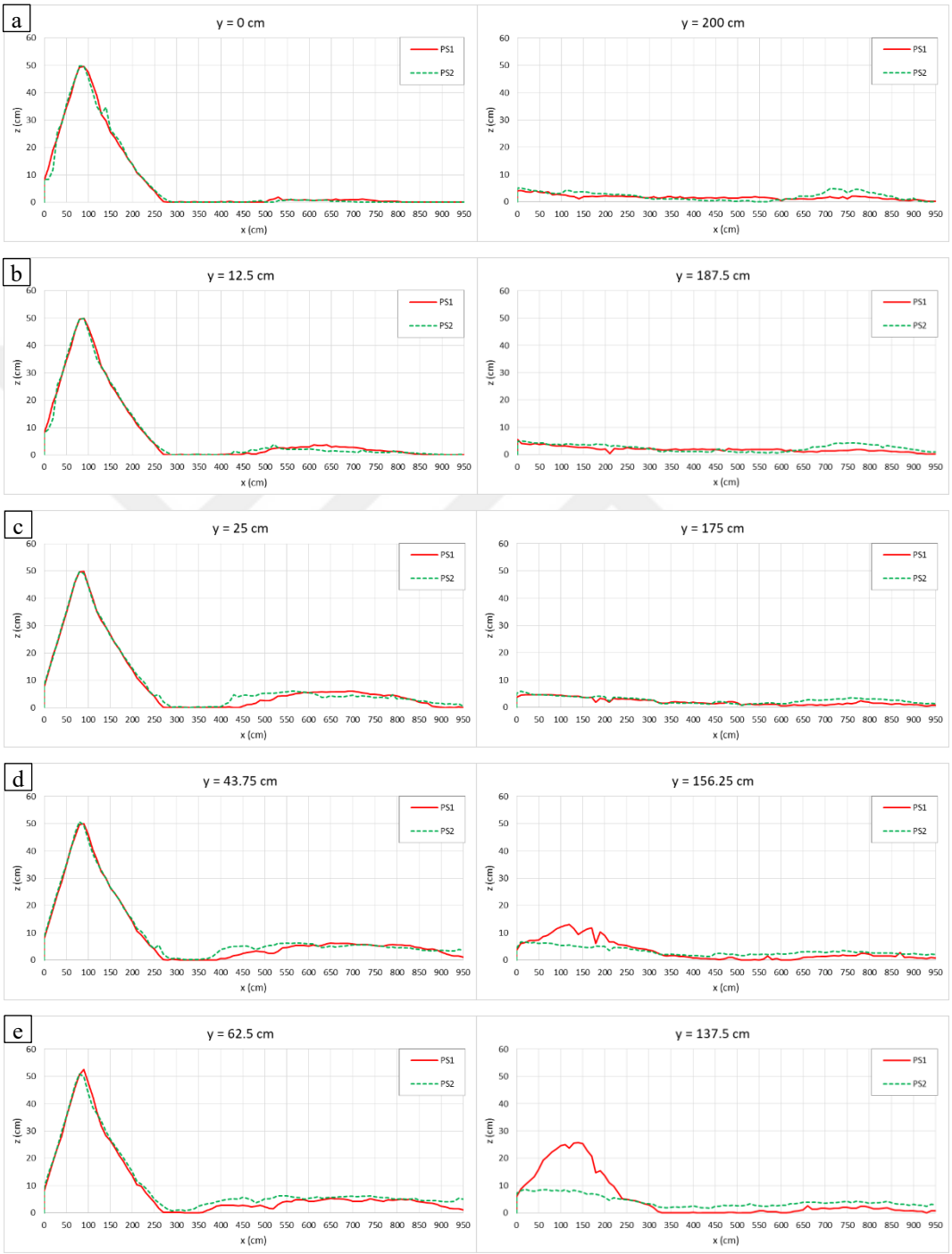

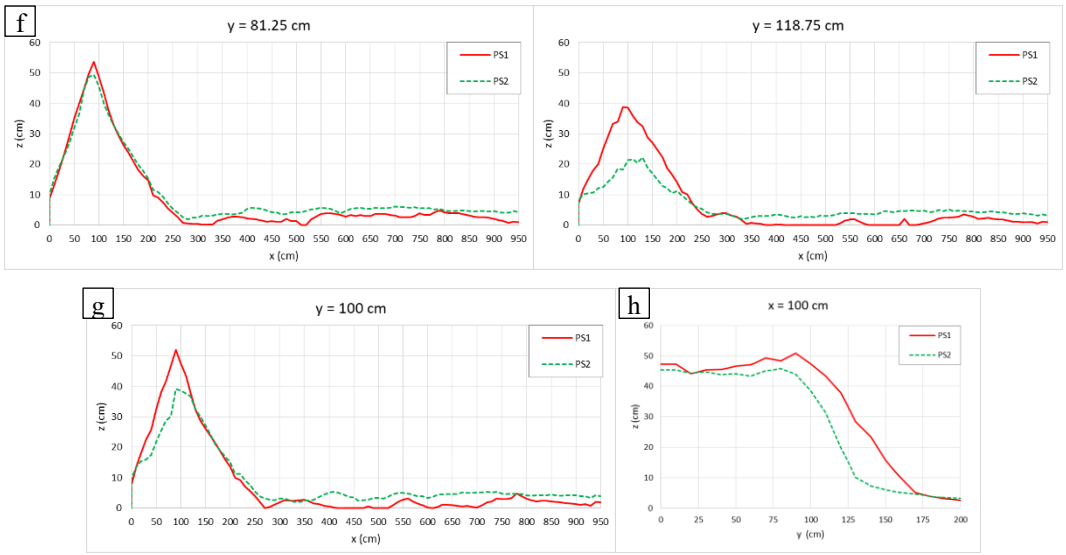


Figure 4.21: Longitudinal sediment height profiles measured at a) y = 0 cm and 200 cm, b) y = 12.5 cm and 187.5 cm, c) y = 25 cm and 125 cm, d) y = 43.75 cm and 156.25 cm, e) y = 62.5 cm and 137.5 cm, f) y= 81.25 cm and 118.75 cm, and g) y = 100 cm and along the channel width and, transversal crest section of the dam at h) x = 100 cm of PS1 and PS2

Figure 4.22 shows the graph of the $R_0$, $R_1$, $R_2$, $R_3$, Probe 1, Probe 2, and Probe 3 measurements of the PS1 and PS2 experiments. Accordingly, it is seen that the $R_1$ and Probe 3, $R_2$, and $R_3$ measurements are compatible with each other.

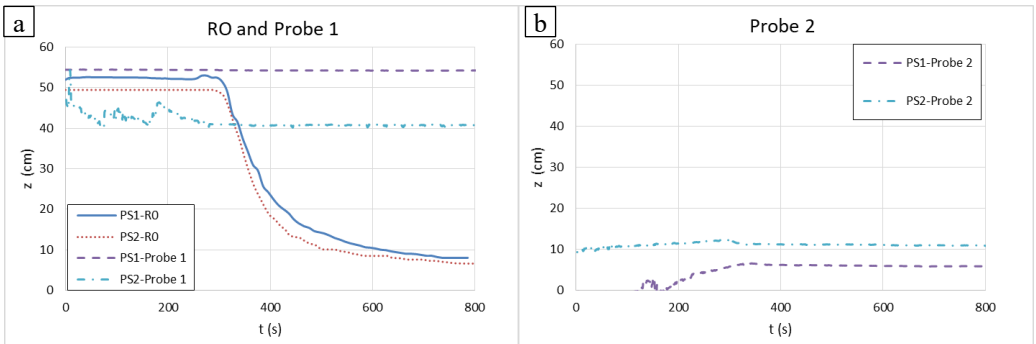

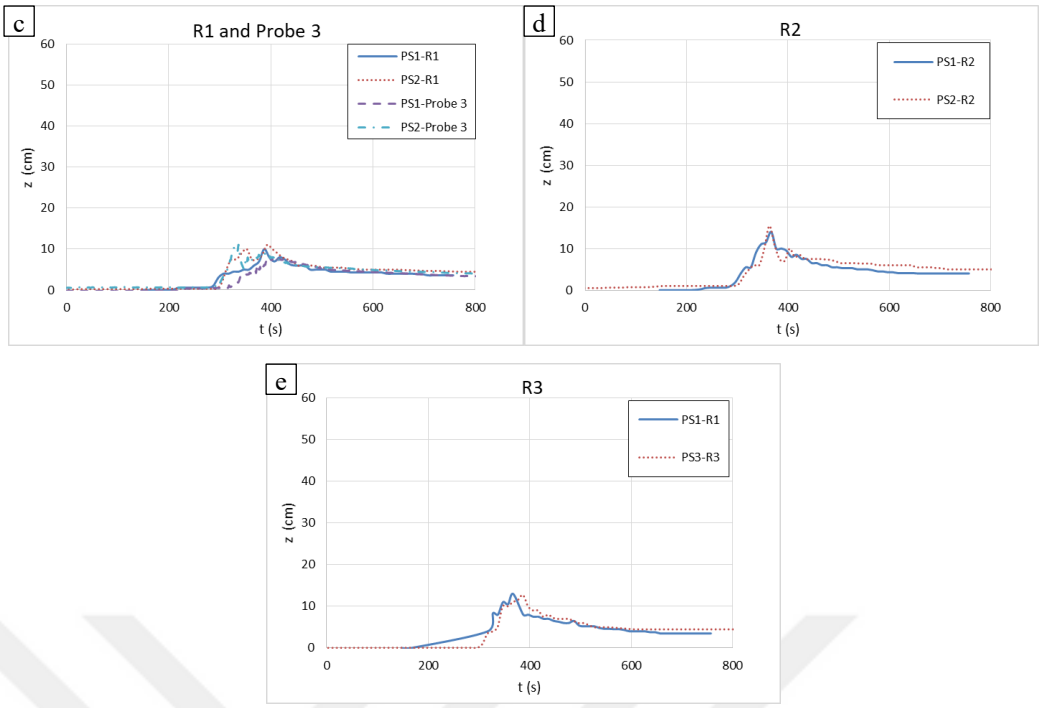


Figure 4.22: Level measurements for experiment PS1 and PS2 experiments measured from a) $R_0$ and Probe 1, b) Probe 2, c) $R_1$ and Probe 3, d) $R_2$, and e) $R_3$

## 4.5 Fourth Scenario: Piping Dam Break Type, Rough Downstream Condition

The simultaneous images of the PR1 experiment in camera 2 (left column) and camera 1 (right column) 175 s, 310 s, 325 s, 340 s, 390 s, and 435 s are given in Figure 4.23. The sediment at the skirt of the dam started to move after 122 seconds. After 175 seconds, almost half of it was eroded (Figure 4.23 a). The body of the dam continued to be eroded up to the crest level until the 310$^{th}$ second, and the crest of the dam thinned and the water overflowed from the left bank over the crest (Figure 4.23 b). From the left bank to the middle of the channel, the breach widened rapidly within 80 seconds as in Figure 4.23 b-e. The mixture of water and sediment covered the roughness region within 15 seconds (Figure 4.23 c). As the water and sediment mixture reaches the concrete blocks, splashes have occurred as seen in Figure 4.23 (b, c, d, e ). These jumps

reached the maximum until the 340$^{th}$ second, and then decreased (Figure 4.23 e) and disappeared (Figure 4.23 f).

44 s after the water started to seepage from the skirt of the dam, it reached the first red line. It took 70 s for the seepage water to reach $R_1$ from the red line, 48 s to reach $R_2$ from $R_1$, and 41 s to reach $R_3$ from $R_2$. After the water and sediment mixture started to propagate downstream, it took 8 s to reach $R_1$, 3 s to reach $R_1$ from $R_2$, and 5 s to reach $R_3$ from $R_2$. Water reached $R_2$ in 154 s and the water and sediment mixture reached $R_2$ in 118 s after water passed the first red line.


Figure 4.23: Camera 2 (flow and sediment transport at downstream area) and Camera 1 (stages of breach formation) at a) 175, b) 310, c) 325, d) 340, e) 390, f) 435 for experiment PR1

Figure 4.24 shows the final sediment propagation after the experiment was completed. As seen in the figure, approximately 50 cm of the dam body from the right wall has been completely eroded, and between 80 cm and 150 cm, the sediment in the dam body has been partially transported. The fact that the flood wave came from the left wall caused the flow to be faster on this axis, and as a result, it caused the sediment to accumulate more on the right wall from the second row of the cubes.

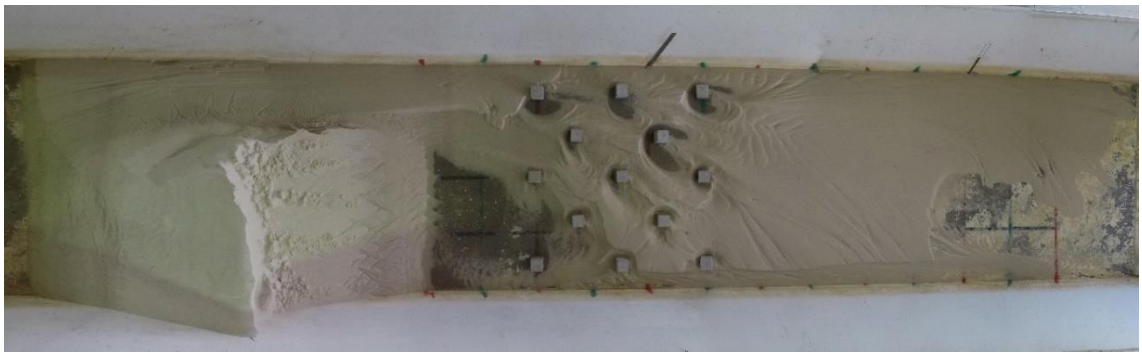

Figure 4.24: Sediment propagation of end the experiment PR1

Contour and bathymetry maps obtained by using the sediment heights obtained as a result of the measurements are presented below in Figure 4.25. According to the bed topography data, the maximum sediment height is higher on the right side of the channel in the roughness region and the sediment height is higher up to about 7 m from the unit of the roughness elements. In the region where the water velocity is high, it is seen that there are values where the sediment depth is 0 around the cubes near the left wall.

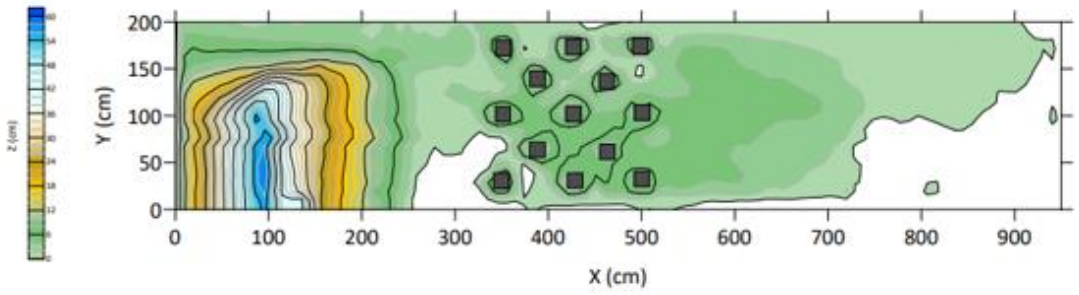

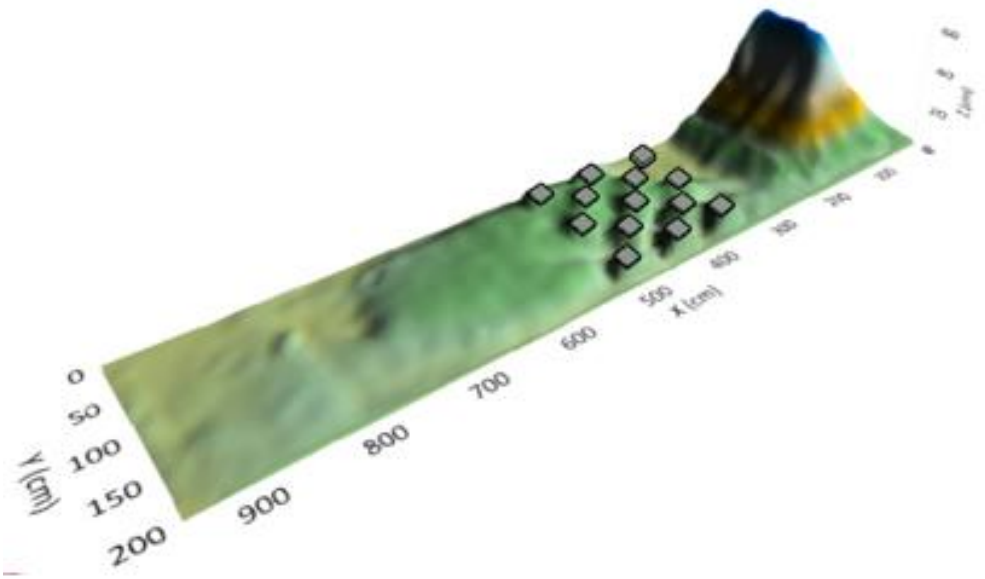


Figure 4.25: 2D and 3D contour maps of sediment distribution at the end of PR1

Symmetrical with respect to the longitudinal axis of experiment PR1, y = 0 cm and 200 cm, y = 12.5 cm and 187.5 cm, y = 25 cm and 125 cm, y = 43.75 cm and 156.25 cm, y = 62.5 cm and 137.5 cm, y= 81.25 cm and 118.75 cm, and y = 100 cm and x = 100 cm with longitudinal and traversal axes graphs of sediment heights are presented in Figure 4.26.

y = 0 cm and y = 200 cm while the maximum sediment height in the dam body is 56.1 cm and 4.8 cm, respectively. The sediment height at x = 2.02 m is 13.2 cm at y = 0 cm and 3.2 cm at y = 200 cm. The maximum sediment height between x = 2 m and x = 4 m is 13.2 cm at y = 0 cm and 3.2 cm at y = 200 cm, between x = 4 m and x = 6 m is 1.6 cm at y = 0 cm and 1.8 cm at y = 200 cm, between x = 6 m and x = 8 m is 1.1 cm at y = 0 cm and 1.8 cm at y = 200 cm, between x = 8 m and x = 9.5 m is 0.2 cm at y = 0 cm and 2.4 cm at y = 200 cm.

y = 12.5 cm and y = 187.5 cm while the maximum sediment heigt in the dam body is 56 cm and 5.1 cm, respectively. The sediment height at x = 2.02 m is 13.4 cm at y = 12.5 cm and 2.9 cm at y = 187.5 cm. The maximum sediment height between x = 2 m and x = 4 m is 13.4 cm at y = 12.5 cm and 4.8 cm at y = 187.5 cm, between x = 4 m and x = 6 m is 3.9 cm at y = 12.5 cm and 3.8 cm at y = 187.5 cm, between

x = 6 m and x = 8 m is 3.2 cm at y = 12.5 cm and 3.6 at y = 187.5 cm, between x = 8 m and x = 9.5 m is 1.1 cm at y = 12.5 cm and 2.3 cm at y = 187.5 cm.

y = 25 cm and y = 175 cm while the maximum sediment height in the dam body is 57.9 cm and 6.4 cm, respectively. The sediment height at x = 2.02 m is 14.8 cm at y = 25 cm and 4.6 cm at y = 175 cm. The maximum sediment height between x = 2 m and x = 4 m is 14.8 cm at y = 25 cm and 9.4 cm at y = 175 cm, between x = 4 m and x = 6 m is 9.7 cm at y = 25 cm and 9.8 cm at y = 175 cm, between x = 6 m and x = 8 m is 8.8 cm at y = 25 cm and 8.5 at y = 175 cm, between x = 8 m and x = 9.5 m is 2.5 cm at y = 25 cm and 2.5 cm at y = 175 cm.

y = 43.75 cm and y = 156.25 cm while the maximum sediment height in the dam body is 57.9 cm and 15.9 cm, respectively. The sediment height at x = 2.02 m is 13.8 cm at y = 43.75 cm and 10 cm at y = 156.25 cm. The maximum sediment height between x = 2 m and x = 4 m is 13.8 cm at y = 43.75 cm and 10 cm at y = 156.25 cm, between x = 4 m and x = 6 m is 8.3 cm at y = 43.75 cm and 6.1 cm at y = 156.25 cm, between x = 6 m and x = 8 m is 6.8 cm at y = 43.75 cm and 5.7 cm at y = 156.25 cm, between x = 8 m and x = 9.5 m is 2.5 cm at y = 43.75 cm and 3.2 cm at y = 156.25 cm.

y = 62.5 cm and y = 137.5 cm while the maximum sediment height in the dam body is 57.9 cm and 36.8 cm, respectively. The sediment height at x = 2.02 m is 14.1 cm at y = 62.5 cm and 14.5 cm at y = 137.5 cm. The maximum sediment height between x = 2 m and x = 4 m is 14.1 cm at y = 62.5 cm and 14.5 cm at y = 137.5 cm, between x = 4 m and x = 6 m is 10.5 cm at y = 62.5 cm and 10 cm at y = 137.5 cm, between x = 6 m and x = 8 m is 6.3 cm at y = 62.5 cm and 5.5 cm at y = 137.5 cm, between x = 8 m and x = 9.5 m is 3 cm at y = 62.5 cm and 3.4 cm at y = 137.5 cm.

y = 81.25 cm and y = 118.75 cm while the maximum sediment height in the dam body is 56.9 cm and 47.4 cm, respectively. The sediment height at x = 2.02 m is 15.1 cm at y = 81.25 cm and 13.9 cm at y = 118.75 cm. The maximum sediment height between x = 2 m and x = 4 m is 15.1 cm at y = 81.25 cm and 13.9 cm at y = 118.75 cm, between x = 4 m and x = 6 m is 8.2 cm at y = 81.25 cm and 8.7 cm at y = 118.75 cm, between x = 6 m and x = 8 m is 6.7 cm at y = 81.25 cm and 5.7 cm at y = 118.75cm, between x = 8 m and x = 9.5 m is 3.8 cm at y = 81.25 cm and 4.6 cm at y = 118.75 cm.

y = 100 cm while the maximum sediment height in the dam body is 57.3 cm. The sediment height at x = 2.02 m is 14.6 cm. The maximum sediment height between x = 2 m and x = 4 m is 14.6 cm, between x = 4 m and x = 6 m is 10.2 cm, between x = 6 m and x = 8 m is 9 cm, between x = 8 m and x = 9.5 m is 4.5 cm.

In addition, the sediment at the downstream skirt of the dam body has shifted from 200 cm to 250 cm at y=0 cm, 12.5 cm, 25 cm, 43.75 cm, 62.5, 81.25, and 100 cm sections. At x = 100 cm, the unbroken right bank height of the dam body decreased from 60 cm to an average of 56 cm.

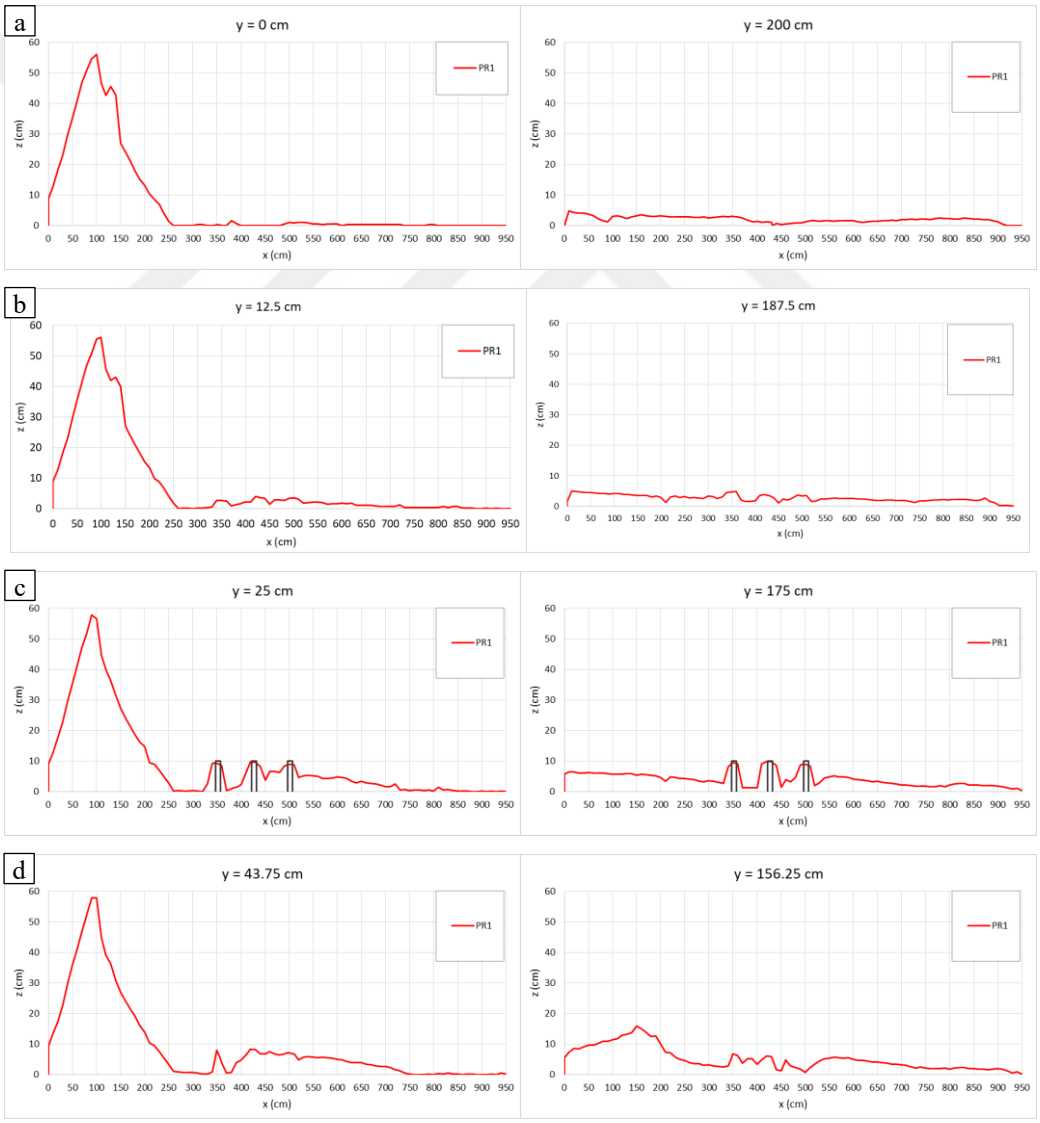

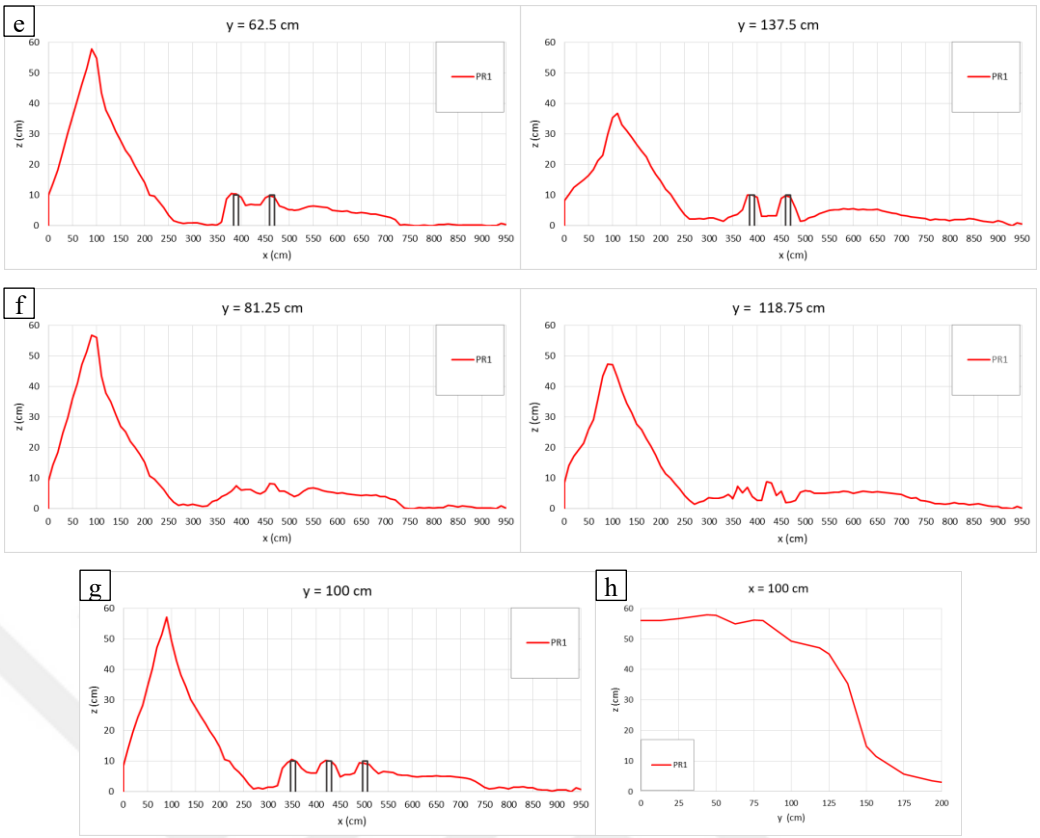


Figure 4.26: Longitudinal sediment height profiles measured at a) y = 0 cm and 200 cm, b) y = 12.5 cm and 187.5 cm, c)y = 25 cm and 125 cm, d) y = 43.75 cm and 156.25 cm, e)y = 62.5 cm and 137.5 cm, f) y= 81.25 cm and 118.75 cm, and g) y = 100 cm and along the channel width and, transversal crest section of the dam at h) x = 100 cm of PR1

Figure 4.27. a shows the levels measured by Probe 1, $R_0$ for PS1, Figure 4.27. b $R_1$, $R_2$, $R_3$, Probe 2 and Probe 3. Accordingly, the decrease in the dam body (Probe 1) in Figure 4.27. a, the decrease in the dam body between 202 s to 330 s, 55.5 cm to 43.1 cm . $R_0$ decreased from 53.5 cm to 8.2 cm at the end of 800 seconds. In Figure 3.5.5.b, the maximum water level is 340 s, 387 s, 377 s, 13 cm, 15 cm, and 12.5 cm at $R_1$, $R_2$, and $R_3$, respectively. The maximum level at Probe 2 is 11.3 cm and maximum water level Probe 3 is 14.3 cm at 345 s and 357 s, respectively.

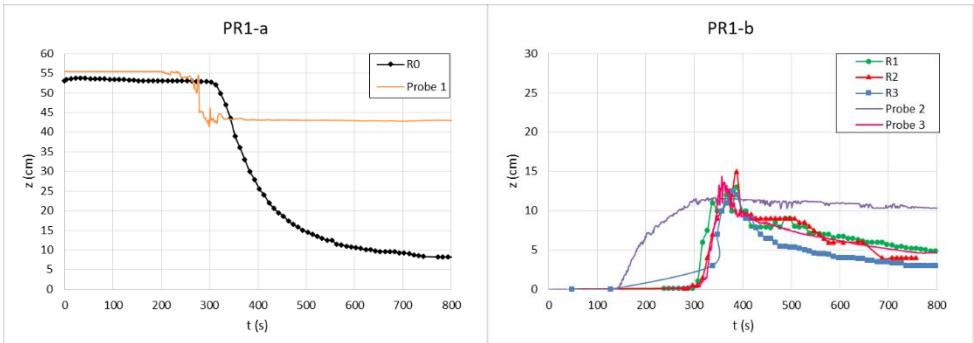


Figure 4.27: Level measurements for PR1 experiment a) measured from $R_0$ and Probe 1, b) measured from $R_1$, $R_2$, $R_3$, Probe 2 and Probe 3

### 4.5.1 Repeatability of Fourth Scenario Experiments

The fourth break scenario was performed in 2 repetitions under the same condition. In Figure 4.28, for experiments PR1 and PR2 sediment height graphs at y = 0 cm and 200 cm, y = 12.5 cm and 187.5 cm, y = 25 cm and 125 cm, y = 43.75 cm and 156.25 cm, y = 62.5 cm, 137.5 cm, y= 81.25 cm and 118.75 cm, y = 100 cm and x = 100 cm are given. Accordingly, it is seen that the sediment section graphs of the experiments carried out in the rough downstream condition are compatible with each other and the sediment distributions are almost the same.

For the PR2 experiment, 602 s after the water started to seepage from the skirt of the dam, it reached the first red line. It took 18 s for the seepage water to reach $R_1$ from the red line, 33 s to reach $R_2$ from $R_1$, and 86 s to reach $R_3$ from $R_2$. After the water and sediment mixture started to propagate downstream, it took 9 s to reach $R_1$, 9 s to reach $R_1$ from $R_2$, and 4 s to reach $R_3$ from $R_2$. Water reached $R_2$ in 133 s and the water and sediment mixture reached $R_2$ in 51 s after water passed the first red line. In the PR 2 experiment, according to PR1, it was 558 s longer for the first red line after the water started to seepage from the skirt of the dam, and 52 s earlier for the water seepage to reach $R_1$ from the red line. It took 15 s earlier from $R_1$ to $R_2$ and 45 s longer from $R_2$ to $R_3$. It took 1 s longer for the water and sediment mixture to reach $R_1$ after it started propagating downstream, 1 s longer for it to reach $R_2$ from $R_1$, and 1 s earlier for it to reach $R_3$ from $R_2$.

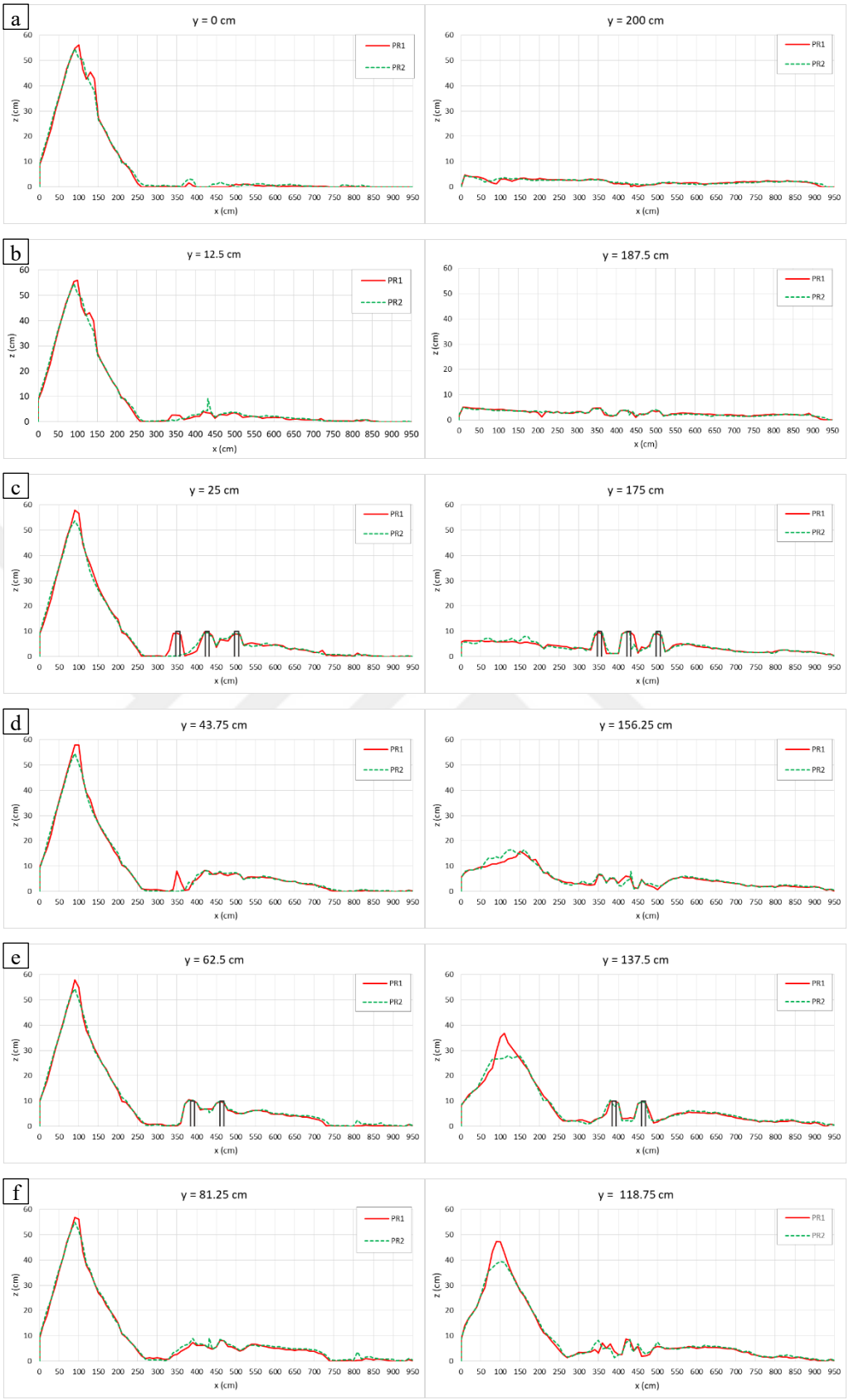
a
y = 0 cm
y = 200 cm
b
y = 12.5 cm
y = 187.5 cm
c
y = 25 cm
y = 175 cm
d
y = 43.75 cm
y = 156.25 cm
e
y = 62.5 cm
y = 137.5 cm
f
y = 81.25 cm
y = 118.75 cm
PR1
PR2
z (cm)
x (cm)

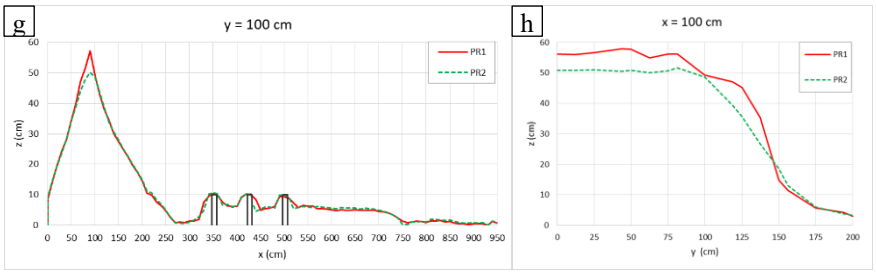


Figure 4.28: Longitudinal sediment height profiles measured at a) y = 0 cm and 200 cm, b) y = 12.5 cm and 187.5 cm, c)y = 25 cm and 125 cm, d) y = 43.75 cm and 156.25 cm, e)y = 62.5 cm and 137.5 cm, f) y= 81.25 cm and 118.75 cm, and g) y = 100 cm and along the channel width and, transversal crest section of the dam at h) x = 100 cm of PR1 and PR2

Figure 4.29 shows the graph of the $R_0$, $R_1$, $R_2$, $R_3$, Probe 1, Probe 2, and Probe 3 measurements of the PR1 and PR2. Accordingly, it is seen that the ruler and probe measurements are compatible with each other in the experiments

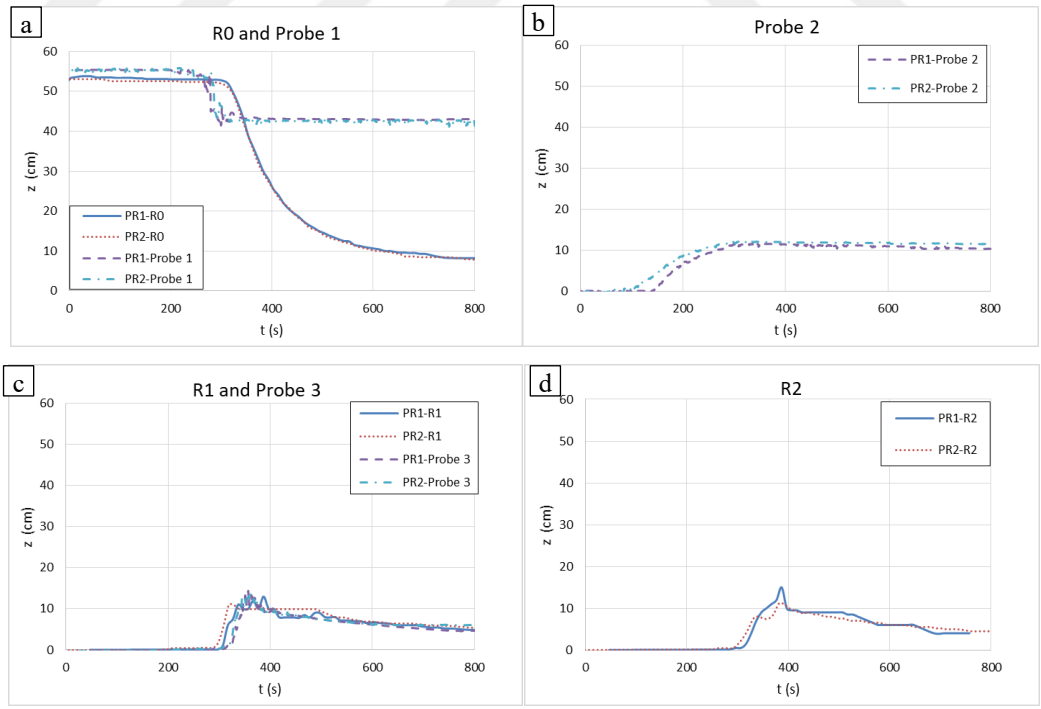

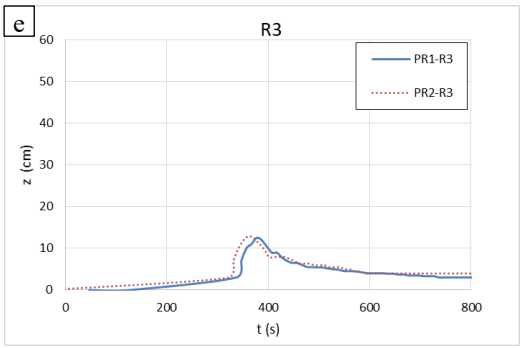


Figure 4.29: Level measurements for experiment PR1 and PR2 experiments measured from a) $R_0$ and Probe1, b) Probe 2, c) $R_1$ and Probe 3, d) $R_2$, and e) $R_3$

## 4.6 Comparison of the Experimental Results

### 4.6.1 Regarding Sediment Distribution: Longiditudinal x-Section, Overtopping and Piping Downstream Conditions

The average of the sediment height of the OS1 and OS2, first scenario experiments is given as smooth, and the average of the sediment height of the OR1 and OR2, second scenario experiments is rough, in Figure 4.30 left side, the sediment section graphs are given. While the sediment distribution in the graphs is higher between 3.50 m - 5 m in the rough experiments, except for this part it propagation at similar heights in the channel. The average of the sediment height of the PS1 and PS2 experiments is given as smooth, and the average of the sediment height of the PR1 and PR2 experiments is rough, in Figure 4.30 rigt side, the sediment section graphs are given. Like overtopping experiments, sediment distribution in the graphs is higher between 3.50 m - 5 m in the rough experiments, except for this part it propagation at similar heights in the channel.

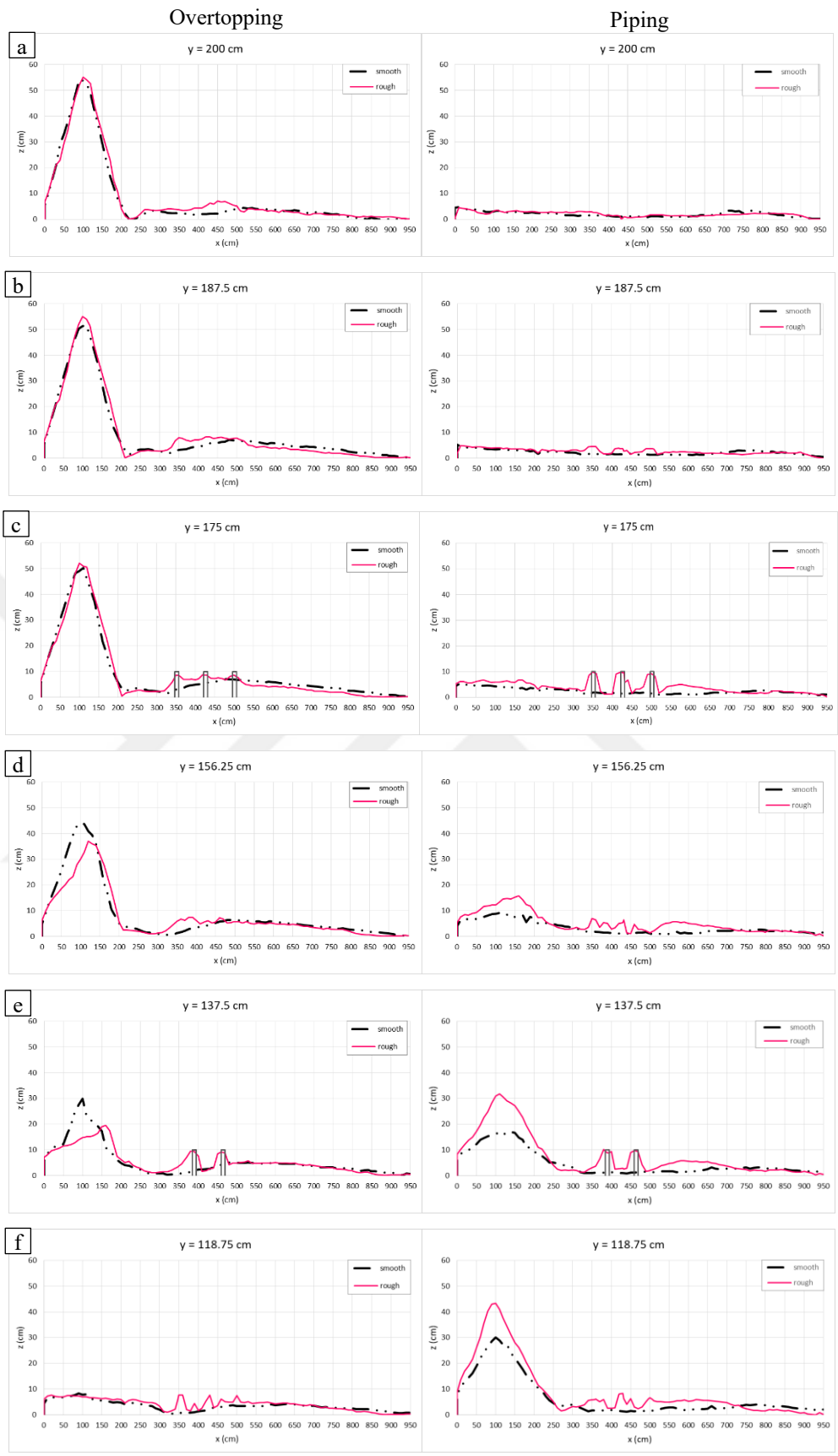
Overtopping
Piping
a
y = 200 cm
b
y = 187.5 cm
c
y = 175 cm
d
y = 156.25 cm
e
y = 137.5 cm
f
y = 118.75 cm
smooth
rough
z (cm)
x (cm)

Overtopping

Piping

g

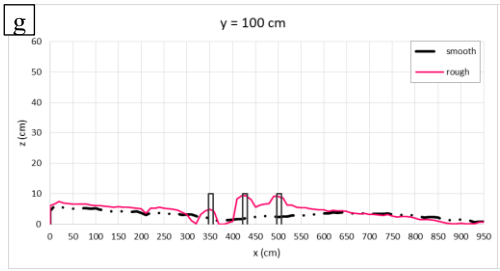


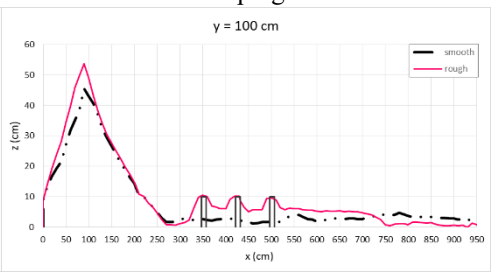


h

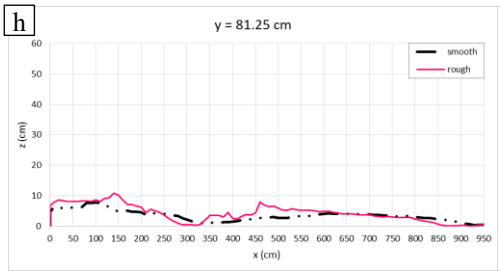


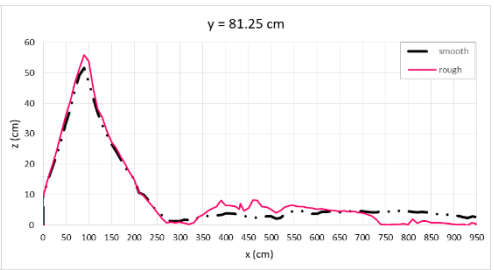


i

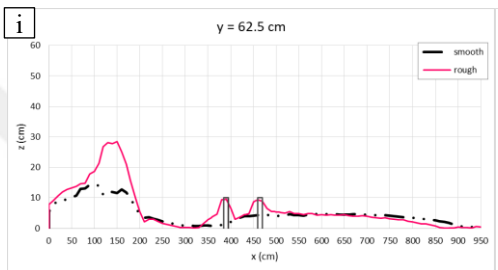


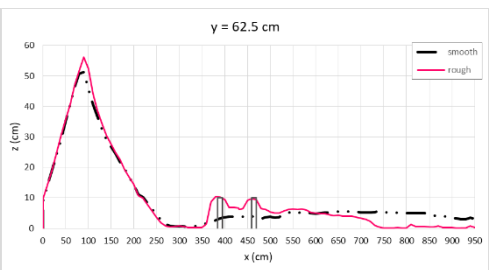


j

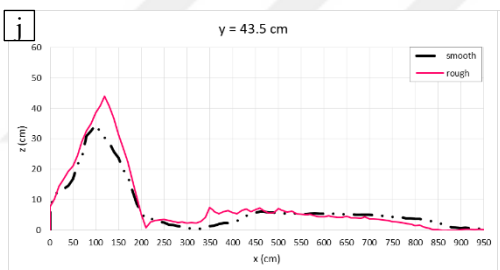


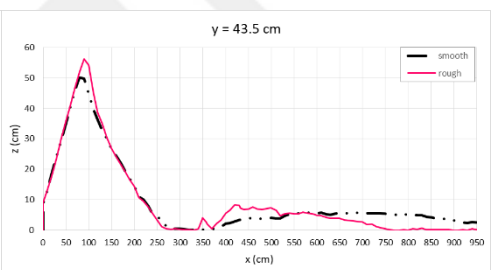


k

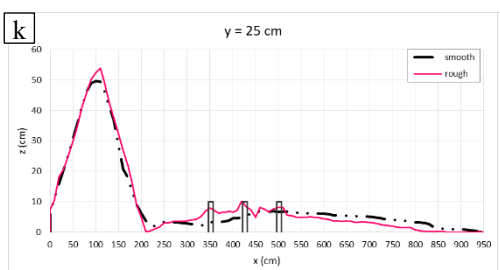


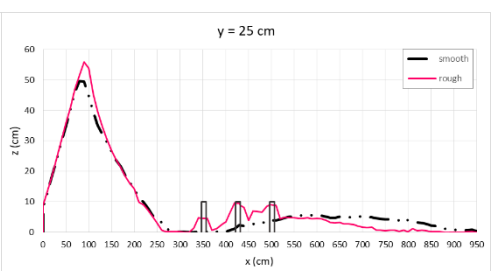


l

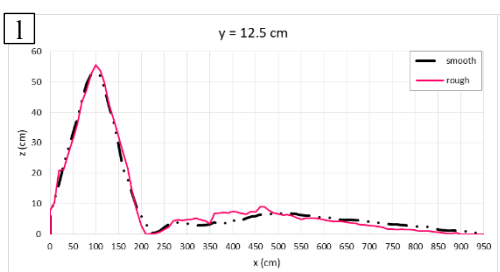


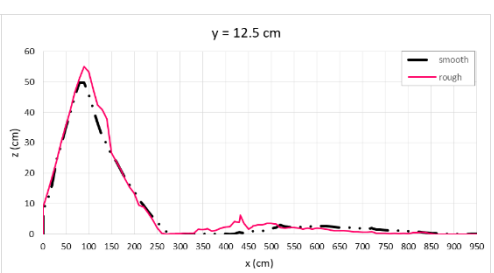

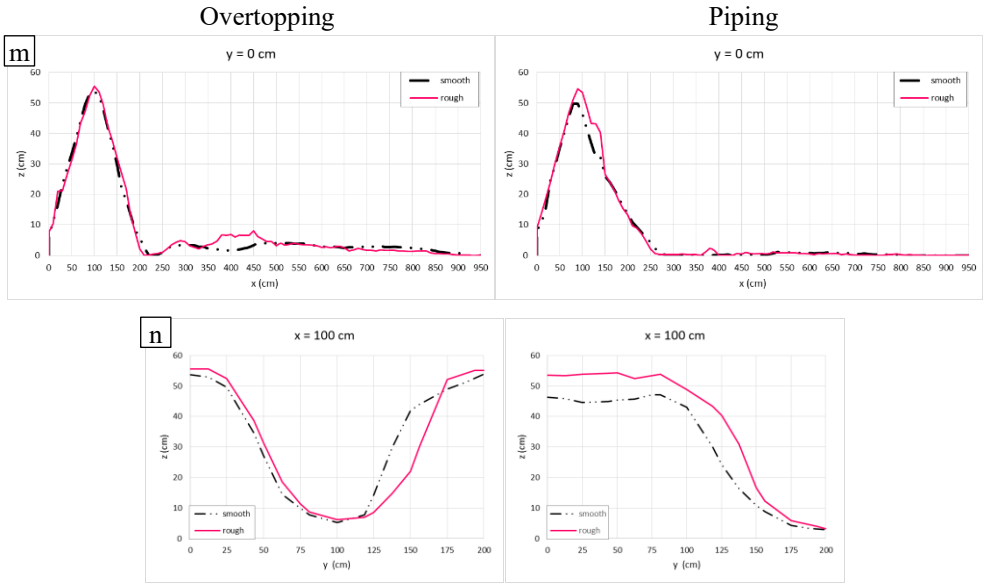


Figure 4.30: Longitudinal sediment height profiles measured at a) y =200 cm, b) y = 187.5 cm, c) 125 cm, d) 156.25 cm, e) 137.5 cm, f) 118.75 cm, and g) y = 100 cm, h) y = 81.25 cm, i) 62.5 cm, j) y = 43.5 cm, k) y = 25 cm, l) y = 12.5 cm, m) y = 0 cm and along the channel width and, transversal crest section of the dam at n) x = 100 cm of average smooth and rough downstream condition for overtopping (left), and piping (right)

According to Figure 4.30;

- In the overtopping experiments the breach widened in the middle of the dam body, the right and left parts of the dam body remained standing and the middle of the dam body propagated downstream. In the piping experiments the dam body broke from the left, and the left parts of the dam body remained standing.

- While the sediment distribution in the graphs is higher between 3.50 m - 5 m in the rough experiments, except for this part it propagation at similar heights in the channel.

- Rough experiment sediment height is higher than smooth experiments.

It has been observed that both the break of the homogeneous earth- fill dam overtopping and piping will cause significant morphological changes in the reservoir of the dam and accumulation in the settlement areas.

### 4.6.2 Regarding Sediment Distribution: Longiditudinal x-Section, Smooth and Rough Downstream Conditions

The average of the sediment height of the overtopping and piping, experiments is given as smooth on the right side, and the average of the sediment height of the overtopping and piping experiments is given as rough on the left side, the sediment section graphs are given in Figure 4.31. Since the break directions of the overtopping and piping experiments are different, the heights of the dam body between 0 cm and 43.5 cm, where the dam body is located, are similar. In this range, sediment propagated heights are higher in the overtopping experiment for both smooth and rough downstream conditions. Sediment heights between 62.5 cm and 118.5 cm are approximately the same. Sediment heights from 137.5 cm to 200 cm are higher for both smooth and rough downstream conditions in the overtopping experiment.

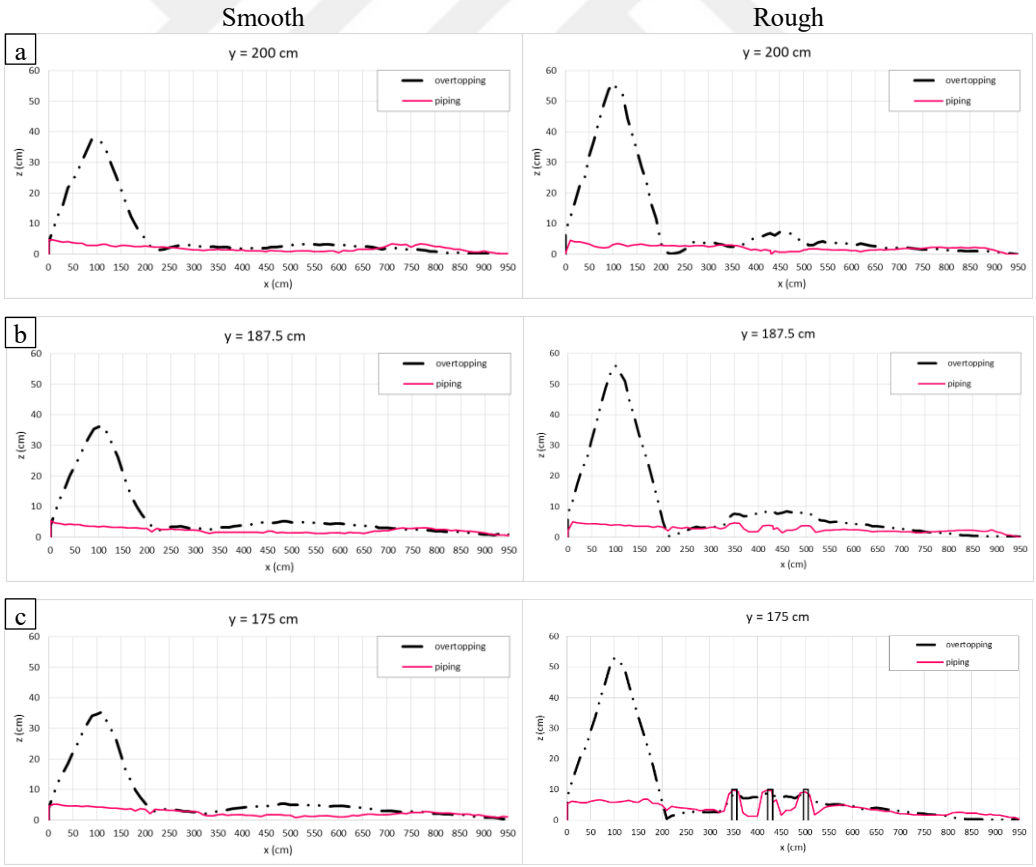

Smooth Rough

d

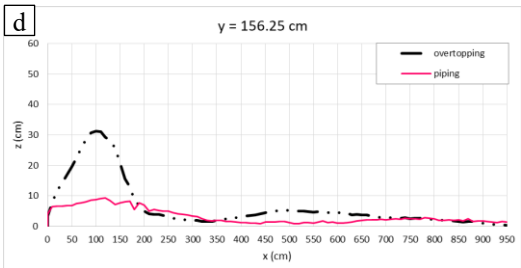


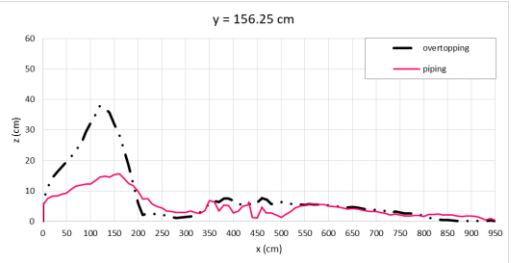


e

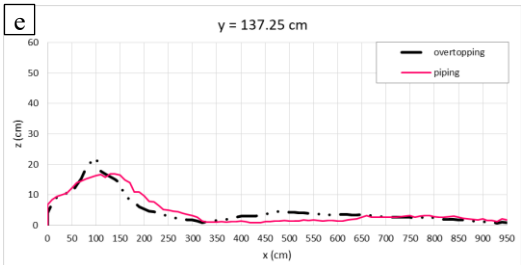


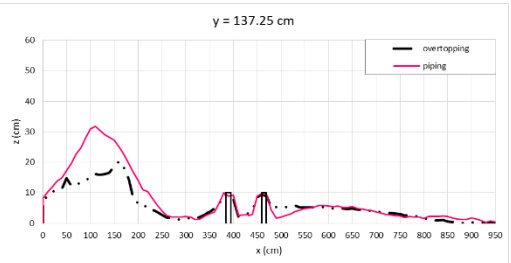


f

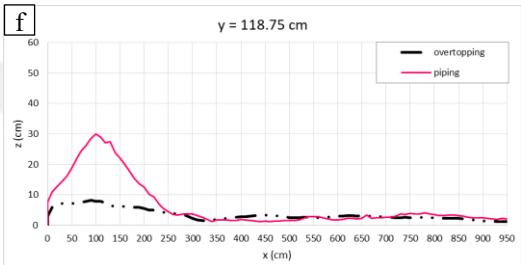


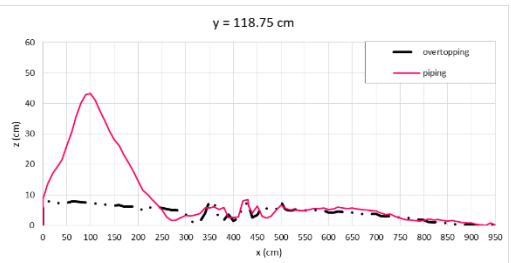


g

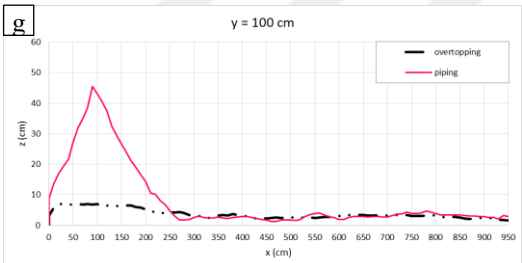


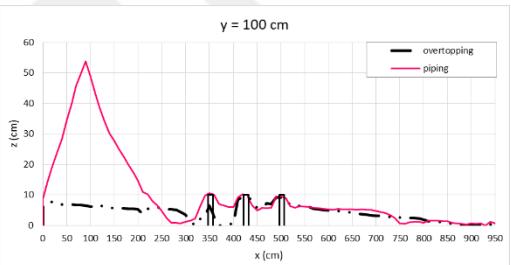


h

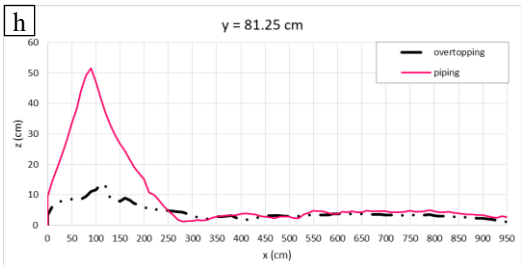


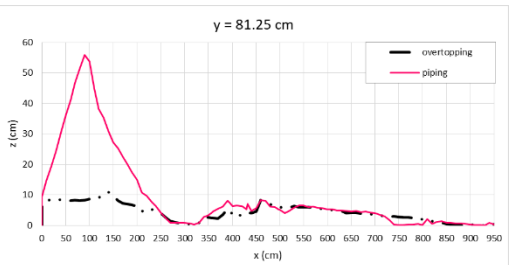


i

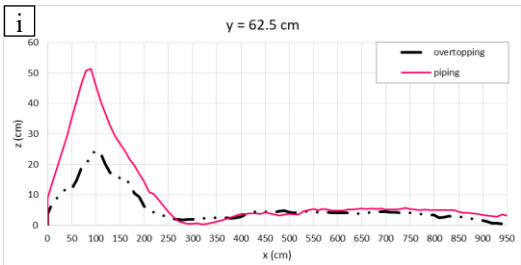


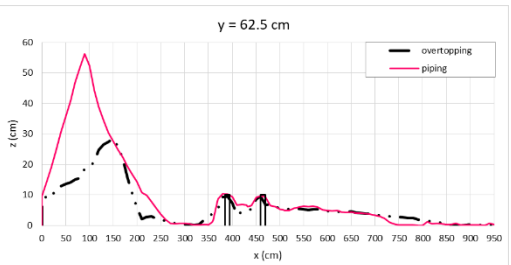

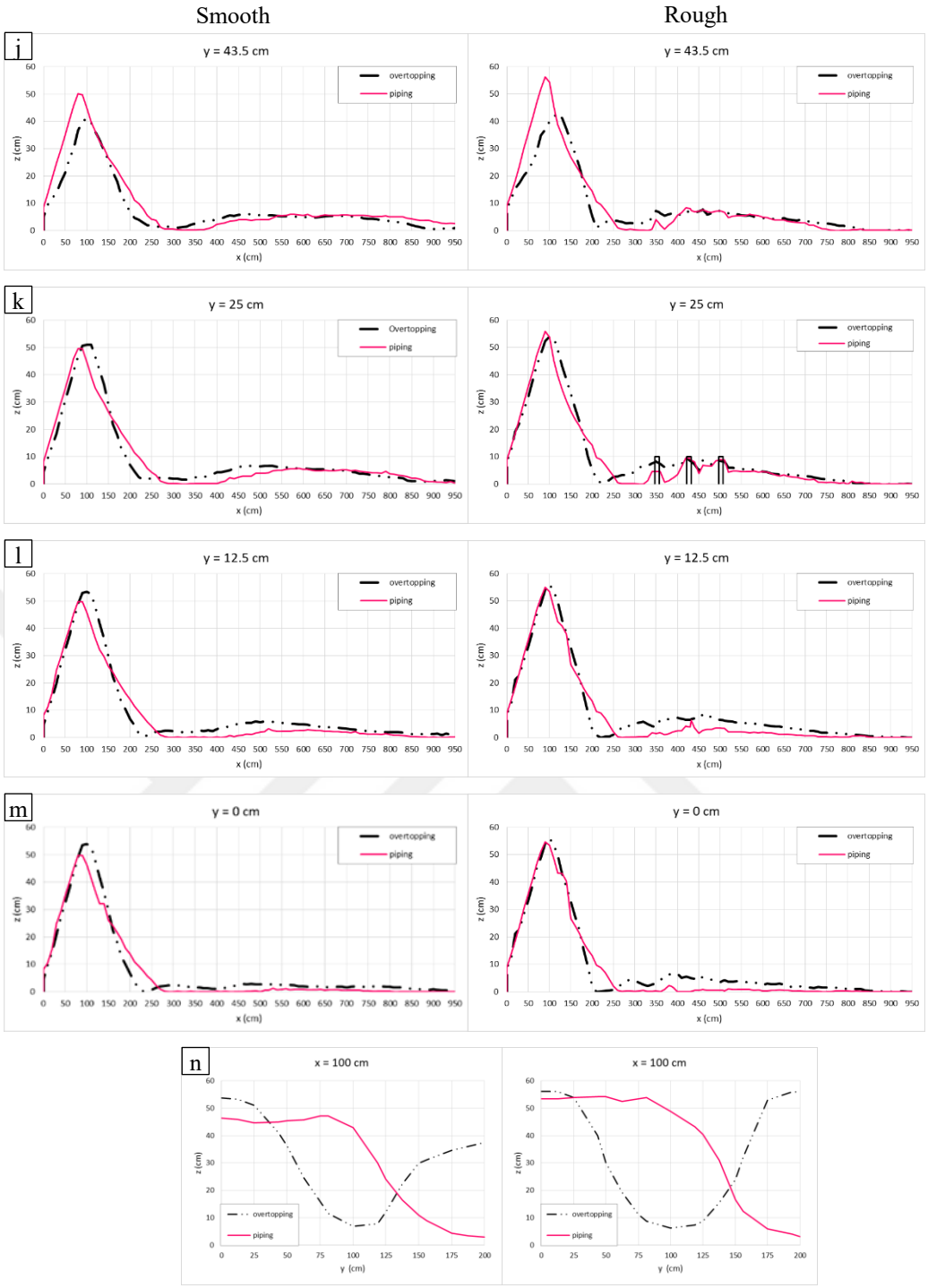


Figure 4.31: Longitudinal sediment height profiles measured at a) y =200 cm, b) y = 187.5 cm, c) 125 cm, d) 156.25 cm, e) 137.5 cm, f) 118.75 cm, and g) y = 100 cm, h) y = 81.25 cm, i) 62.5 cm, j) y = 43.5 cm, k) y = 25 cm, l) y = 12.5 cm, m) y = 0 cm and along the channel width and, transversal crest section of the dam at n) x = 100 cm of average smooth and rough downstream condition for smooth (left), and rough (right)

### 4.6.3 Regarding Sediment Distribution: Plan View

The contour graphs of the sediment propagated along the channel as a result of the break of the dam by overtopping and piping are presented in Figure 4.32. The left side of the figure shows the overtopping experiment, and the right side shows the piping experiment. The first line shows the experiment for the smooth downstream condition, and the bottom line shows the experiment for the rough downstream condition.

According to Figure 4.32;

- In the experiments, the sediment was propagated to the downstream region, covering both the width and the length of the channel.
- Sediment depths are not equally propagated along the channel. In regions where the flood wave is fast, the sediment depths are lower.
- In the smooth downstream condition experiments, the sediment depths are thicker in the opposite direction of the dam break.
- When the dam breaks flow coming from the right wall, the sediment heights of the sections close to the left wall in the downstream region are higher. When the dam breaks flow coming from the middle section, the sediment heights in the sections close to the right and left walls are higher.
- The roughness elements placed downstream of the dam caused the sediment to accumulate around the cubes. It has been observed that the sediment height is high in the parts that are not under the impact of the flood wave in the areas close to the roughness area.
- In the roughness region, the flood wave prevented sediment accumulation around the cube hit by the flood wave. The upstream sediment heights of some cubes are 0.

Overtopping

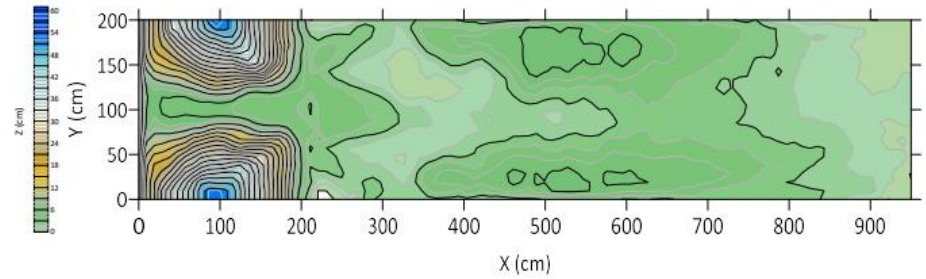


Smooth

Piping

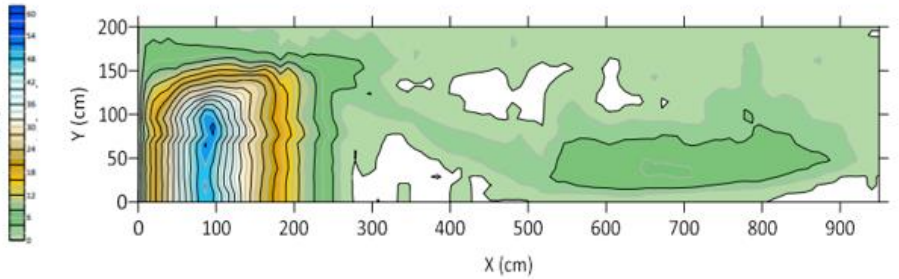


Smooth

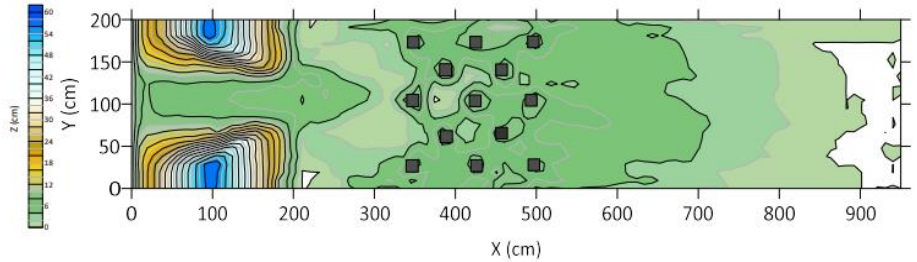


Rough

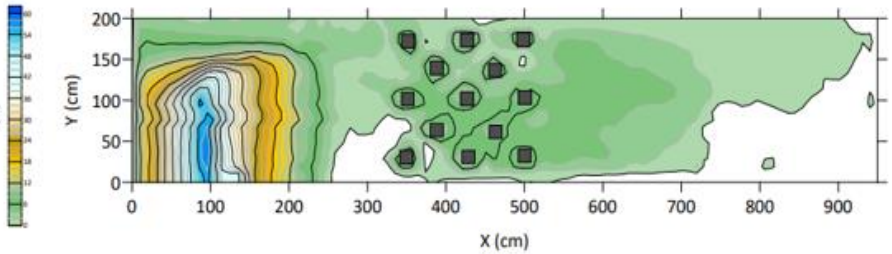


Rough

Figure 4.32: The contour graphs of the experiments sediment propagated along the channel

## 4.6.4 Regarding Water Level

Overtopping and piping experiments average smooth and rough condition graphs for ruler 2 (x = 4.5 m), ruler 3 (x = 7.5 m), and probe 3 (x = 6 m) measurements are given in Figure 4.33.

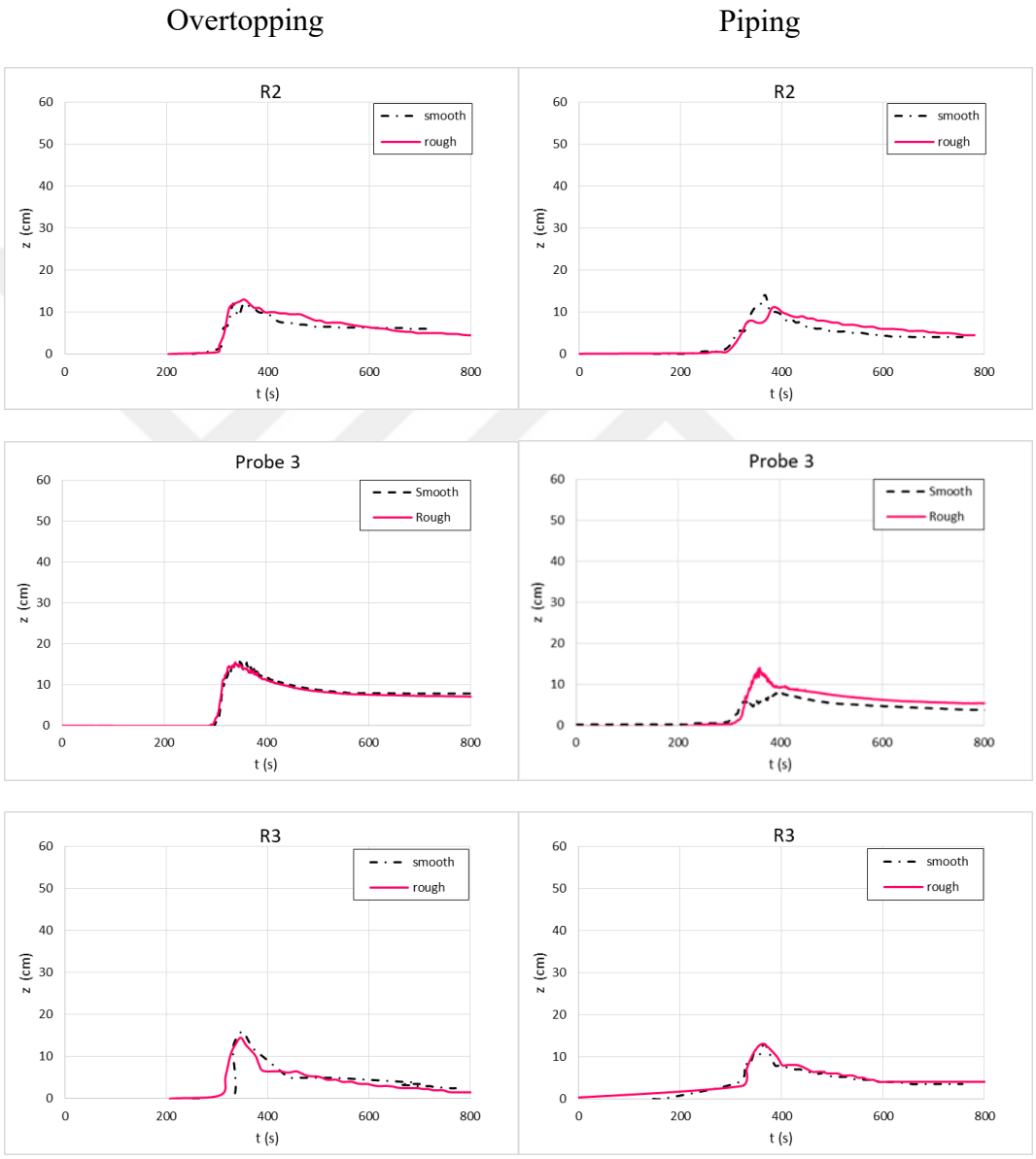


Figure 4.33: Average water depth for overtopping and piping experiments in smooth and rough downstream conditions

According to Figure 4.33;

- Overtopping smooth and rough experiments rulers and probes measurements are almost the same.
- Piping experiments have the same water curve but in rough experiments, the water level is higher than in smooth experiments. The reason can be for these differences in piping experiments breaking the left bank and water propagating the channel from the left bank.

Table 4.1, Table 4.2 and Table 4.3 shows the progress times of sediment and water flow from specific points of the channel to the overtopping experiments. In the Table 4.1 the average time for the water to reach the first red line after crossing the breach is 45 s. In Figure 34 as shown water pass from the breach (a) and water crossed the first red line (b). Figure 4.35 is shown water crossed the $R_2$.

Table 4. 1: Time differences between the water pass from the breach to the red line

| | Average Δt |
|---|---|
| Water pass from the breach | |
| | 45 s |
| Water crossed the first red line (x = 2.52 m) | |

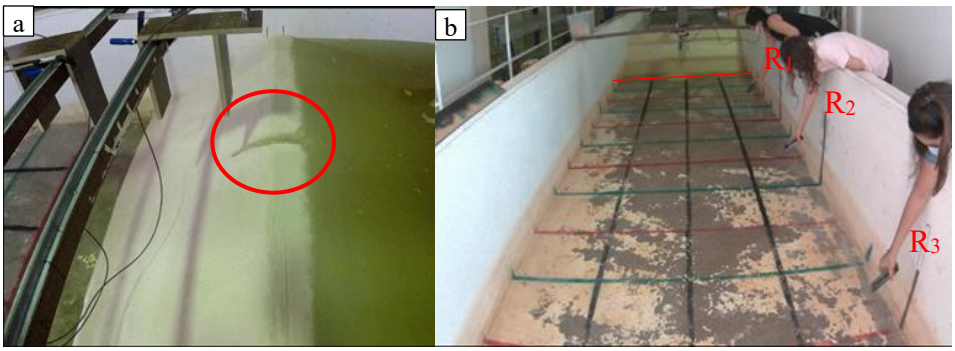


Figure 4.34: Water pass from the breach (a) and water crossed the first red line (b)

Table 4. 2: The time differences between the water crossed the red line to $R_2$

| Δt | smooth | rough |
|---|---|---|
| Water crossed the first red line (x = 2.52 m) | | |
| $R_2$ (x = 6 m) | 24 s | 24 s |

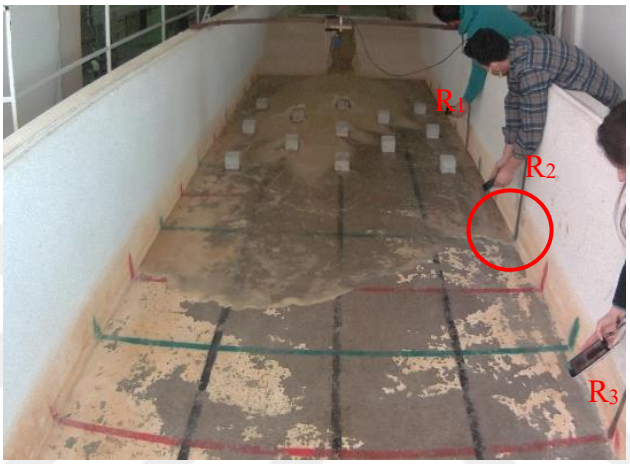


Figure 4.35: Water crossed the $R_2$

Table 4. 3: The average time differences between the water crossed the red line to $R_1$, $R_1$ to $R_2$, and $R_2$ to $R_3$ for smooth and rough experiment

| Δt | smooth | rough |
|---|---|---|
| Water crossed the first red line (x = 2.52 m) | | |
| $R_1$ (x = 4.5 m) | 19 s | 19 s |
| $R_2$ (x = 6 m) | 5 s | 5 s |
| $R_3$ (x = 7.5 m) | 3 s | 4 s |

Acording to Table 4.2 and Table 4.3 time differences between $R_1$-$R_2$ is higher than the $R_2$-$R_3$. Since the water has passed through the breach, the water has moved faster in the mixture of water and sediment. With the widening of the breach, the transport rate of the sediment increased. When smooth and rough experement were compared, roughness did not have a significant effect on the water wave propagation speed.

Table 4.4 is shown piping experiments, the differences between the starting time of the sediment on the downstream skirt of the dam and the starting time of the water to seepage in an average of 15 s for all piping experiments. Table 4.4 is also shown time disfferences between water passing from the red line and sediment passing from the red line. These difference average 27 s. In Figure 4.36. a is shown water seepage start from dam body skirt and Figure 4.36. b sediment passing from the red line.

Table 4. 4: The average time differences between water seepage and sediment movement start from the dam body skirt and, water and sediment passing from the red line

| | Average Δt |
|---|---|
| Water seepage start from dam body skirt | 15 s |
| Sediment movement start from dam body skirt | Average Δt |
| Water passing from the red line x = 2.52 | 27 s |
| Sediment passing from the red line | |

In the overtopping experiments, the sediment movement starts by propagating to the downstream region after crossing the breach. In the piping experiments, first come to seepage water from the dam skirt, in order for the sediment to propagate to the downstream region, the downstream face of the dam was exposed to erosion and the

dam skirt slipped 50 cm downstream on average, and the downstream sediment and flood wave propagated after the downstream slope of the dam was minimum 28 ˚

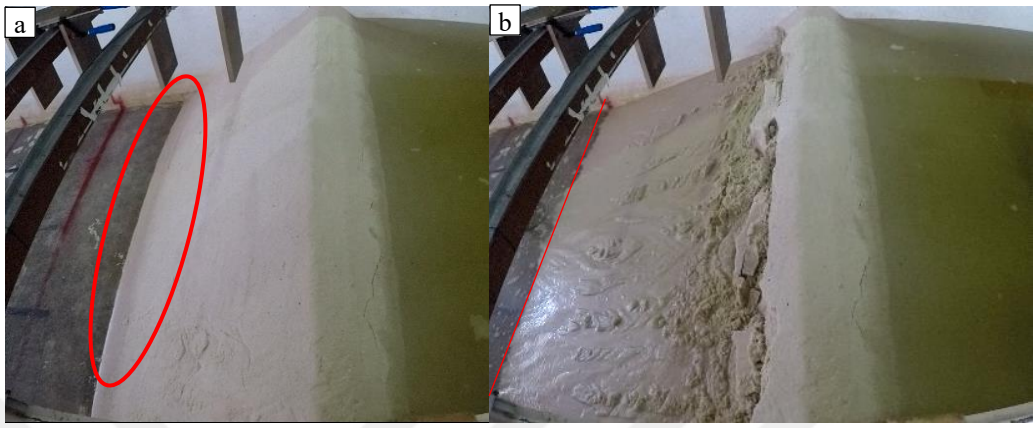


Figure 4.36: Water seepage start from dam body skirt (a) and sediment passing from the red line (b)

Table 4.5 shows the piping experiments' propagation time of water and sediment at specific points of the channel for the piping experiments. In Figure 4.37 is shown seepage water coming from dam body and in Figure 4.38 is shown flood wave water coming to $R_1$, $R_2$ and $R_3$. According to this Table 4.5 important difference is that the time difference between the arrival of the first seepage to $R_1$ and the arrival of the second flood wave to $R_1$ is greater than the time between the first and second waves arriving at $R_2$ and $R_3$. In the $R_3$ scale, the time difference between the arrival of the first and second waves is the shortest in all experiments. Accordingly, it is possible to say that the velocity of the water in the reservoir increases as it progresses along the channel. In all piping experiments, the differences between the starting time of the sediment on the downstream skirt of the dam and the starting time of the water to seepage in are close to each other. In addition, the time for water to cross the red line and for the sediment to come to the red line is almost the same, except for the $PS_2$ experiment. Since the water has passed through the breach, the water has moved faster in the mixture of water and sediment. With the widening of the breach, the transport rate of the sediment increased. For piping experiments, the first seepage water coming from the dam skirt to $R_1$ and the coming of the second flood wave to $R_1$ is greater than

the time between the first and second wave coming at $R_2$ and $R_3$. When smooth and rough experement were compared for piping experiments, roughness increases the propagation time of the water wave.

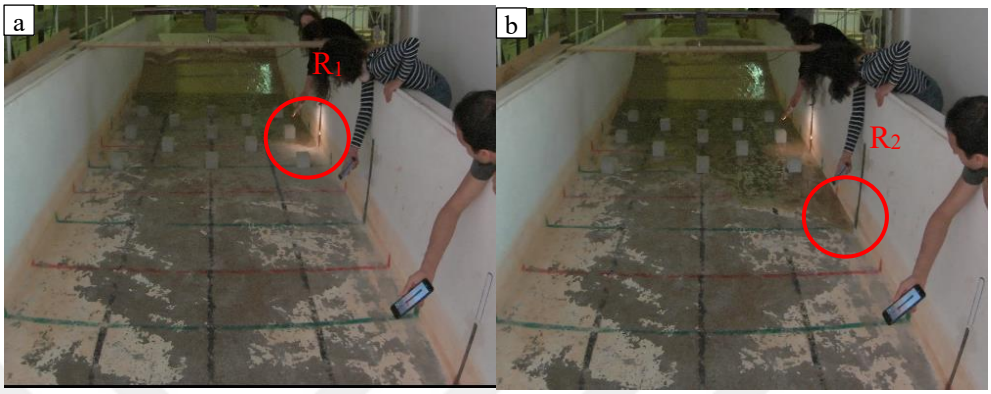


Figure 4.37: Water seepage reach $R_1$ (a) and water seepage reach $R_2$ (b)

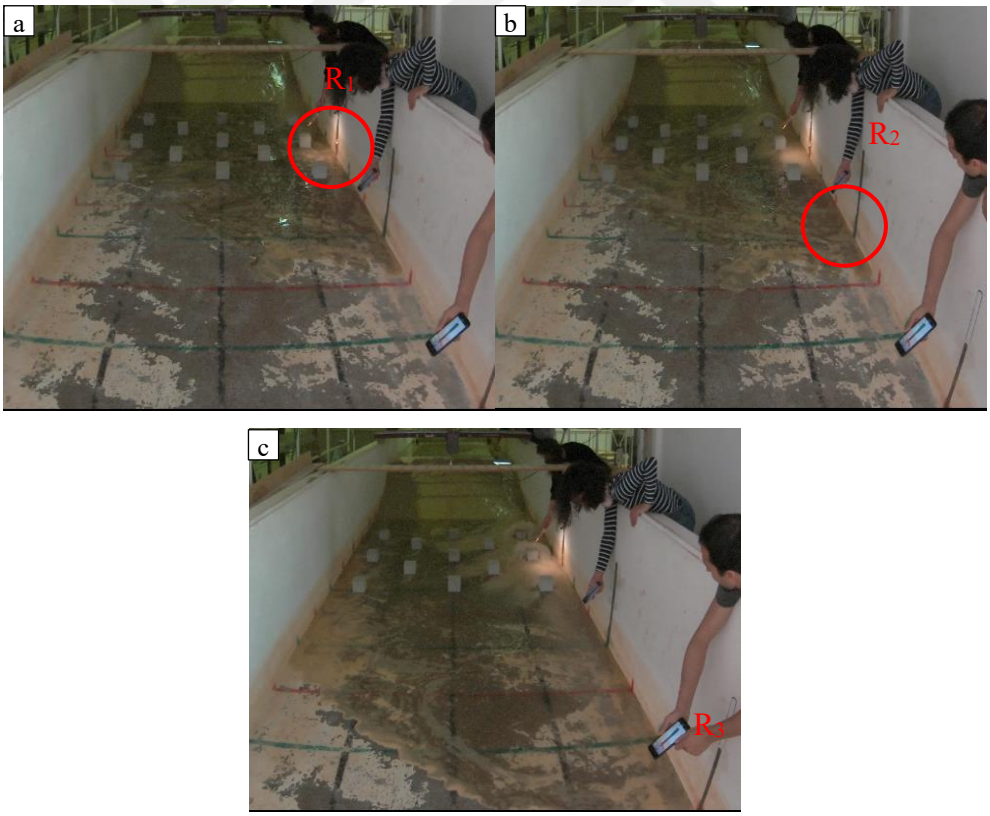


Figure 4.38: Flood wave reach a) $R_1$, b) $R_2$, c) $R_3$

Table 4. 5: The piping experiments propagation time of water and sediment at specific points of the channel for the piping experiments

| Δt | smooth | rough |
|---|---|---|
| $R_1$ first (x = 4.5m) | | |
| | 51 s | 41 s |
| $R_2$ first (x = 6 m) | | |
| | 76 s | 64 s |
| $R_3$ ( x = 7.5m) | | |
| Δt | smooth | rough |
| $R_1$ second ( x = 4.5 m) | | |
| | 5 s | 4 s |
| $R_2$ second (x= 6 m) | | |
| | 4 s | 5 s |
| $R_3$ ( x = 7.5 m) | | |
| Δt | smooth | rough |
| $R_1$ first ( x = 4.5 m) | | |
| | 106 s | 111 s |
| $R_1$ second ( x = 4.5 m) | | |
| Δt | smooth | rough |
| $R_2$ first ( x = 6 m) | | |
| | 69 s | 82 s |
| $R_2$ second ( x = 6 m) | | |

# Chapter 5

# Conclusion

In this study, the changes in the bed morphology of the sediment propagation to the downstream region by the flood wave as a result of the break of the homogeneous earth-fill dam, and the determination of the propagation of the sediment were investigated. In a long and wide laboratory channel, 8 experiments were carried out under 4 different break scenarios, with 2 replications of two different types of a break as overtopping piping, in smooth and rough downstream conditions. Accordingly, 2 of the 4 overtopping experiments were carried out in smooth and 2 in rough downstream conditions. Likewise, piping experiments were carried out in 2 rough and 2 smooth downstream conditions. The videos taken from two cameras placed in the channel during the experiments, the water level measurements taken from the rulers placed in certain parts of the channel during the experiment, and the measurements taken from the ULS40-D device placed on the longitudinal axis of the channel were used to evaluate the results of the experiments. At the end of the experiment, maps of the height of the sediment were obtained with the height measurements taken to determine the sediment heights.

According to the obtained data, the following results were obtained, it has been observed that both the break of the homogeneous earth- fill dam from the top and the break as a result of piping will cause significant morphological changes in the reservoir of the dam and accumulation in the settlement areas. Since the water has passed through the breach, the water has moved faster in the mixture of water and sediment. With the widening of the breach, the transport rate of the sediment increased. Sediment depths are not evenly propagated along the channel. In regions where the flood wave is fast, the sediment depths are lower. The roughness elements placed downstream of the dam caused the sediment to accumulate around the cubes. It has been observed that

the sediment height is high in the parts that are not under the impact of the flood wave in the areas close to the roughness area. In the repetitions of all scenario experiments, the increases and decreases in the rulers and probes measurements are compatible with each other. In all experiments, hydraulic jumps were observed shortly after the flood wave and sediment began to propagate to the downstream region. It was observed that the sediment accumulation increased with the passing of the effect of the hydraulic jump. According to smooth and rough downstream conditions, rough experiments sediment hight is higher. According to overtopping and piping experiment, overtopping type dam break sediment hight is higher than piping type. In water depth and propagation of water, there are no specific differences between experiments.

It can be useful to diversify these experimental scenarios, to determine the spread of the flow and sediment to the downstream region, and to approve the numerical modeling studies. At the same time, experimental data to be obtained from different break-type scenarios of existing dams and numerical modeling results can lead to the necessary planning by determining the risky areas that may occur during break and the areas to be affected.

# References


[1] Dams and Development A New Framework The Report Of The World Commission On Dams, Earth-scan Publications Ltd; 2000.

[2] International Commission on Large Dams, Deterioration of Dams and Reservoirs, Examples and Their Analysis, 1983. http://www.icold-cigb.org

[3] Snorteland, N. J., Shaffner, P. and Paul, D. Fontentelle Dam. Ririe Dam and Teton Dam-An Examination of the Influence of the Organizational Culture on Decision Making. USACE Stanford Risk Symposium; 2015.

[4] Urzica, A.; Mihu-Pintilie, A.; Stoleriu, C.C.; Cîmpianu, C.I.; Hu¸tanu, E.; Pricop, C.I.; Grozavu, A. Using 2D HEC-RAS Modeling and Embankment Dam Break Scenario for Assessing the Flood Control Capacity of a MultiReservoir System (NE Romania). Water 2021, 13, 57. https://doi.org/ 10.3390/w13010057

[5] Brunner, G.. Using HEC-RAS for Dam Break Studies, TD-39. US Army Corps of Engineers—Hydrologic Engineering Center (Hec), 1–74.

[6] Costa, J. E. Floods from Dam Failures; Open File Report. US Geological Survey: Denver, CO, USA, 54, 1985; 85-560.

[7] Bozkuş Z Afet yönetimi için yönetime için baraj yıkılma analizleri. Teknik Dergi 2004; 15(4), 3335-3350.

[8] Abay, O., Baykan, N., Baykan, N.O. The Reasons for Getting Out of Dams Through out History. 4th Water Structures Symposium, Congress Symposium Proceedings, 157-166, 19-21 November 2015, Istanbul.

[9] Living with Dams, Know Your Risks, FEMA Federal Emergency Management Agency, FEMA 2013; P-956, 2013.

[10] https://en.wikipedia.org/wiki/Dam_failure

[11] Kocaman, S. Baraj Yıkılması Probleminin Deneysel ve Teorik Olarak İncelenmesi (doctoral thesis). Çukurova Üniversitesi Fen Bilimleri Enstitüsü, Adana; 2007.

[12] Xiong Y. A Dam Break Analysis Using HEC-RAS, Journal of Water Resource and Protection, 2011; 3(6). 370-379.

[13] Güngör M. TOPRAK DOLGU BARAJLARDAKİ SIZMA OLAYININ SONLU ELEMANLAR MODELİ. Pamukkale Üniversitesi Mühendislik Bilimleri Dergisi. 1995; 1(1): 33-38.

[14] Zorluer İ. Toprak Dolgu Barajlarda Borulanma ve Bir Borunlanma Göçmesi: Teton Barajı. Afyon Kocatepe Üniversitesi Fen Ve Mühendislik Bilimleri Dergisi. 2001; 1(1): 135-146.

[15] Foster, M., Fell, R., ve Spannagle, M. (2000). The statistics of embankment dam failures and accidents. Canadian Geotechnical Journal, 37(5), 1000-1024.

[16] Tingsanchali, T. and Chinnarasri C.. 'Numerical modelling of dam failure due to flow overtopping', Hydrological Sciences Journal,2001; 46(1), 113-130, DOI: 10.1080/02626660109492804

[17] Capart, H. & Young, D.L. 1998. Formation of a jump by the dam-break wave over a granular bed. Journal of Fluid Mechanics 372: 165-187.

[18] Fell, Robin, Chi Fai Wan, John Cyganiewicz, and Mark Foster. 2003. "Time for Development of Internal Erosion and Piping in Embankment Dams." Journal of Geotechnical and Geoenvironmental Engineering 129 (4): 307–14. https://doi.org/10.1061/(asce)1090-0241(2003)129:4(307).

[19] Hanson, G. J., Cook, K. R., ve Hunt, S. L. (2005). Physical modeling of overtopping erosion and breach formation of cohesive embankments. Transactions of the ASAE, 48(5), 1783-1794.

[20] Wu, W. and Wang, S.S.. One-Dimensional Modeling of Dam-Break Flow over Movable Beds. Journal of Hydraulic Engineering, ASCE.2007.

[21] Alcrudo, F. and Mulet J. (2007). 'Description of the Tous Dam break case study (Spain)', *Journal of Hydraulic Research*, 45(sup1), 45-57, DOI: 10.1080/00221686.2007.9521832.

[22] Zhang J.Y., Xiang, L.G. Xuan, G.X., Wang, X.G. and Li J. (2009) 'Overtopping breaching of cohesive homogeneous earth- dam with different cohesive strength', Science in China Series E Technological Sciences, 52(10),3024-3029, DOI: 10.1007/s11431-009-0275-1.

[23] Carrivick L., Dam break – Outburst flood propagation and transient hydraulics: A geosciences perspective,Journal of Hydrology,Volume 380, Issues 3–4, 2010; 338-355,ISSN 0022-1694, DOI: S0022169409007185.

[24] Kocaman S., Güzel H. Baraj Yikilmasi Taşkın Dalgası Yayılmasının 3-Boyutlu Deneysel Ve Nümerik Karşılaştırılması. Engineering Sciences. 2011; 6(1): 406-414.

[25] Wu, W. , Altinakar, M., Al-Riffai, M., Bergman, N., Bradford, S., Cao, Z., et al. (2011). Earth-en Embankment Breaching. J. Hydraul. Eng. 137, 1549–1564. DOI:10.1061/(ASCE)HY.1943-7900.0000498

[26] Zhang, J, Guo, Z., Cao, S.,, Yang, F.. Experimental study on scour and erosion of blocked dam, Water Science and Engineering, 2012; 5(2): 219-229.

[27] Hsu, H.C, F, A. Hsu, T.C, Hwung , H.. Numerical And Experimental Study Of Dam-Break Flood Propagation And Its Implication To Sediment Erosion, Coastal Engineering Proceedings, 2012; 1(33).DOI:10.9753/icce.v33.sediment.7,

[28] Guney, M.S., Tayfur, G., Bombar, G., and Elci, S. "Distorted pyhsical model to study sudden partial dam break flows in an urban area", Journal of Hydraulic Engineering, 2014; 140(11):05014006-1-11, DOI: 10.1061/ (ASCE) HY.1943-7900.0000926.

[29] Okeke, A.CU., Wang, F. Critical hydraulic gradients for seepage-induced failure of landslide dams. Geoenviron Disasters Volume 3, Page 9, 2016. https://doi.org/10.1186/s40677-016-0043-z

[30] Msadala, V.P.C. 2016. Sediment transport dynamics in dam-break modeling. PhD Thesis, Stellenbosch University, South Africa.

[31] Haltas, Ismail; Tayfur, Gokmen; Elci, Sebnem Two-dimensional numerical modeling of flood wave propagation in an urban area due to Urkmez dam-break, Izmir, Turkey.' NATURAL HAZARDS Volume: 81 Issue: 3 Pages: 2103-2119 Published: APR 2016

[32] Haltas, Ismail; Elci, Sebnem; Tayfur, Gokmen Numerical Simulation of Flood Wave Propagation in Two Dimensions in Densely Populated Urban Areas due to Dam Break.' WATER RESOURCES MANAGEMENT Volume: 30 Issue: 15 Pages: 5699-5721 Published: DEC 2016

[33] Elçi Ş. , Tayfur G. , Haltas İ. , Kocaman B. Baraj Yıkılması Sonrası İki Boyutlu Taşkın Yayılımının Yerleşim Bölgeleri İçin Modellenmesi. Teknik Dergi. 0017; 28(3): 7955-7975.

[34] Zhong, Q., Chen,S., Deng,Z. A simplified physically-based model for core dam overtopping breach, Engineering Failure Analysis, Volume 90, 2018, Pages 141-155,https://doi.org/10.1016/j.engfailanal.2018.03.032.

[35] Chen, H.-X., Li, J., Feng, S.-J., Gao, H.-Y., and Zhang, D.-M. (2019). Simulation ofInteractions Between Debris Flow and Check Dams on Three-Dimensional Terrain. Eng. Geol. 251, 48–62. DOI:10.1016/j.enggeo.2019.02.001.

[36] Khosravi K., Chegini A.H.N., Cooper J., Mao L., Habibnejad M., Shahedi K., Binns A., A laboratory investigation of bed-load transport of gravel sediments under dam break flow,International Journal of Sediment Research,Volume 36, Issue 2, Pages 229-234, ISSN 1001-6279, 2021, https://doi.org/10.1016/j.ijsrc.2020.08.005.

[37] Azeez, O., Elfeki, A., Kamis, A.S., Chaabani, A.. Dam break analysis and flood disaster simulation in arid urban environment: the Um Al-Khair dam case study, Jeddah, Saudi Arabia. Natural Hazards, 2020; 100, 995–1011.

[38] Urzica, A., Pintilie, A.M., Stoleriu, C.C., Cîmpianu C.I., Hutanu E., Pricop C.I. ve Grozavu A. . Using 2D HEC-RAS Modeling and Embankment Dam Break

Scenario for Assessing the Flood Control Capacity of a Multi-Reservoir System (NE Romania). Water, 2020; 13(1), 57.

[39] Yavuz, S. & Deveci, M. (2015). İSTATİKSEL NORMALİZASYON TEKNİKLERİNİN YAPAY SİNİR AĞIN PERFORMANSINA ETKİSİ. Erciyes Üniversitesi İktisadi ve İdari Bilimler Fakültesi Dergisi, 0 (40) , 167-187. https://dergipark.org.tr/en/pub/erciyesiibd/issue/5897/78019.

# Appendices

# Appendix A

# Overtopping Smooth 2

Figure A.A.1: Camera 2 (flow and sediment transport at downstream area) and Camera 1 (stages of breach formation) at a) 291 sec, b) 311 sec, c) 331 sec, d) 351 sec, e) 361 sec, d) 375 sec for experiment OS2

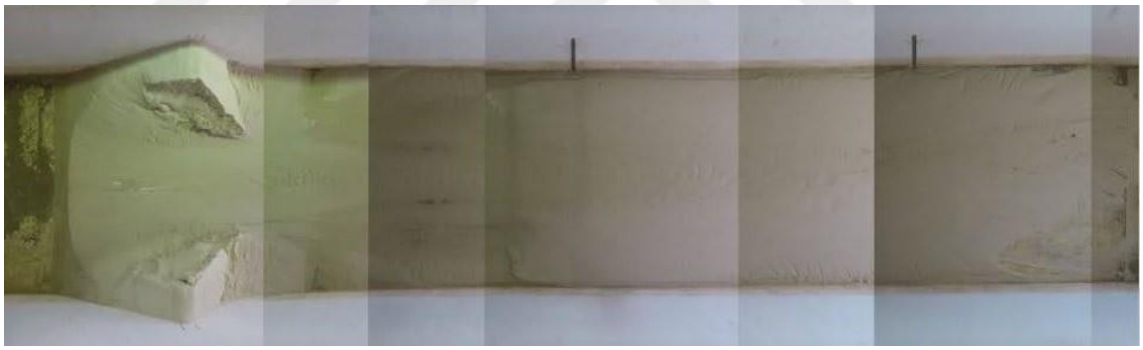

Figure A.A.2: Sediment propagation of end the experiment OS2

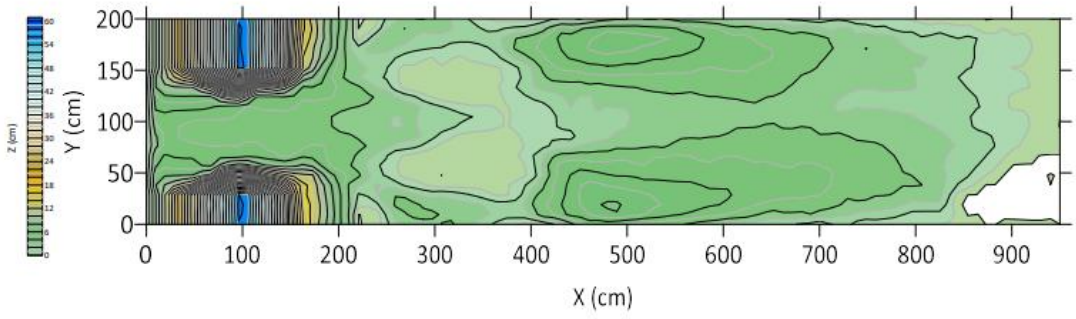

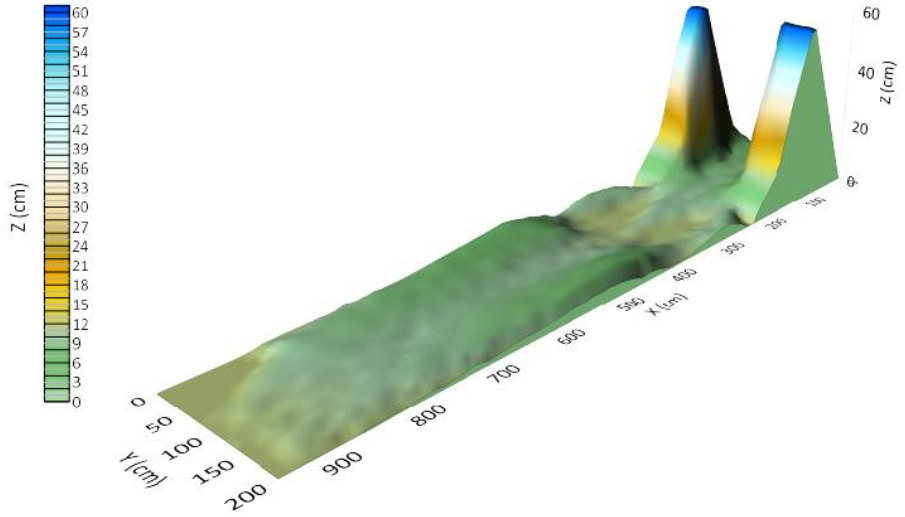


Figure A.A.3: 2D and 3D contour maps of sediment distribution at the end of OS2

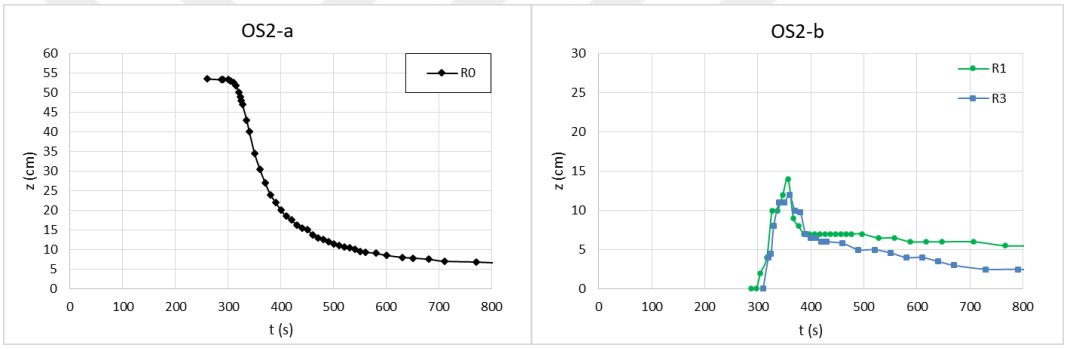


Figure A.A.4: Level measurements for OS2 experiment a) measured from $R_0$ and Probe1, b) measured from $R_1$, $R_2$, $R_3$, Probe 2 and Probe

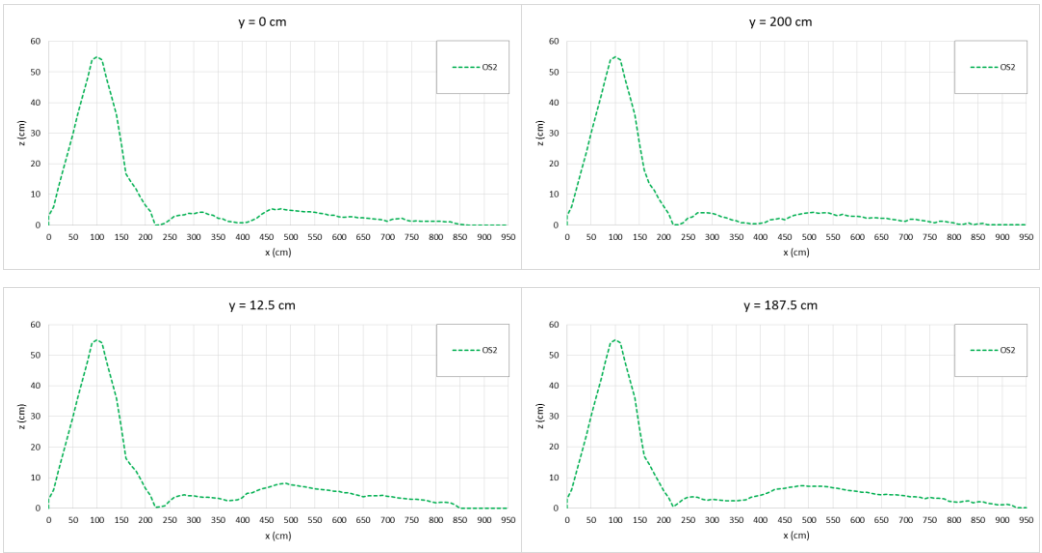


Figure A.A.5: Longitudinal sediment height profiles measured at a) y = 0 cm and 200 cm, b) y = 12.5 cm and 187.5 cm, c)y = 25 cm and 125 cm, d) y = 43.75 cm and 156.25 cm, e)y = 62.5 cm and 137.5 cm, f) y= 81.25 cm and 118.75 cm, and g) y = 100 cm and along the channel width and, transversal crest section of the dam at h) x = 100 cm of OS2

# Appendix B

# Overtopping Rough 2

Figure A.B.1: Camera 2 (flow and sediment transport at downstream area) and Camera 1 (stages of breach formation) at a) 249 sec, b) 300 sec, c) 305 sec, d) 316 sec, e) 354 sec, f) 384 sec for experiment OR2

Figure A.B.2: Sediment propagation of end the experiment OR2

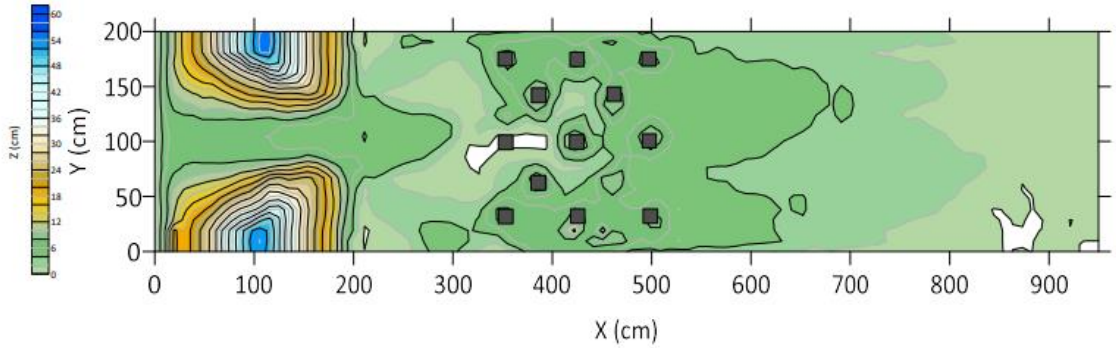

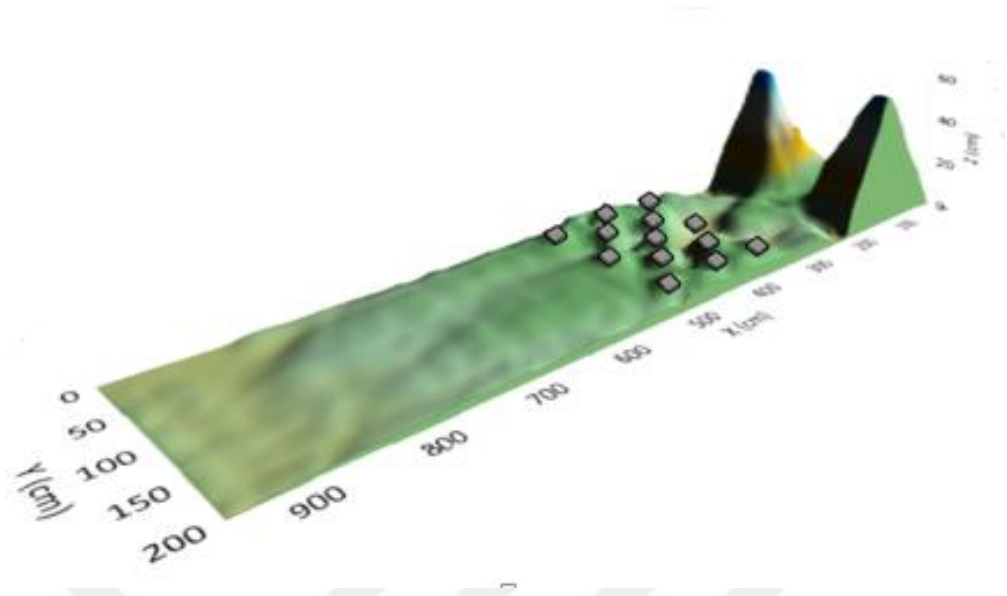


Figure A.B.3: 2D and 3D contour maps of sediment distribution at the end of OR2

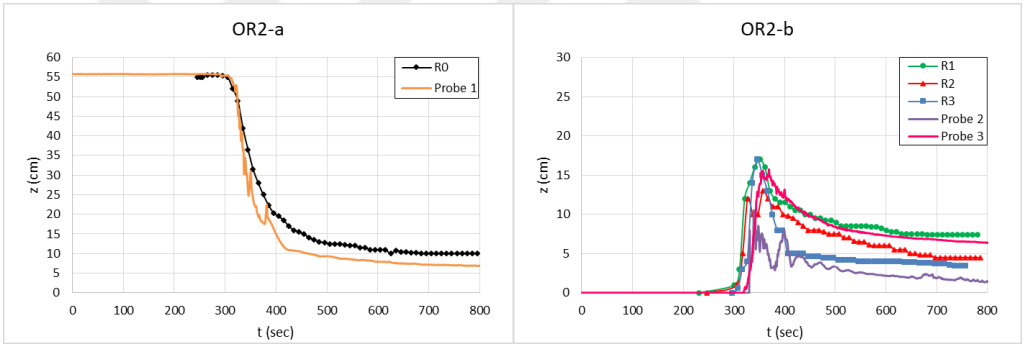


Figure A.B.4: Level measurements for OR2 experiment a) measured from $R_0$ and Probe1, b) measured from $R_1$, $R_2$, $R_3$, Probe 2 and Probe 3

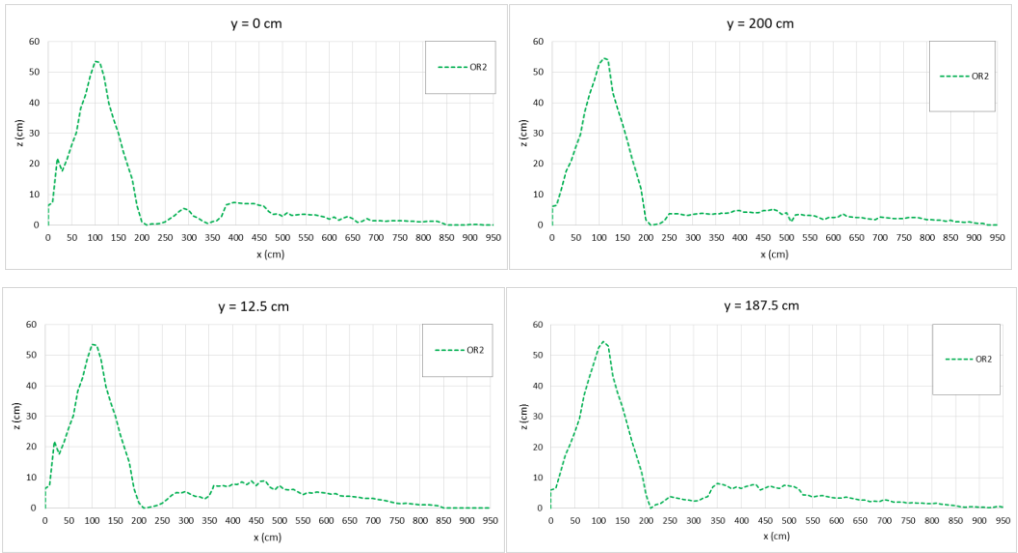

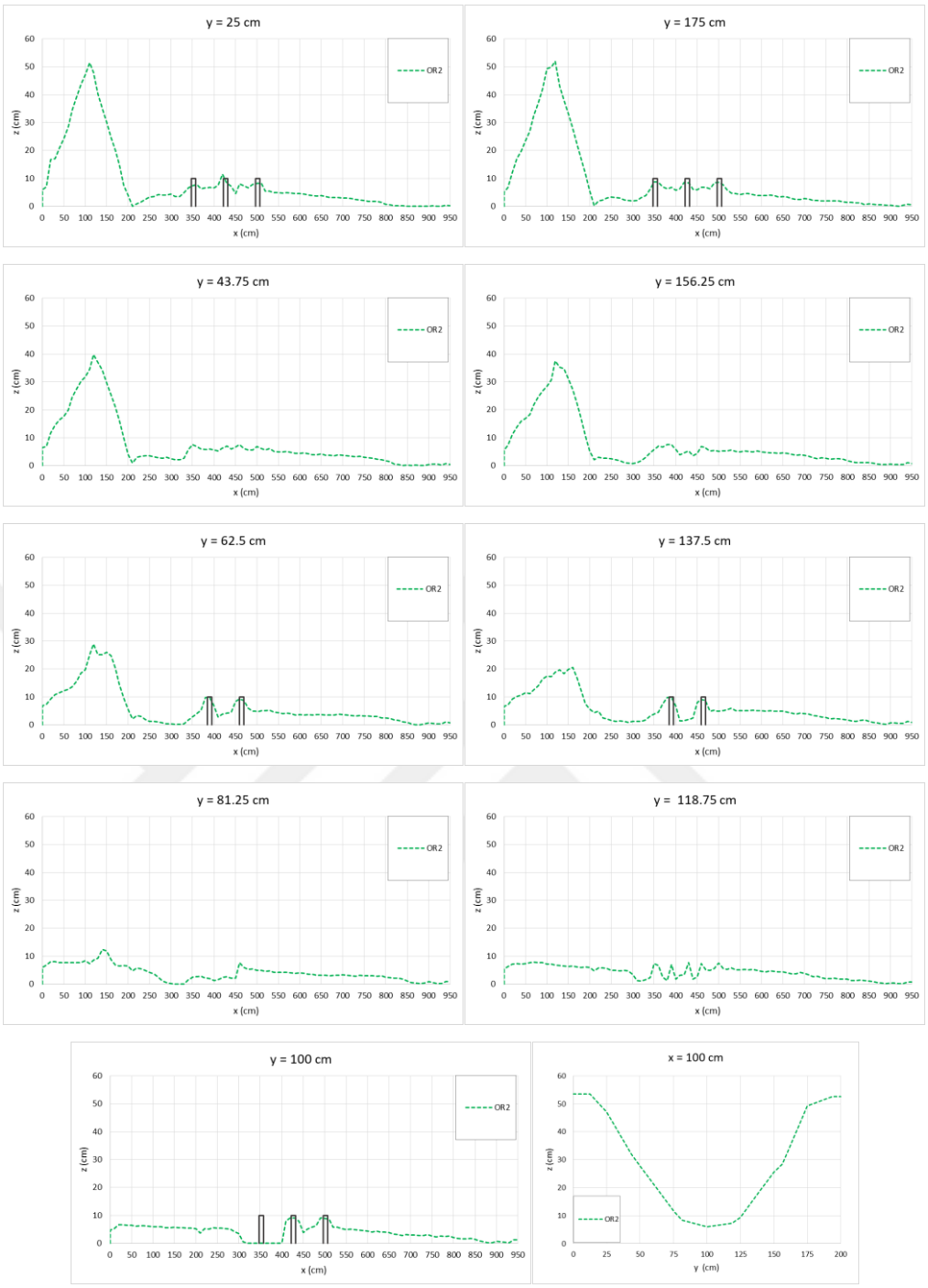


Figure A.B.5: Longitudinal sediment height profiles measured at a) y = 0 cm and 200 cm, b) y = 12.5 cm and 187.5 cm, c)y = 25 cm and 125 cm, d) y = 43.75 cm and 156.25 cm, e)y = 62.5 cm and 137.5 cm, f) y= 81.25 cm and 118.75 cm, and g) y = 100 cm and along the channel width and, transversal crest section of the dam at h) x = 100 cm of OR2

# Appendix C

# Piping Smooth 2

Figure A.C.1: Camera 2 (flow and sediment transport at downstream area) and

Camera 1 (stages of breach formation) at a) 0 sec, b) 292 sec, c) 337 sec, d) 352 sec, e) 362 sec, f) 493 sec for experiment PS2

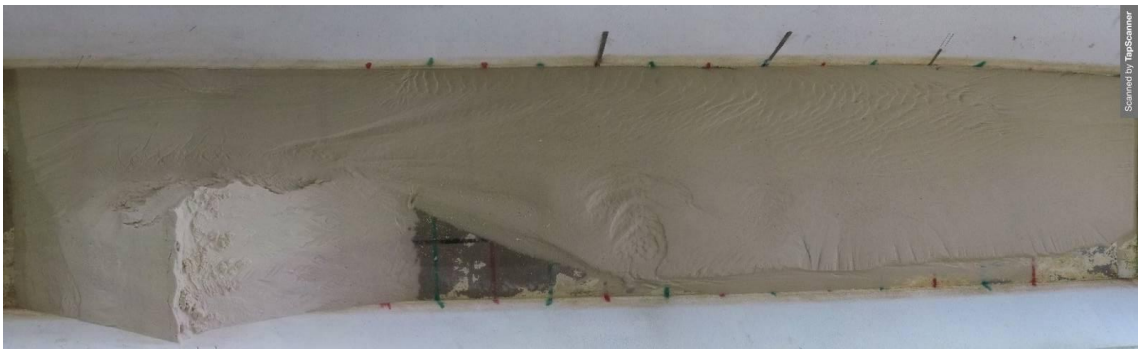

Figure A.C.2: Sediment propagation of end the experiment PS2

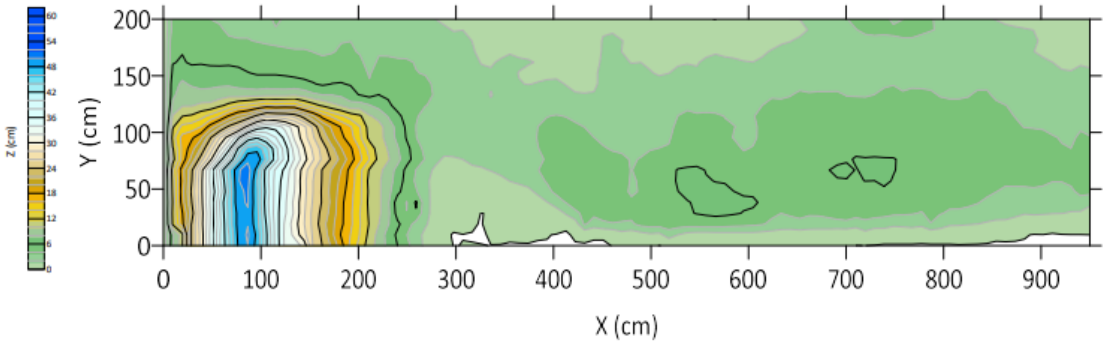


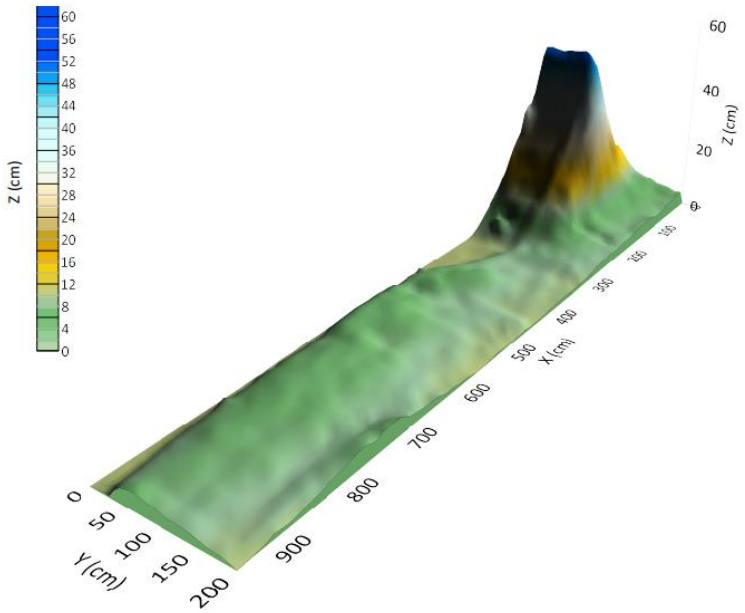


Figure A.C.3: 2D and 3D contour maps of sediment distribution at the end of PS2

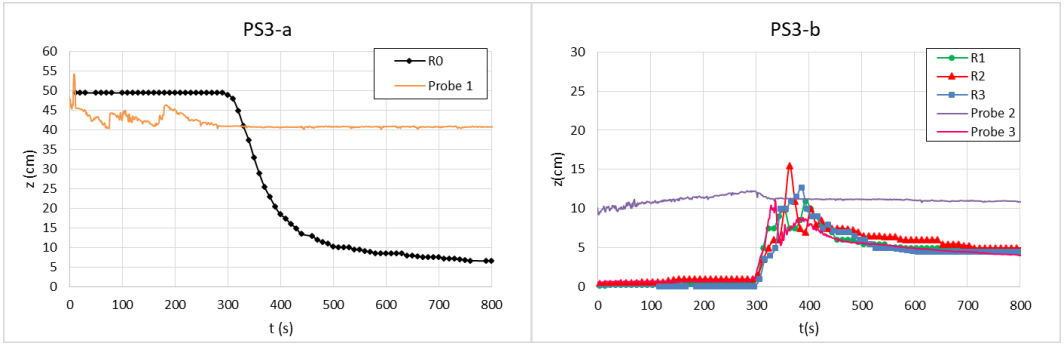


Figure A.C.4: Level measurements for PS2 experiment a) measured from $R_0$ and Probe1, b) measured from $R_1$, $R_2$, $R_3$, Probe 2 and Probe 3

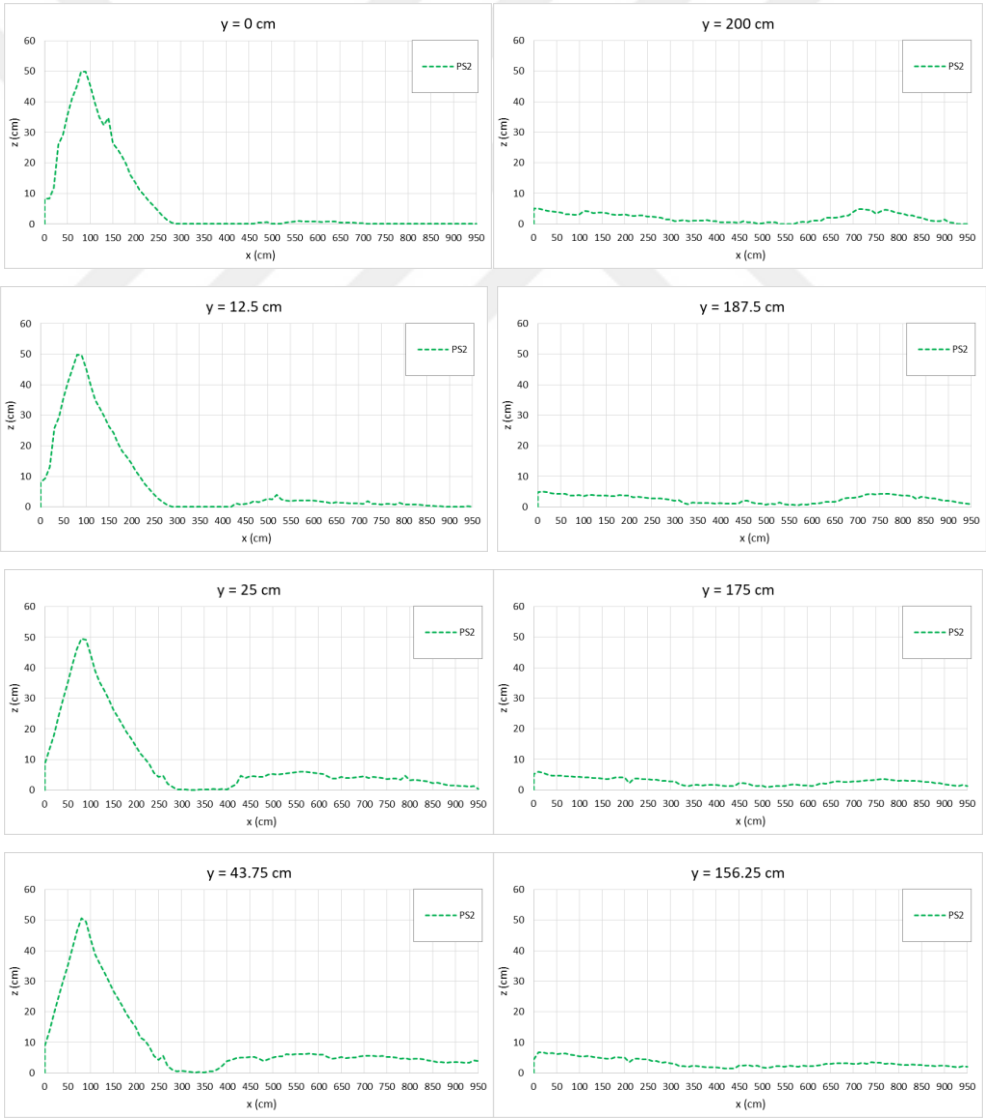

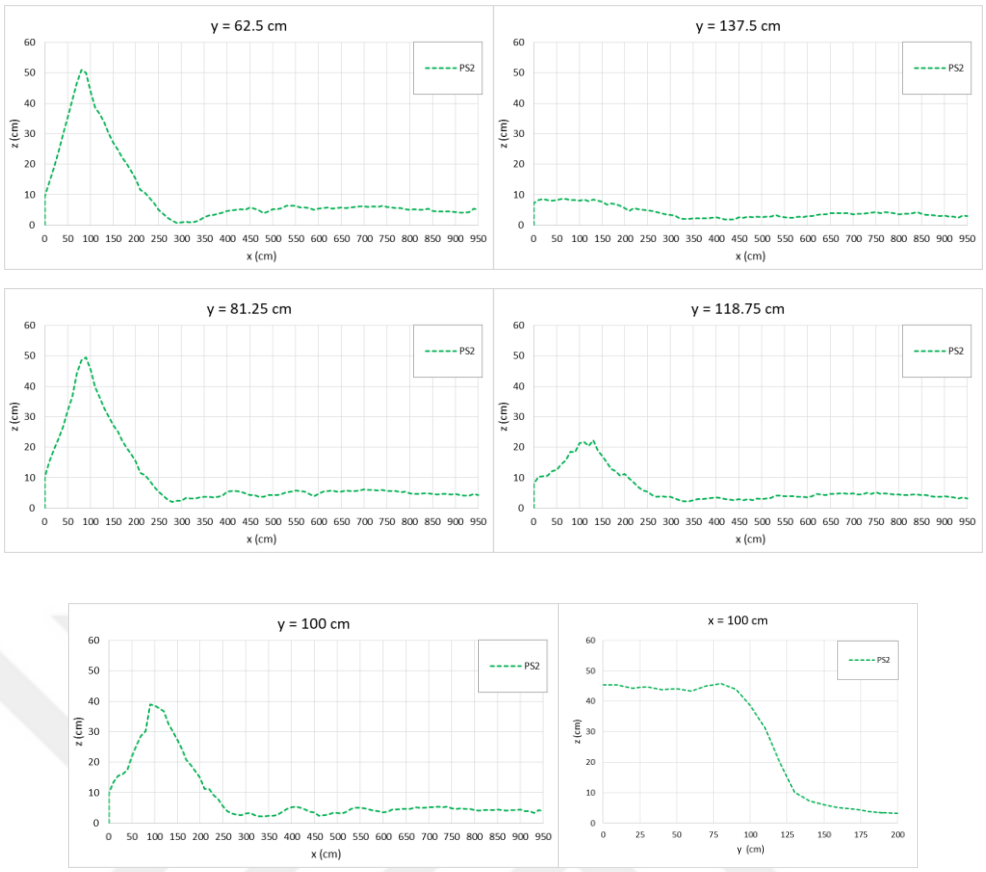


Figure A.C.5: Longitudinal sediment height profiles measured at a) y = 0 cm and 200 cm, b) y = 12.5 cm and 187.5 cm, c)y = 25 cm and 125 cm, d) y = 43.75 cm and 156.25 cm, e)y = 62.5 cm and 137.5 cm, f) y= 81.25 cm and 118.75 cm, and g) y = 100 cm and along the channel width and, transversal crest section of the dam at h) x = 100 cm of PS2

# Appendix D

# Piping Rough 2

Figure A.D.1: Camera 2 (flow and sediment transport at downstream area) and Camera 1 (stages of breach formation) at a) 141 sec, b) 281 sec, c) 300 sec, d) 303 sec, e) 321 sec, f) 366 sec for experiment PR2

Figure A.D.2: Sediment propagation of end the experiment PR2

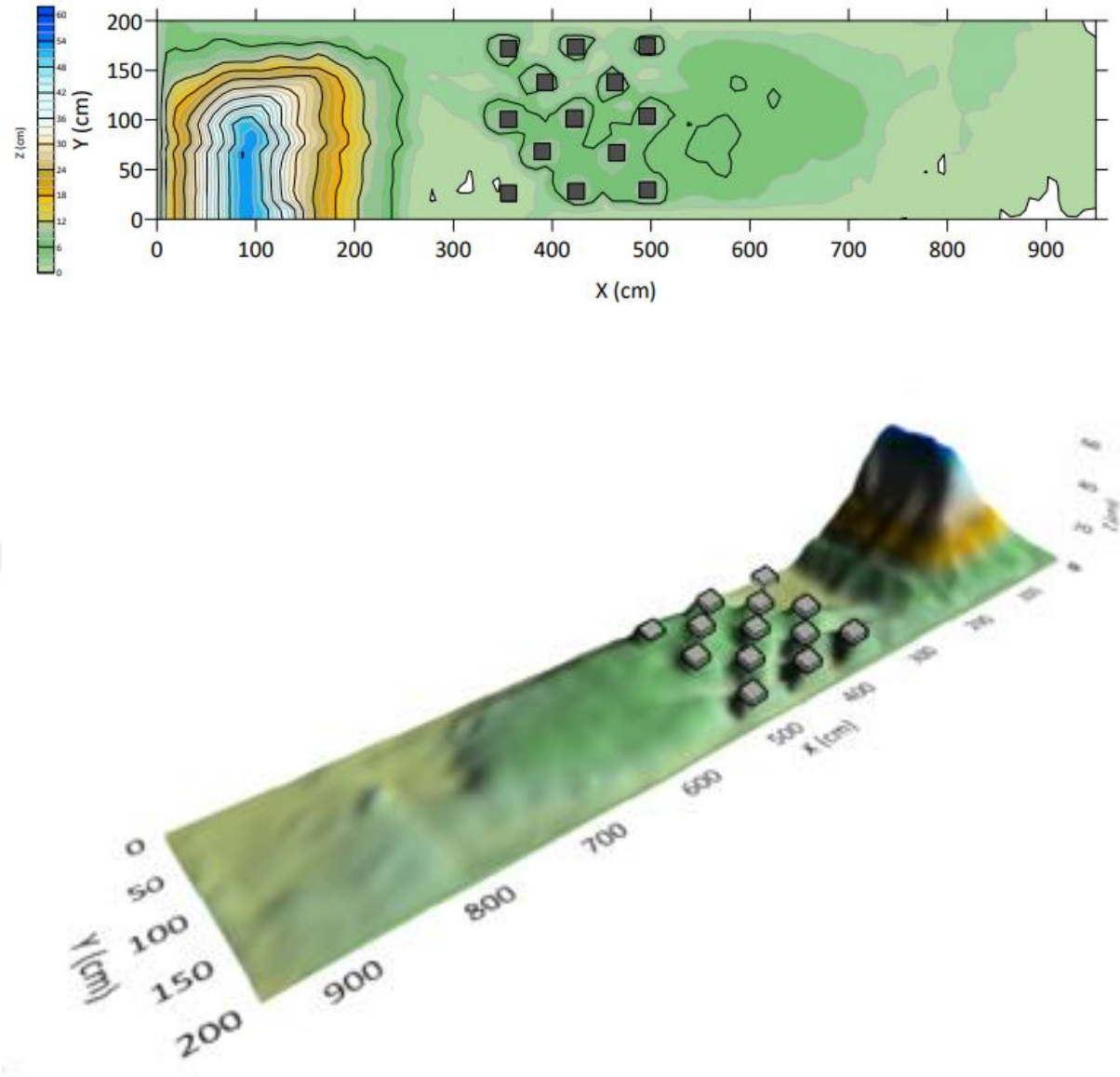


Figure A.D.3: 2D and 3D contour maps of sediment distribution at the end of PR2

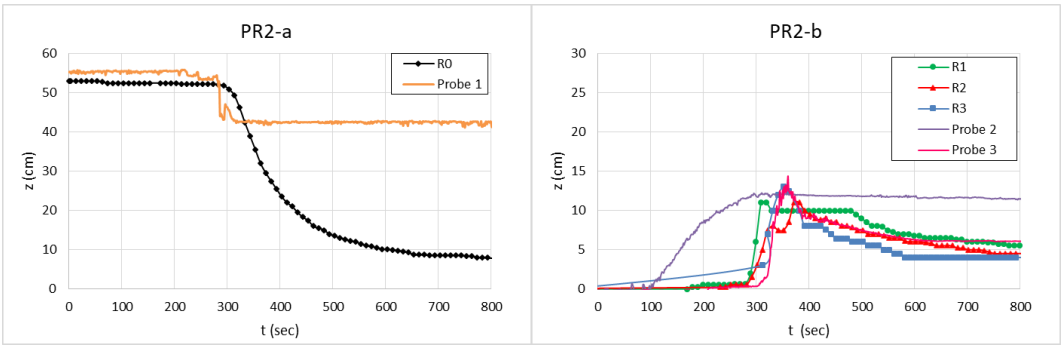


Figure A.D.4: Level measurements for PR2 experiment a) measured from $R_0$ and Probe1, b) measured from $R_1$, $R_2$, $R_3$, Probe 2 and Probe 3

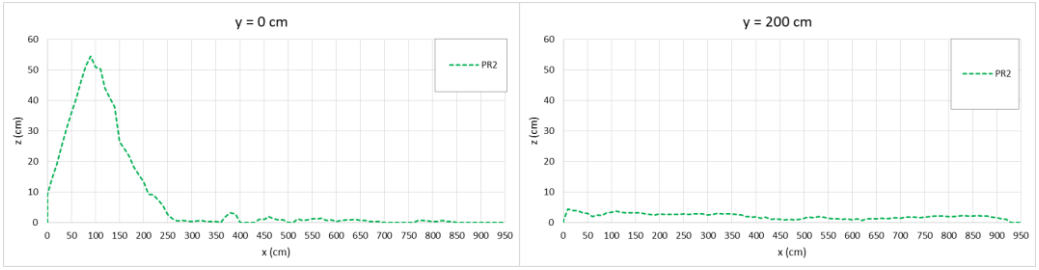
y = 0 cm
PR2
z (cm)
x (cm)


y = 200 cm
PR2
z (cm)
x (cm)

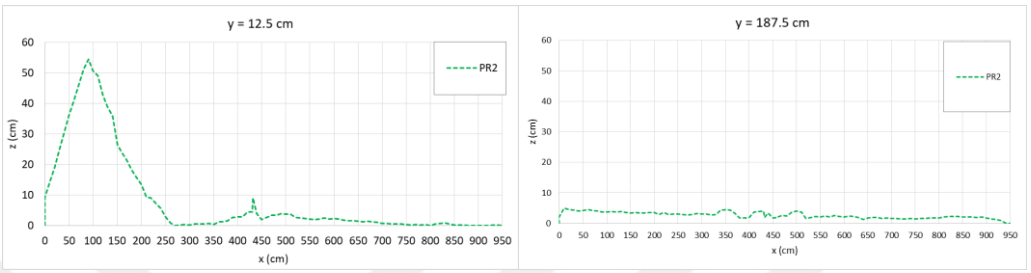
y = 12.5 cm
PR2
z (cm)
x (cm)


y = 187.5 cm
PR2
z (cm)
x (cm)

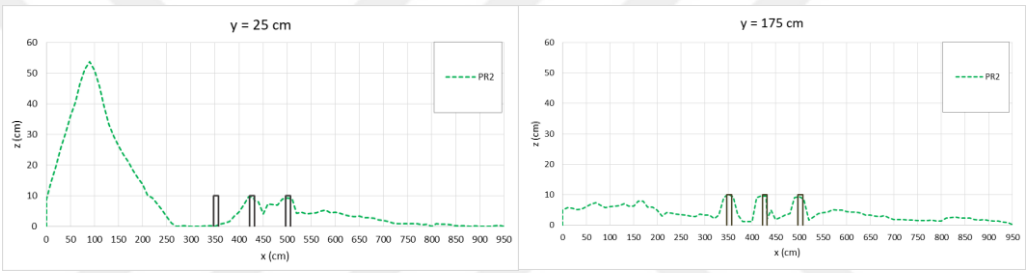
y = 25 cm
PR2
z (cm)
x (cm)


y = 175 cm
PR2
z (cm)
x (cm)

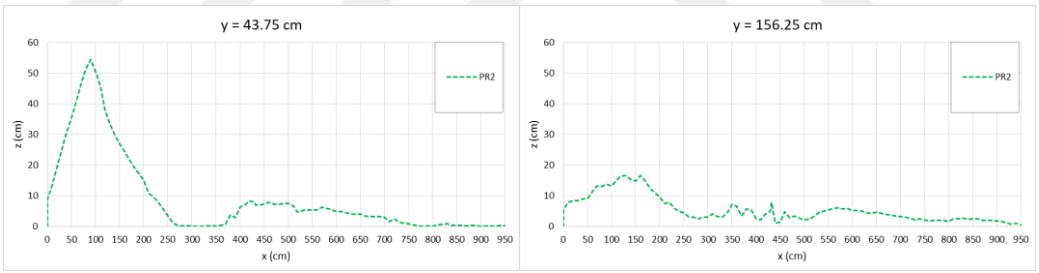
y = 43.75 cm
PR2
z (cm)
x (cm)


y = 156.25 cm
PR2
z (cm)
x (cm)

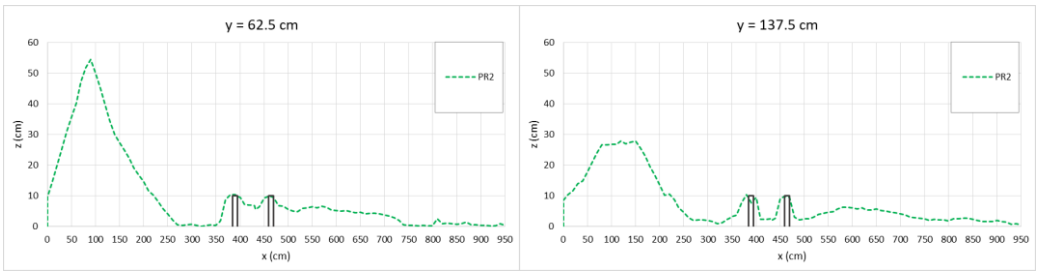
y = 62.5 cm
PR2
z (cm)
x (cm)


y = 137.5 cm
PR2
z (cm)
x (cm)

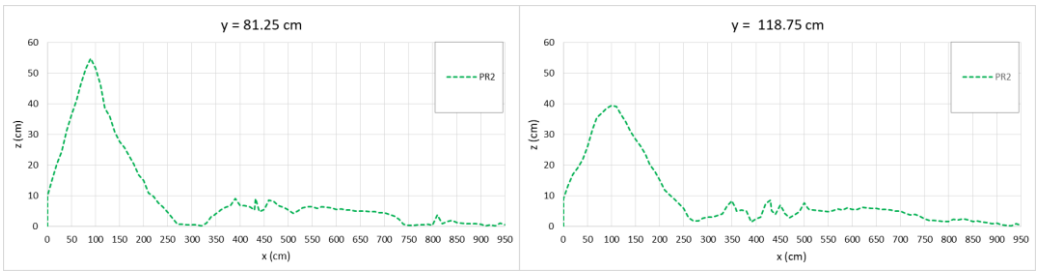
y = 81.25 cm
PR2
z (cm)
x (cm)


y = 118.75 cm
PR2
z (cm)
x (cm)

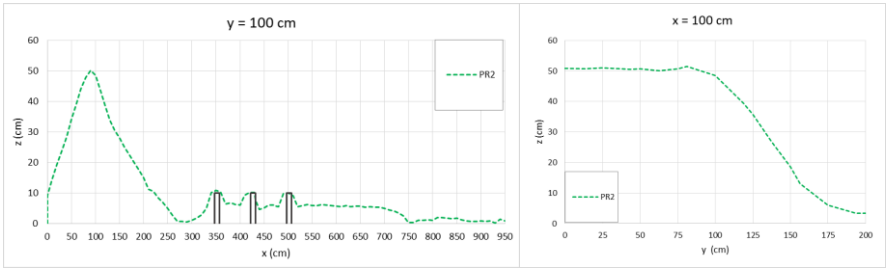


Figure A.D.5: Longitudinal sediment height profiles measured at a) y = 0 cm and 200 cm, b) y = 12.5 cm and 187.5 cm, c)y = 25 cm and 125 cm, d) y = 43.75 cm and 156.25 cm, e)y = 62.5 cm and 137.5 cm, f) y= 81.25 cm and 118.75 cm, and g) y = 100 cm and along the channel width and, transversal crest section of the dam at h) x = 100 cm of PR2

# Appendix E

# Publications from the Thesis

**Conference Papers**

**1**. Taşkaya, E., Büyüker, Z., Öztürk, B., Bombar, G., Tayfur, G., 2022, "Overtopping Failure of a Homogeneous Earth-Fill Dam with Two Different Breach Sizes and Rough Downstream Conditions", River Flow 2022, the 11th International Conference on Fluvial Hydraulics, 8-9 November 2022, Ottawa, Kanada, oral presentation, full text.

**2.** Taşkaya, E., Büyüker, Z., Bombar, G., Tayfur, G., "Homojen Toprak Dolgu Baraj Yıkılmasının Mansap Bölgesindeki Sediment Yayılımı Üzerine Deneysel Çalışma" XI. International Hyrology Congress, 13-14 October,2022, Gaziantep Universitesi, Gaziantep, Türkiye, presentation, full text.

**Journal Articles**

**1**. Taşkaya, E., Bombar, G., Tayfur, G., "Experimental Investigation of Sediment Movement as a Result of Homogeneous Earth-fill Dam Overtopping Break over a Simplified Urban Area", Journal of Hydrology, 2022

**Projects**

**1**. Project numbered 119M959 supported by TÜBİTAK

Republic of Turkey

İzmir Kâtip Çelebi University

Graduate School of Natural and Applied Sciences

# Experimental Investigation of Propagation of Sediment Due to Earth-fill Dam Break



Department of Civil Engineering

Master's Thesis

Ebru Taşkaya

ORCID 0000-0003-1265-600X

Thesis Advisor: Ass. Prof. Dr. Gökçen BOMBAR

November 2023

| | | | |
|---|---|---|---|
| TASKAYA | Experimental Investigation of Propagation of Sediment Due to Earth-fill Dam Break | MASTER'S THESIS | 2023 |

# Curriculum Vitae

Name Surname : Ebru TAŞKAYA

Education:

2015–2019 İzmir Kâtip Çelebi University, Dept. of Civil Eng.

Work Experience:

02.2021 – 09.2022 TUBITAK Project Scholar

09.2019 – 04.2020 TUBITAK Project Scholar

07.2019 – 09.2019 Instituto Superior Técnico - Intern

Publications (if any):

1. Taşkaya, E., Bombar, G., Tayfur, G., "Experimental Investigation of Sediment Movement as a Result of Homogeneous Earth-fill Dam Overtopping Break over a Simplified Urban Area", Journal of Hydrology, 2022.

2. Taşkaya, E., Büyüker, Z., Öztürk, B., Bombar, G., Tayfur, G., 2022, "Overtopping Failure of a Homogeneous Earth-Fill Dam with Two Different Breach Sizes and Rough Downstream Conditions", River Flow 2022, the 11th International Conference on Fluvial Hydraulics, 8-9 November 2022, Ottawa, Kanada, oral presentation, full text.

3. Taşkaya, E., Büyüker, Z., Bombar, G., Tayfur, G., "Homojen Toprak Dolgu Baraj Yıkılmasının Mansap Bölgesindeki Sediment Yayılımı Üzerine Deneysel Çalışma" XI. International Hyrology Congress, 13-14 October,2022, Gaziantep Universitesi, Gaziantep, Türkiye, presentation, full text.

4. Taşkaya, E., Büyüker, Z., Öztürk, B., Bombar, G., Tayfur, G., 2022, “Experimental Study of a Homogeneous Dam Break with a Breach”, 14th of the International Conference on Hydroscience & Engineering, ICHE 2022, Izmir, Turkey, 26-27 May 2022, oral presentation, full text.

5. Büyüker, Z., Taşkaya, E., Bombar, G., Tayfur, G., 2022, “Pürüzlü Mansaba Sahip Homojen Toprak Dolgu Barajın Yıkılma Senaryosunun Deneysel Olarak İncelenmesi”, 6th International Students Science Congress, 20-21 May 2022, İzmir, Turkey, oral presentation, full text.

6. Taşkaya, E., Bombar, G., Tayfur, G., 2021, “Homojen Dolgu Baraj Yıkılması Üzerine Deneysel bir Çalışma”, 5th International Students Science Congress, 18-19 September 2021, İzmir, Turkey, oral presentation, full text.

7. Taşkaya, E., Bombar, G., Tayfur, G., 2021, “Experimental Investigation of a Failure of a Homogeneous Earth-en Dam by Overtopping”, 14th International Congress on Advances in Civil Engineering, ACE, 6-8 September, 2021, İstanbul, Türkiye, oral presentation, full text.

8. Taşkaya, E., Büyüker, Z., Bombar, G., Cardoso, A.H., 2022, “Experimental Investigation On The Geometry Of Scour Holes Around A Cylinder Pier”, 14th of the International Conference on Hydroscience & Engineering, ICHE 2022, Izmir, Turkey, 26-27 May 2022, oral presentation, full text.